CELLULAR AND GENETIC CHARACTERIZATION OF OCULAR MELANOSIS IN THE CAIRN TERRIER DOG

By

Ethan Dawson-Baglien

A DISSERTATION

Submitted to
Michigan State University
in partial fulfillment of the requirements
for the degree of

Genetics – Doctor of Philosophy

2017

PUBLIC ABSTRACT

CELLULAR AND GENETIC CHARACTERIZATION OF OCULAR MELANOSIS IN THE CAIRN TERRIER DOG

By

Ethan Dawson-Baglien

Ocular melanosis (OM) is an inherited eye disease seen in the Cairn terrier dog breed. The disease is very common in Cairn terriers – although the exact number of dogs affected by the disease is not known, surveys of Cairn terrier breeders and owners frequently rank it near the top of health concerns in the breed. The disease progresses through several stages, starting off as a thickening and darkening of the iris. Eventually, dark brown-black pigment begins to appear in patches in abnormal areas of the eye, such as the sclera (the whites of the eye). These patches gradually grow and expand over time. Within the eye, pigmented material is shed into the anterior chamber of the eye (the fluid-filled space between the iris and the front of the eye). This pigmented material clogs up the eye's internal drainage pathways, and fluid builds up within the anterior chamber, leading to an increase in pressure within the eye. This increase in pressure can lead to painful glaucoma, and eventually blindness, in the dogs with the most severe cases of OM. The underlying causes of OM are not currently known. Two different methods were used to attempt to find out more about the disease – a cell culture method and a gene sequencing method.

In the cell culture method, donated eyes from dogs with and without OM were used to isolate and grow uveal melanocytes – the pigmented cells of the eye which grow and migrate in OM. These cells were then tested using a variety of different cellular assays to determine how the melanocytes from affected eyes differed from those in unaffected eyes. The only tests

where the melanocytes from the OM-affected dogs showed any difference from those in unaffected dogs were in pigmentation – the melanocytes from OM-affected dogs had much more pigment, and made new pigment more quickly, than those from unaffected dogs.

Gene sequencing methods were also used to try to find where in the genome the mutation that causes OM was located. To determine the general location of the mutation, a whole-genome SNP array was used to test 94 dogs at 170k markers from all around the 2.8 billion base pairs of the canine genome, to see if any of the markers was associated with the disease. This identified a 7.5 million base-pair long region of chromosome 11 that was significantly associated with the disease. Next, the entire genome of 10 dogs was sequenced, 5 OM-affected and 5 unaffected, to look for the exact mutation causing OM. Analysis of the sequencing data failed to identify a likely causal variant, either within the identified region or in known genes related to pigmentation disorders. Finally, RNA sequencing was performed on eye tissues from 12 dogs; 7 OM-affected and 5 unaffected, to determine whether there were any differences in gene expression between the two populations. Six genes were identified that were expressed differently between the two populations that were in pathways known to be associated with cancer metastasis.

Although a causal variation for OM has not yet been discovered, several promising new clues have been identified that can be followed up on, including the general location of the causal DNA mutation on chromosome 11, and a number of genes whose expression are altered in OM-affected dogs. Following these leads may finally allow us to identify the underlying cause of OM.

ABSTRACT

CELLULAR AND GENETIC CHARACTERIZATION OF OCULAR MELANOSIS IN THE CAIRN TERRIER DOG

By

Ethan Dawson-Baglien

Ocular melanosis (OM) is an inherited eye disease characterized by a thickening of the iris root due to expansion of a melanocyte population and an abnormal progressive deposition of pigment in areas of the eye such as the sclera and episclera. The disease is inherited in an autosomal dominant fashion, and occurs almost exclusively in Cairn terrier dogs, in whom the disease is very common. OM is relatively recent in origin, leading us to suspect that it has a single causative underlying mutation, which spread through the Cairn population via a founder effect. In this work, two different approaches were used to attempt to characterize the OM phenotype – a cellular and a genetic approach.

A method for isolating and culturing canine uveal melanocytes without contamination from other cell types was initially developed. This was then used to isolate melanocytes from OM-affected and control dogs which were then compared using various assays of physiological behavior. These included a battery of standard cell behavior tests to evaluate doubling time, migration rate, anchorage independence, ability to migrate through a membrane, extracellular matrix preference, and melanin content and rate of production. In all aspects, melanocytes from OM-affected dogs and those from unaffected dogs were identical *in vitro*, except for melanin content and production rate – after initial culture, OM-affected melanocytes contained much more melanin than unaffected cells, and produced more melanin as well. These changes

were eventually lost in later passages, but differences were statistically significant ($p<0.05$) in early-passage cells.

Attempts to identify a causal mutation for OM based using a candidate gene approach had not previously been successful, so a whole-genome SNP array was used to examine 94 Cairn terriers at ~170k evenly spaced markers throughout the genome. This identified a 7.5 megabase (Mb) region of chromosome 11 that was significantly associated with the disease. Sanger sequencing of positional candidate genes selected from the region of interest did not reveal any variants associated with the disease. Whole-genome sequencing was performed on 10 dogs; 5 affected and 5 unaffected, but no genes either within the region detected via the SNP array or within a list of genes known to be associated with pigmentation disorders contained any polymorphism that segregated with the disease. Finally, RNA sequencing was performed on 12 samples, 7 affected and 5 affected, and the transcriptomes of OM-affected and unaffected dogs were compared. Although no individual genes had a statistically significant difference in expression level, pathway analysis of the genes with the lowest p-values revealed 6 genes with differential expression levels that were part of 1 of 2 pathways known to be associated with cell migration in metastatic cancer.

Although further studies are needed, the identification of both a region associated with OM and a putative pathway which may be involved in the migratory component of the disease functions are major steps toward identifying the underlying cause of the disease.

TABLE OF CONTENTS

LIST OF TABLES

LIST OF FIGURES

KEY TO ABBREVIATIONS

Mb – megabase pairs

bp – base pairs

OM – ocular melanosis

ICC – immunocytochemistry

IOP – Intraocular pressure

IHC – immunohistochemistry

SNP – single nucleotide polymorphism

WGS – whole-genome sequencing

qRT-PCR – quantitative real-time PCR

CHAPTER 1

INTRODUCTION

1.1 The dog as a model organism for inherited disease

1.1.1 The dog as a model organism

Although a relative newcomer compared to the established traditional model organisms of biology such as *Drosophila melanogaster*, *Arabidopsis thaliana*, and *Mus musculus*, the domestic dog has many qualities which lend themselves well to disease research in the era of genomic science. The dog combines a huge amount of phenotypic variation, in terms of size, shape, and behavior, with a well-characterized and annotated genome and many excellent tools designed to facilitate the analysis of large-scale genomic data. The wide variety of genetic backgrounds present in the form of different dog breeds combined with certain breeding practice leads to the occurrence of many spontaneous models of human disease. Since dogs usually share an environment with their owners, and are more similar in size, behavior, and physiology, orthologous diseases in the dog often more useful as models for human diseases than those in traditional models like the mouse and rat.

1.1.2 The canine genome

In terms of raw size, the canine genome is roughly as large as the mouse genome (2.41 billion base pairs in dogs vs. 2.60 billion base pairs in mice), and slightly smaller than the human genome (2.91 billion base pairs) (1-3). It is subdivided into 39 pairs of chromosomes, 38 autosomal pairs and one pair of sex chromosomes. The first high-quality draft of the canine genome was completed in 2005 using whole-genome shotgun sequencing at a coverage of approximately 7.5X to sequence the genome of a female boxer dog (1, 6).

In addition to having numerous and well-established tools that exist for working with the canine genome, the dog genome also benefits from the unique population structure that centuries of selective breeding have created. Through the process of selecting for certain behavioral and physiological traits in certain breeds, dogs display an enormous amount of variation between breeds, but very little variation within breeds (10). This can be expressed in terms of intrabreed vs interbreed linkage disequilibrium (LD), the non-random association of alleles at a given loci due to physical linkage. Intrabreed canine LD is on the order of megabases, whereas the interbreed LD is on the order of kilobases, nearly 100 times shorter than the LD seen within breeds. In fact, LD between breeds is similar to what is seen in some well-characterized human populations (1). The large LD blocks seen within single breeds can be very useful for applications where a disease inherited within a limited number of breeds is being mapped – the large LD blocks seen in single breeds allow for marker-based studies like genome-wide association studies to map genes with a high degree of power using only a very small number of markers, around 10,000 for an average breed (1).

Although they may differ from humans in terms of LD, dogs are similar to them in terms of the number of coding genes they possess. The dog genome was originally projected to contain roughly 19,300 total genes, compared with around 22,320 in humans, 23,062 in mice, and 24,147 in zebrafish, but recent studies suggest that up to 70% of the difference in gene number between dogs and other established model organisms is the result of real canine genes failing to be called by prediction algorithms, suggesting that the total number of true canine genes is probably closer to 21,400 (1, 3, 11-13).

1.2 Anatomy of the canine eye and uvea

1.2.1 General overview of the eye

The canine eye is composed of three basic layers – the fibrous tunic, the uvea, and the nervous coat (Figure 1.1) (5, 14-16). Fibrous tunic is a tough, mostly avascular outer layer which helps the eye maintain its rigid shape. It is subdivided into the cornea and the sclera. The uvea is the middle layer, and it is further subdivided into the choroid, the ciliary body, and the iris. The uvea is heavily vascularized and pigmented, and helps to adjust intraocular light levels and to provide nutrients to the other layers of the eye. The nervous coat is the innermost layer, and it is composed of the retina and the optic nerve head. The retina contains the light-sensitive cells that are responsible for converting light signals into electrical impulses which can then be transmitted to the brain via the optic nerve (5, 14-16). For purposes of this work, we will primarily be focusing on the various components of the uvea, as well as the fibrous layer to a somewhat lesser extent.

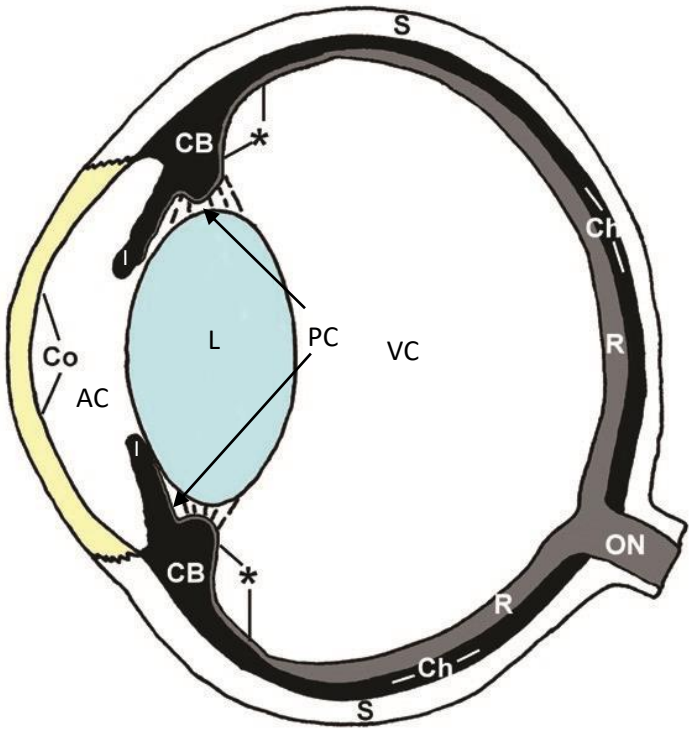

Figure 1.1 – Diagram of the three basic layers of the canine eye The fibrous tunic is shown in yellow (Co, cornea) and white (S, sclera). The uvea is shown in black, consisting of the choroid (Ch), the ciliary body (CB), and the iris (I). The nervous tunic is shown in grey, and is composed of the retina (R) and the optic nerve (ON). Between the cornea and the iris lies the anterior chamber (AC). The large cavity at the posterior of the eye is the vitreous chamber, and the small space between the iris and the lens (L) is the posterior chamber (PC). Modified from (5).

1.2.2 The fibrous tunic

1.2.2.a The cornea

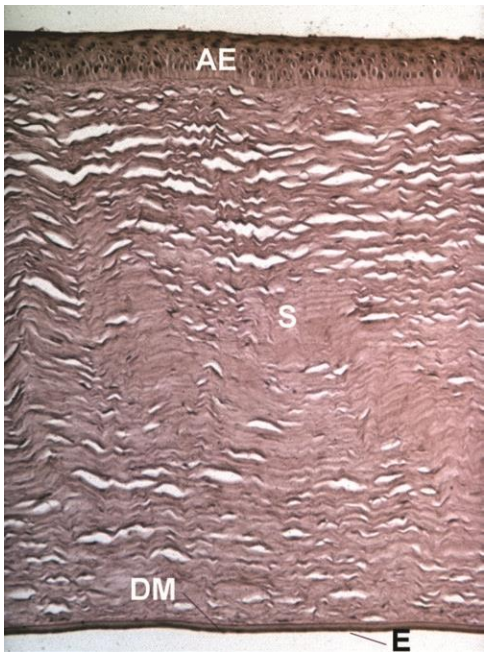

Figure 1.2 – Layers of the canine cornea Anterior epithelium (AE), the stroma (S), Descemet's Membrane (DM), and the corneal endothelium (E). Figure reproduced from (5).

The cornea is the most anterior portion of the fibrous tunic, comprising roughly one-fifth of the tunic's total area. It is transparent, allowing the transmission of light through to the lens and the retina, and is avascular. It receives the majority of its nutrients from the aqueous humor. The cornea is made up of four layers: the anterior epithelium, the stroma, Descemet's membrane, and the corneal endothelium (Figure 1.2). The anterior epithelium is 25-40 µm thick and consists of a single layer of basal columnar cells, 2-3 layers of polyhedral cells, and 2-3 layers of nonkeratizined squamous cells. The basal cell layer is attached to a basement membrane which adheres the anterior epithelium to the underlying stroma. The stroma makes up the bulk of the cornea, roughly 90% of the overall thickness, and it contains primarily of

transparent parallel sheets of collagen fibrils along with a small number of keratocytes which form and maintain the lamellae. Descemet's membrane is a homogenous acellular layer of collagen fibrils produced by the basement layer of the corneal endothelium. Descemet's membrane is under tension, and helps to maintain the shape of the eye. The corneal endothelium is the innermost layer of the cornea, and it consists of a single layer of metabolically active cells which help to maintain Descemet's membrane (5, 14, 17, 18).

1.2.2.b The sclera

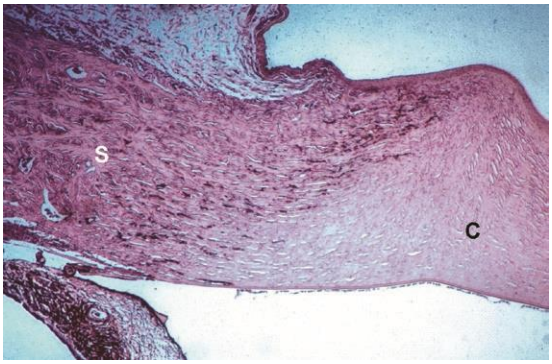

Figure 1.3 – The canine limbus This image shows the junction between the highly regular, parallel collagen fibers of the transparent cornea (C) and the irregular fibers of the opaque sclera (S). Figure reproduced from (5).

The remaining four-fifths of the fibrous tunic compose the sclera, what is usually known as the "white" of the eye. The fibrous tunic transitions from the transparent cornea to the opaque sclera at a transition zone known as the limbus. At this transition zone, the layer that had been the corneal epithelium expands and thickens and the stroma loses the regular parallel arrangement of the collagen fibers that allowed it to transmit light, becoming opaque (Figure 1.3). The sclera is divided into four layers. The outermost layer is the episclera, a thin collagenous membrane that connects to Tenon's capsule (a thin sheath separating the eye from the interior of the eyesocket), and the conjunctiva (the inner lining of the eyelids). Blood vessels

originating in the conjunctiva serve to vascularize the episclera. The remaining layers, the stroma, the basal cell layer, and the endothelium, are continuous with and serve the same function as their counterparts in the cornea, although unlike the cornea, the sclera contains blood vessels (5, 14, 17-19).

1.2.3 The uvea

1.2.3.a The choroid

The choroid is the posterior portion of the uvea. It connects directly to the sclera, and is composed of four layers. The outermost layer is the suprachoroidea, followed by the stroma with large vessels, the stroma with medium-sized vessels and the tapetum (a layer of reflective tissue which reflects light which has passed through the retina), and the choriocapillaris. Like most of the uvea, the choroid is pigmented and heavily vascular (5, 14-16, 20).

1.2.3.b The ciliary body

The ciliary body, along with the iris, makes up the anterior uvea. It is located near the limbus, and is roughly triangular in shape – one edge connects to the sclera, another to the lens (via the lens zonular fibers), and the third to the iris (Figure 1.4). It helps to provide nutrients to and remove waste from the avascular cornea by producing aqueous humor, an optically clear fluid which contains diffuse proteins and nutrients for delivery to the cornea. Keeping the proper volume of aqueous humor in the anterior chamber at all times is critical for proper functioning of the eye – aqueous humor generates intraocular pressure (IOP). An impediment to aqueous humor drainage leads to an increase in IOP which can eventually cause painful glaucoma and blindness. Reduced aqueous humor production leads to a

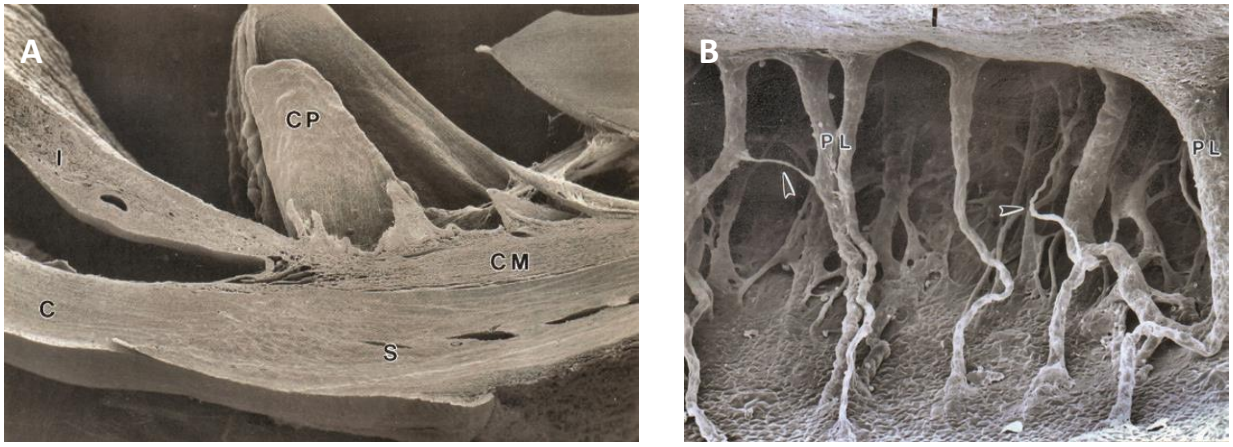

Figure 1.4 – SEM image of the canine limbus and iridocorneal angle (A) is a SEM image of the area near the limbus of a canine eye. Shown are the cornea (C), the stroma (S), the iris (I), and the ciliary body (CM and CP). Notice the fine, porous meshwork near the junction of I and CP. (B) is a SEM image of the canine iridocorneal angle. The iris is denotes with (I) near the top of the frame, and the pectinate ligaments that bridge the gap between iris and cornea are marked with a (PL). The arrowheads denote connections between the pectinate ligaments and the finer trabecular meshwork behind them. Figure modified from (5).

drop in IOP, which can affect the eye's ability to maintain a rigid shape. The anteriormost component of the ciliary body is the iridocorneal angle (ICA, Figure 1.4). At the ICA, pectinate ligaments extend from the limbic junction down to the root of the iris (which extends anteriorly from the ciliary body), attaching the iris to the fibrous tunic. Behind these ligaments is the trabecular meshwork, a network of interwoven collagen cords through which aqueous humor is filtered on its way out of the anterior chamber. Under normal circumstances, the aqueous humor is produced from the ciliary body epithelium into the posterior chamber, flows through the pupil into the anterior chamber, and exits through the iridocorneal angle/trabecular meshwork (5, 15, 16, 20).

1.2.3.c The iris

The iris is a thin layer of pigmented, vascular tissue extending out from the ciliary body that divides the anterior compartment of the eye into anterior and posterior chambers. It is

divided into four tissue layers – the anterior border layer, the stroma, the sphincter muscle, and the posterior epithelium. The anterior border layer is a porous cell layer primarily composed of fibroblasts and melanocytes. The stroma is a loosely arranged network of collagen fibers containing fibroblasts. The stroma is organized into dense sheaths where it surrounds blood vessels and nerves, and melanocytes tend to be found in close proximity to these features. The iridal sphincter muscle is a thin band of unstriated muscle that changes the shape of the iris in response to light levels, and the posterior epithelium, which is continuous with the choroid (5, 16, 20).

1.3 Melanocyte biology

Melanocytes are a type of cell specialized for the production of melanin, the pigment which gives color to the skin, eyes, hair, and other tissues. They contain a specialized membrane-bound organelle called a melanosome where melanin production can take place sequestered from the remainder of the cell. This physical separation is required due to the fact that some intermediates of melanin production are toxic to the cell. Although melanocytes have been most extensively studied in the skin, physiologically distinct populations of melanocytes also exist at a number of extracutaneous sites such as the ear, the meninges, various mesenchymal tissues, and, most notably for this work, the eye (8, 21).

1.3.1 Melanocyte development

Melanocytes, regardless of the tissue in which they are found, are all originally derived from the neural crest. Initially, neural crest cells differentiate into a mixed-fate progenitor cell capable of developing into either a melanoblast or a glial cell progenitor (22). Both of these lineages are specified by the transcription factors Paired Box 3 (*PAX3*) and SRY-Box 10 (*SOX10*). The expression of two additional transcription factors, Forkhead-box D3 (*FOXD3*) and SRY-Box 2 (*SOX2*), determine whether this bipotent cell will further develop into a melanocyte or into a glial cell. PAX3 and SOX10 are transcription factors that act synergistically to activate microphthalmia-associated transcription factor (MITF), which is the master regulator of melanocyte identity (8). *FOXD3* is expressed in glial progenitor cells – it interacts with PAX3 and prevents it from activating the *MITF* promoter. *SOX2*, on the other hand, regulates *MITF* directly, by binding to its promoter and repressing its expression. Therefore, progenitor cells develop into melanoblasts when FOXD3 and SOX2 are downregulated, although the

mechanisms for how these transcription factors are controlled are not well understood, and appear to vary between organisms. Once *MITF* expression is induced, it appears to be self-reinforcing, as MITF expression causes the rapid downregulation of *SOX2 (23)*. These cells also begin to express dopachrome tautomerase (DCT, also commonly called TRP2), a melanocyte-specific protein which is responsible for converting DOPAchrome to 5,6-dihydroxyindole-2-carboxylic acid (DHICA) rather than the 5,6-dihydroxyindole (DHI) it would otherwise form spontaneously (Figure 1.6) (24). The melanoblast cells follow two distinct migratory paths, some ventrally, and some dorsolaterally (25). The gene for KIT receptor tyrosine kinase (*KIT*) is expressed by the melanoblast throughout migration, and the presence of KIT and its ligand is essentially for melanoblast survival during migration (26). Post-migration, although a large number of melanoblasts differentiate into melanocytes, it has been shown that at least mammalian melanocyte populations associated with hair follicles maintain reservoirs of melanocyte stem cells, and that these follicular melanocyte stem cell reservoirs are capable of replenishing depleted epidermal melanocyte populations (27). These stem cells are dedifferentiated melanoblasts, who lose expression of *MITF* but maintain expression of *DCT*. These stem cells can be activated to create differentiating, transit-amplifying daughter cells which are then used to replenish depleted populations of differentiated melanocytes in the epidermis or hair follicle (28).

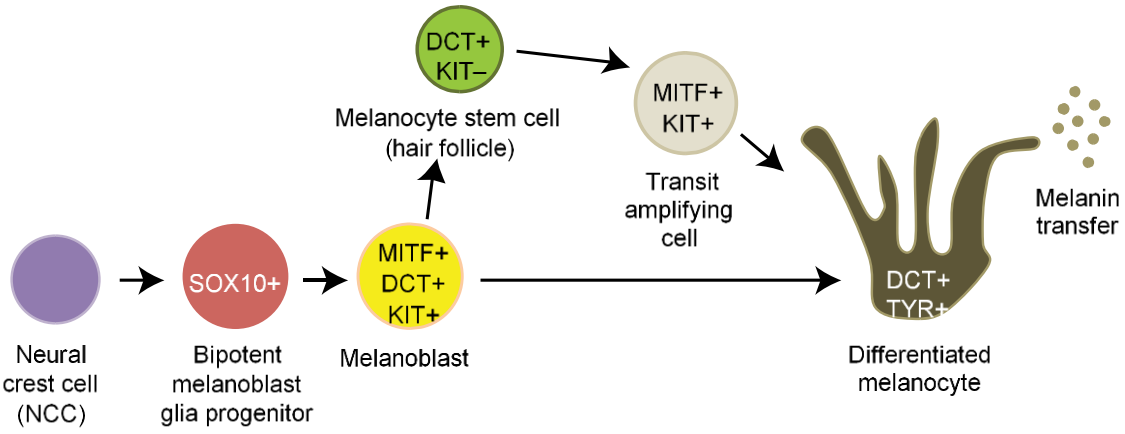

Figure 1.5 – **Brief overview of mammalian melanocyte development** A neural crest cell progenitor becomes specified as a SOX10-positive bipotent progenitor that can potentially develop into either a melanoblast of a glial cell. Activation of MITF specifies the cell as a melanoblast, which activated DCT. KIT is expressed during migration. Once migration is complete, some portion of the cells differentiate into mature melanocytes and produce melanin to transfer to keratinocytes. Another portion of the melanoblasts instead dedifferentiates, becoming melanocyte stem cells. These stem cells replenish the differentiated melanocyte population via MITF-positive, KIT-positive transit amplifying cells. Modified from (8).

1.3.2 Melanin production

Melanocytes are capable of producing two different types of melanin, the black-brown eumelanin (further subdivided into the darker-black DHI-melanin and the lighter-brown DHICA-melanin) and the red-yellow pheomelanin. The pathway for determining which type of melanin is produced is illustrated in Figure 1.6 (7). As was previously mentioned, melanin is produced within specialized membrane-bound organelles called melanosomes, which mature through four stages of development during melanin synthesis (Figure 1.7). Initially, melanosomes are small, spherical vesicles commonly thought to originate from the endoplasmic reticulum (stage 1), but this is still a matter of some debate (29). In stage II of melanosome development, the previously spherical vesicle begins to elongate, and glycoprotein fibrils begin to form an

organized matrix. Tyrosinase (TYR) and tyrosinase-related proteins 1 and 2 (TRP1 and TRP2) can be detected within the organelle. Melanogenesis begins in stage III, and the melanosome takes on a light brown color as newly synthesized melanin begins to settle on the matrix fibrils. By stage IV, the melanosome is densely pigmented and dark in color – it is completely filled with melanin, and loses tyrosinase activity at this point (7, 30).

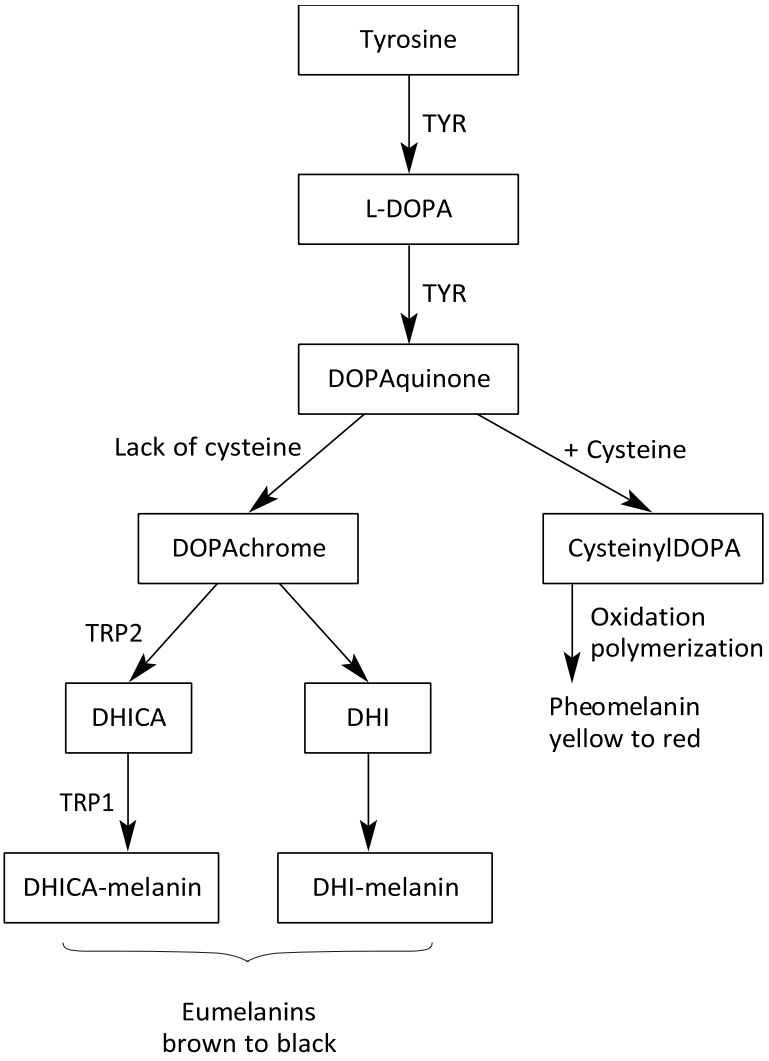

Figure 1.6 – **The melanogenesis pathway** Tyrosine is converted by tyrosinase (TYR) to L-DOPA which is then converted to DOPAquinone. In the presence of cysteine, DOPAquinone reacts and polymerizes to form the red-yellow pheomelanin. In the absence of cysteine, DOPAquinone spontaneously cyclicalizes to DOPAchrome. If tyrosinase-related protein 2 (TRP2, or DCT) is present, the cell can convert DOPAchrome to DHICA, which is then converted by tyrosinase-related protein 1 (TRP1) to the light brown DHICA-melanin, a eumelanin. In the absence of TRP2, DOPAchrome oxidized to form a dark brown-black DHI-melanin, the other eumelanin. Figure reproduced from (7).

Melanosom features	Stage I	Stage II	Stage III	Stage IV
				
Shape	Spherical	Elongated	Elliptical, ellipsoidal	Elliptical, ellipsoidal
Internal structure	–	Matrix fibrils are visible	Matrix fibrils are visible	Matrix fibrils are covered by polymerized melanin
TYR	–	+	+	+
TYRP1	–	+	+	+
TYRP2	–	+	+	+
Melanin synthesis	–	–	Begins, settle on internal fibrils	Filled by melanin
Color			Brown	Dark brown to black

Figure 1.7 – **Melanosome development by stage** Figure reproduced from (7).

1.3.3 Uveal melanocytes

Uveal melanocytes differ in several significant ways from those seen in the epidermis or in hair follicles. Epidermal and follicular melanocytes retain very little of their own cellular melanin over the long term, transferring the melanin granules they produce to keratinocytes of the skin or hair. These cells are highly dendritic and transfer melanosomes to large numbers of associated keratinocytes – 30-40 keratinocytes for epidermal melanocytes, and 5-10 for follicular ones (31). Uveal melanocytes, in contrast, have relatively few dendritic processes, and retain most of their melanin throughout their life, producing more only under specific stimuli.

1.3.4 Invasiveness in uveal melanocytes

Aggressive metastatic uveal melanomas possess the ability to invade through the matrix surrounding them, the basement membrane, and into the vasculature. Compared to normal

uveal melanocytes, melanoma cells that display this phenotype usually display elevated integrin expression, and adhere more readily to endothelial cells and all types of extracellular matrix (ECM) substrates (32). Due to the lack of lymphatics in the eye, many highly invasive uveal melanomas are capable of vasculogenic mimicry – essentially creating their own pseudo-vasculature through a re-shaping of the surrounding ECM (33, 34). These channels are even capable of undergoing anastomosis with existing blood vessels. Although invasive melanoma cells are capable of harnessing existing ECM for these purposes, it should be noted that they are often also capable of generating their own ECM components as necessary, expressing fibronectin, laminin, collagen IV, and collagen VI as needed to provide the raw materials necessary to create a pseudo-vasculature through which to migrate.

1.4 Ocular melanosis

Ocular melanosis (OM) is an inherited eye disease seen primarily in Cairn terrier dogs. Briefly, the disease is characterized by the bilateral proliferation of abnormal pigmented cells into the anterior uvea and into other areas of the eye such as the sclera. Over time, this pigmented material can block the anterior chamber drainage angle, leading to a buildup of pressure in the anterior chamber, as the aqueous humor is unable to properly drain. The resulting rise in intraocular pressure is known as glaucoma. Glaucoma can cause pain and blindness which may necessitate enucleation of the affected eyes to alleviate the pain. The disease has a highly variable age of onset and progression, and appears to be autosomal dominant in its mode of inheritance(4, 9, 35).

1.4.1 Physiological description

The clinical description of ocular melanosis includes four stages of development. The changes associated with the transition through these stages are illustrated in Figure 1.8 (9). In stage 1, a dark, donut-shaped thickening of the iris root is observed, but no other morphological changes are apparent. Stage 2 is characterized by a continuing thickening of the iris root, as well as the appearance of small pigmented plaques in the sclera and episclera. The pigmented plaques initially appear spicule-shaped, but as the disease progressed more appear and the existing ones enlarge and often become circular. Small deposits of pigment may also be observed coating the ventral pectinate fibers at this stage of the disease. In stage 3, the iris surface of some dogs takes on a lumpy, uneven appearance, while others continue to display the circumferentially thickened donut-shaped iris observed in earlier stages. The previously

small scleral and episcleral plaques expand in size, becoming several millimeters in diameter. At this stage, it is sometimes possible to see particles of free-floating pigment suspended in the aqueous humor, and pigment deposition along the ventral drainage angle is much more pronounced. Finally, stage 4 is usually characterized by the development of secondary glaucoma as pigment completely obscures the drainage angle, leading to a buildup of pressure as aqueous humor is prevented from draining out of the anterior chamber. At this point, most changes observed are those typical of chronic glaucoma, such as loss of vision, lens subluxation, and globe enlargement (4, 9, 36, 37). Additional pigment deposition into the sclera/episclera patches is also observed at this stage of the disease. Ocular melanosis is always bilateral, although there may be differences in the rate of pigment deposition and the development of glaucoma between eyes.

1.4.2 Identification of pigmented cells

One of the most striking characteristics of OM is the appearance of large, densely pigmented cells within the anterior segment and the sclera. Although the fact that the cells in question were densely pigmented suggested a melanocytic origin, a clinically similar condition observed in Boxers and Labradors had been shown to involve the accumulation of large numbers of melanophages, phagocytic cells which have engulfed melanosomes, but which are not themselves melanocyte-derived (36). Immunohistochemistry and transmission electron microscopy were used to determine the identity of these cells in Cairn terrier uveal tissue (4). Sectioned uveal tissue samples showed that the majority of the large, pigmented cells characteristic of OM were immunoreactive for HMB45, MITF, and vimentin. HMB45 recognizes gp100, an organelle-specific protein that localizes to immature melanosomes (38, 39). Normal

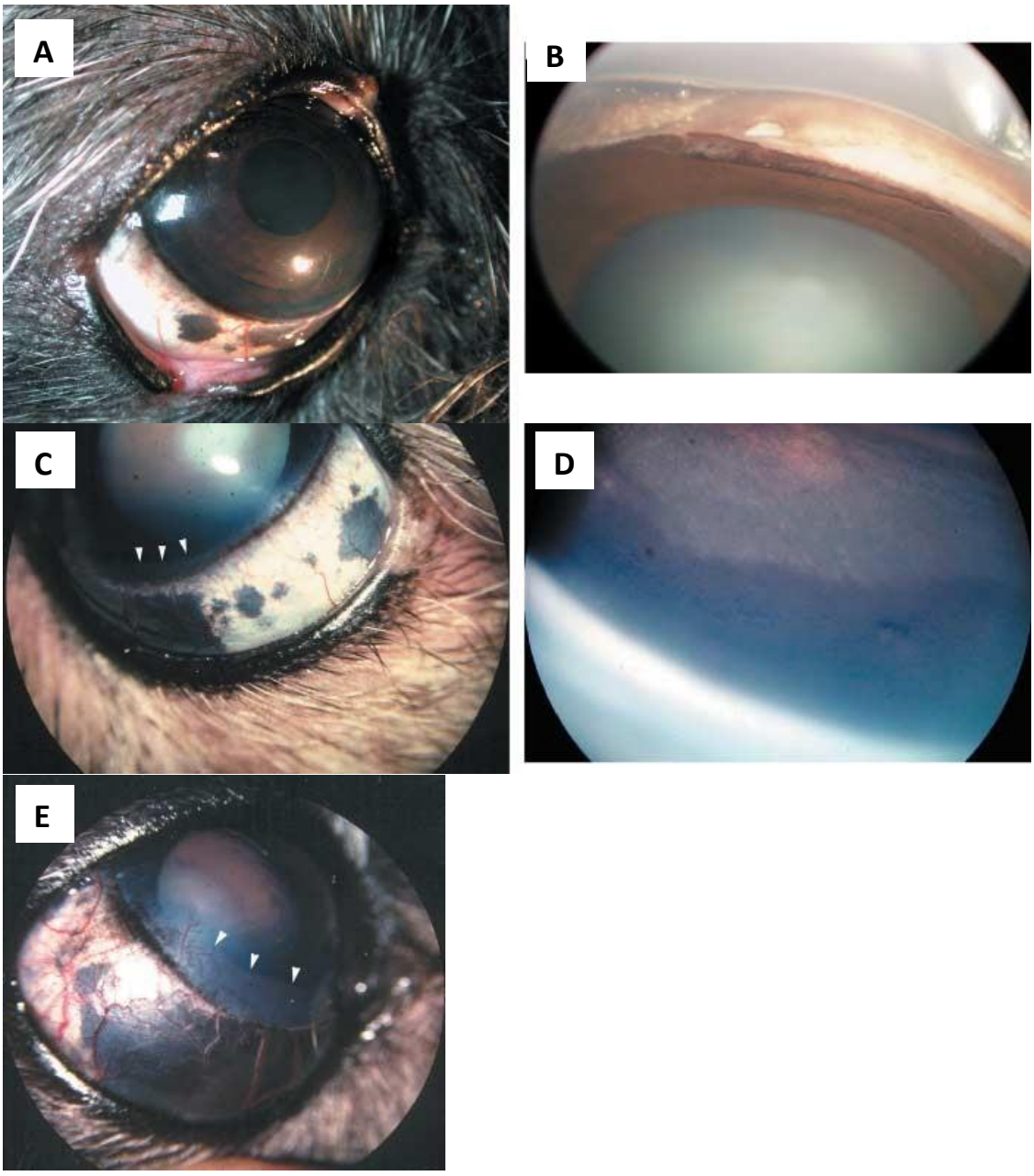

Figure 1.8 – Ocular melanosis in the Cairn terrier (A) shows a Cairn with stage 2 OM – the thickening of the iris root can be seen ventrally, and the pigmented plaques on the sclera are clearly visible. (B) is the view across the anterior chamber of the eye shown in (A). Notice the thickening of the iris root. (C) shows a Cairn with stage 3 OM – the plaques on the sclera are larger, and floating pigment particles can be seen in the pupil. The arrows highlight pigment sedimentation on the corneal endothelium. (D) is the view across the anterior chamber of the eye shown in (C). Notice the dense deposits of pigment particles that completely block the drainage angle from view. (E) shows a stage 4 OM eye – there is heavy pigment sedimentation on the corneal endothelium, and the pigment plaques take up a large portion of the eye's surface area. Figure reproduced from (9).

adult uveal melanocytes are usually HMB45 negative, as resting adult melanocytes do not usually produce melanin and therefore do not have any immature melanosomes to mark. However, HMB45 does mark fetal melanocytes and melanoma cells that are actively producing melanosomes, suggesting that these cells are melanocytic (Figure 1.9). This was further confirmed by the fact that many of the large pigmented cells were also immunoreactive for MITF, a melanocyte nuclear transcription factor critical for melanocyte development and postnatal survival, and vimentin is a marker for mesenchymal cells expressed by melanocytes (40). Taken together, this strongly suggests that the majority of the large abnormal pigmented cells observed in the OM uvea are melanocytic in origin. Interestingly, some of the pigmented cells also stained positively for CD18, an integrin known to be involved in mediating cell adhesion.

Transmission electron micrographs of pigmented cells present in the iris also support a melanocytic origin for the cells (Figure 1.10). The majority of the large, pigmented cells were observed to contain melanosomes of varying sizes and stages of development in the cytoplasm and rough endoplasmic reticulum, traits characteristic of melanocytes (4, 41, 42). A small number of cells displayed multiple membrane-bound melanosomes, characteristic of melanophages which have phagocytosed melanosomes, indicating the presence of at least some melanophages in the uvea of affected dogs as well (4). In contrast, the uveal melanocytes seen in eyes of unaffected Cairn terriers were less rounded than those seen in affected dogs, and they contained only the mature melanosomes expected in a quiescent melanocyte (4).

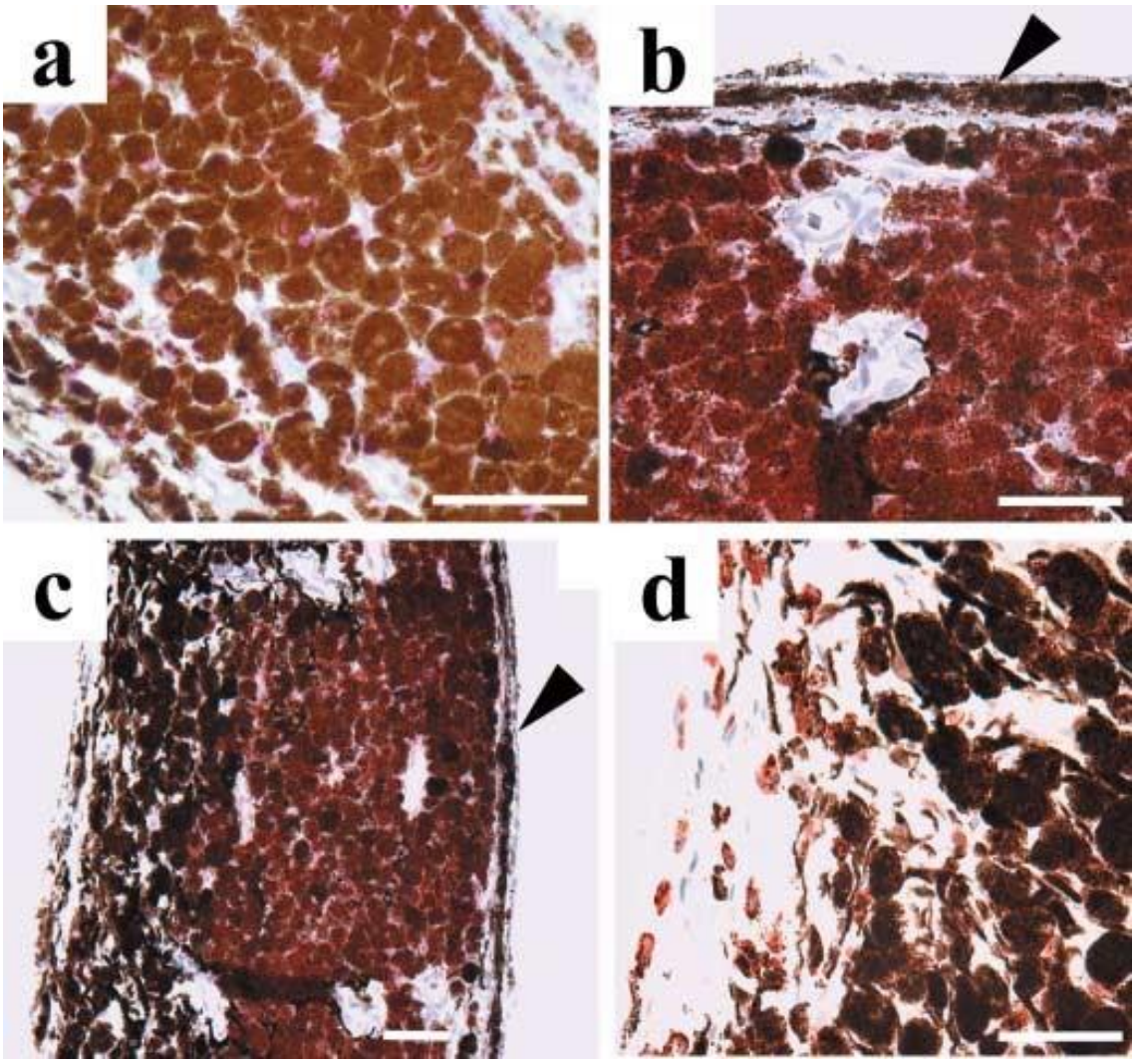

Figure 1.9 – Immunohistochemical expression of markers in sections of OM-affected and unaffected globes (a) shows MITF staining pigment-laden cells in the iris of an OM affected dog – note the pink stained nuclei denoting positive cells, as MITF is a transcription factor. (b) shows HMB45 staining in the ciliary body of an OM-affected eye. The ciliary body epithelium is denoted by an arrowhead and is negative for HMB45, but the pigmented cells seen below stain positively for HMB45 (pink). (c) shows the iris of an OM-affected eye stained for HMB45. The arrowhead denotes the posterior iridal epithelium, which was negative for HMB45. The iridal stroma, however, was infiltrated with many large pigmented cells which stained positive for HMB45 (pink). (d) shows the anterior iris of an OM-affected eye stained for CD18. Some staining in of the large, pigmented cells is observed (pink). Bar = 50 µm. Figure reproduced from (4).

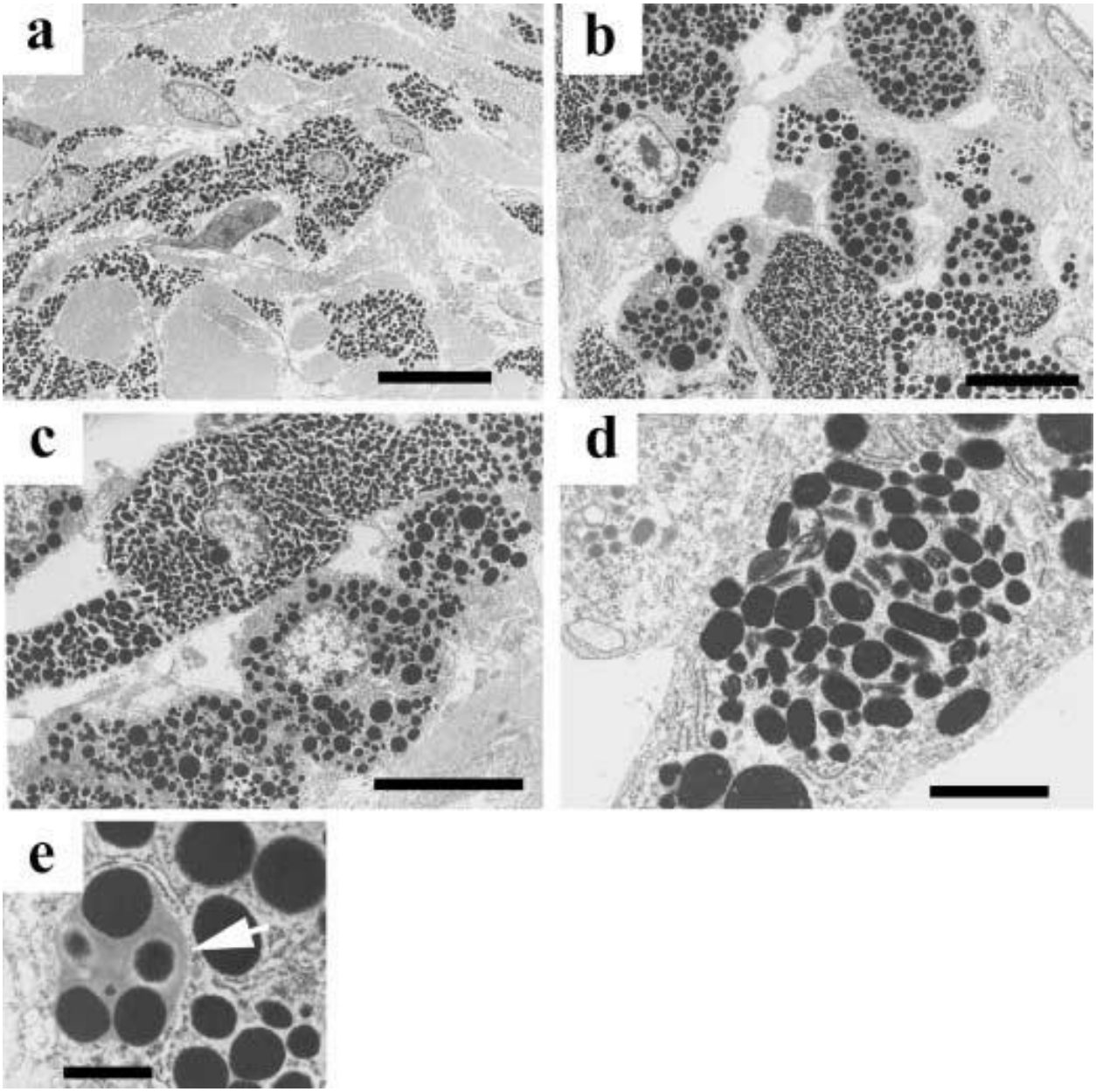

Figure 1.10 – Transmission electron micrograph of pigmented cells within the iris (a) shows the iris of a normal control dog, whereas b-e show the iris of an OM-affected Carin terrier. Note the increased size of the pigmented cells in (b) and (c) relative to (a). Bar = 10 µm. (d) shows a higher magnification image of the melanosomes of an affected dog – note the size and shape differences indicating the presence of immature melanosomes. Bar = 2 µm. (e) shows several membrane-bound melanosomes bound together as a single compound melanosome (arrow), suggesting that the melanosomes in question may have been engulfed by a melanophage. Bar = 1 µm.

1.4.3 Breed prevalence and history

The earliest reference to ocular melanosis in the literature was in a conference proceedings from 1984, when Covitz *et al* described a condition they called pigmentary glaucoma in Cairn terriers which was characterized by the proliferation of ocular pigment and secondary glaucoma arising from a blockage of the anterior drainage angle by pigmented material (43). Subsequent publications further describing the disease in Cairn terriers began to use the term ocular melanosis to differentiate the disease from other known forms of pigmentary glaucoma with different etiologies (35, 36, 44, 45). The fact that this disease had not been reported in Cairn terriers prior to only a few decades ago suggests that the disease may have a fairly recent origin, and has been propagated through the breed by means of a founder effect (9).

Although the precise incidence of the disease is not known in Cairn terriers, its prevalence within the breed is thought to be relatively high. A 2005 survey of the Cairn terrier breeders and owners listed OM as the second most common health concern for the breed. Fifty-eight percent of respondents agreed that OM was a major concern for the breed, and 14 percent of owners surveyed reported having owned at least one Cairn terrier with OM (46). Additionally, the prevalence of glaucoma in Cairn terriers is estimated to be 1.82%, more than double the species-wide prevalence of 0.89% (47). As no other predisposition to glaucoma is known to exist in Cairn terriers, it is likely that the increase in glaucoma prevalence is primarily due to glaucoma caused by late-stage OM (46).

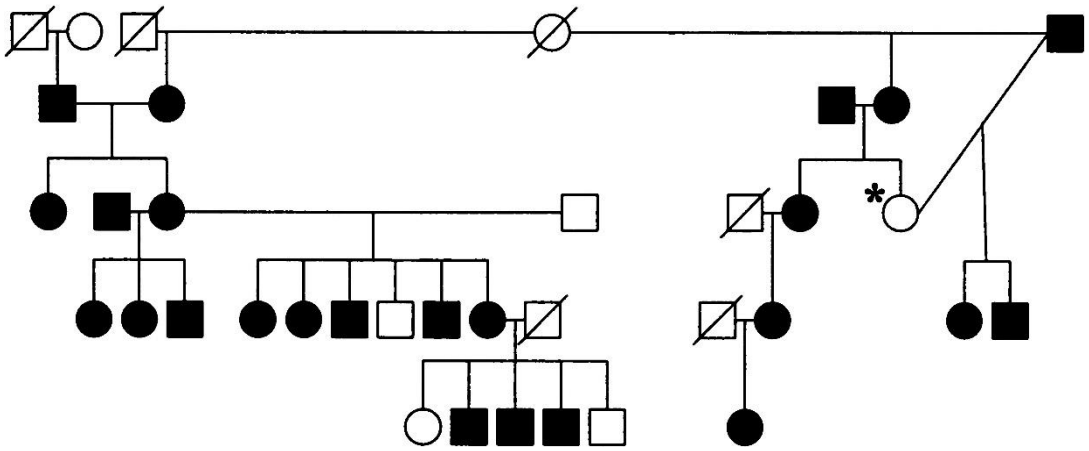

Figure 1.11 – A representative pedigree of a Cairn terrier lineage with ocular melanosis
Male dogs are represented as squares, females as circles. Filled symbols represent OM-affected dogs, and open symbols represent unaffected dogs age 8+. Symbols with a slash are of unknown phenotype. The dog indicated with a * is the unaffected offspring of two affected parents, suggesting that the disease is autosomal dominant rather than recessive. Figure reproduced from (9).

1.4.4 Inheritance pattern

Based on pedigree analysis, ocular melanosis appears to be an autosomal dominant disease possibly with incomplete penetrance (4, 9). A representative pedigree is shown in Figure 1.11 (9). The disease does not skip any generations, as would be expected from a recessive condition, and the disease occurs in roughly equivalent proportions of male and female dogs, suggesting that it is not sex-linked. No instances have been observed of unaffected parents producing affected offspring, although there have been a small number of instances of two affected parents producing an offspring which appears to be unaffected, which suggests that the disease is likely autosomal dominant. However, as previously noted, this is complicated by the fact that OM has a widely variable age of onset. The average lifespan of a Cairn terrier is estimated at 12-15 years, and there have been multiple instances where a Cairn

terrier which had previously been diagnosed as OM-free will first begin to show signs of the disease at age 12 or later (9).

1.4.5 Comparisons to human disease

Ocular melanosis has similarities to certain forms of pigment dispersion syndrome (PDS), an eye disease seen in humans. PDS, like OM, is characterized by a release of pigment into the anterior chamber which eventually blocks drainage pathways and leads to secondary glaucoma (48). The disease appears to be genetically heterogeneous, however, as different loci have been mapped with the disease in different populations (49, 50). The disease appears to have different etiologies in different populations – the disease has been most extensively studied in white populations, where it is thought that pigment is released due to mechanical shearing caused by the lens rubbing against the iris due to a defect in iris which is not seen in Cairn terriers (51, 52). However, a distinct form of PDS is seen in black patients which lacks the iris defect thought to cause the disease in white populations (53, 54). According to an analysis of PDS inheritance in black populations, this form of PDS has an autosomal dominant mode of inheritance, although it may not be completely penetrant (55). The exact prevalence of disease in black populations is not known, it is thought that the disease is under-diagnosed, as difficulties in detecting the increased pigmentation against the darker iris background seen in black populations make the disease very hard to detect (55, 56). Although there have not to date been any studies done to determine whether any of the loci mapped in white populations associate with the form of the disease seen in black populations, the differences in disease phenotype suggest that it is unlikely that they share a causative mutation (53).

Currently, the available treatments for PDS primarily treat the symptoms of the secondary glaucoma caused by the disease rather than the disease itself. The most common treatment is the non-specific reduction of IOP using drugs designed to suppress new aqueous production, although there has been some suggestion that these drugs worsen pigment dispersion (53, 57). When this approach fails, selective laser trabeculoplasty has been successful for reducing IOP in patients suffering from PDS, although the exact mechanism, by which it does so is not well understood (58). Surgical intervention to remove pigment debris from the trabecular meshwork is also possible, although it has not been successful at controlling PDS long-term (59).

1.4.6 Comparisons to mouse models

The DBA/2J mouse has an interesting phenotype which appears at least superficially similar to OM. These mice develop severe glaucoma as a result of increased intraocular pressure caused by pigmented cell debris occluding the ocular drainage angles, but the rate of disease progression is variable and can develop at different speeds between eyes of the same affected mouse, similar to the variable progression we see in OM (60, 61). This phenotype is the result of two separate mutations in genes related to the normal functioning of the melanosomes, *Gpnmb* and *Tyrp1* (60). On their own, both of these mutations produce a milder phenotype – mice with mutations in *Gpnmb* alone caused a milder form of pigmentary glaucoma, similar to PDS in humans. Mutations in *Tyrp1* alone produced atrophy of the iris stroma. The GPNMB and TYRP1 proteins share many structural similarities, and are thought to be part of a common gene family – specifically, a family of glycoproteins responsible for maintaining the structure of the developing melanosome. Epistasis experiments showed that

the presence of these mutations in mice which produced low levels of pigmentation did not experience the glaucoma phenotype, or shed cell debris into the anterior chamber. This suggests that the phenotype seen in the DBA/2J mice is dependent on the production of pigment. It is hypothesized that the severe glaucoma associated with the disease arises from melanocyte cell death in the iris of affected mice caused by structurally weakened melanosomes releasing cytotoxic melanogenesis intermediates.

1.5 Target gene testing

Based on the phenotype that ocular melanosis presents in affected Cairn terriers, 11 genes either known to have a role in melanocyte and melanosome development or known to be associated with other ocular pigmentation disorders were chosen as potential candidate genes to be screened for possible association with ocular melanosis, including the genes implicated in the DBA/2J mouse phenotype (60, 62). A complete list of candidate genes and the markers used to genotype them is shown in Table 1.1. All candidate genes were assayed by performing an association-based exclusion analysis. In an association-based exclusion analysis, variable genomic markers (in this case, SNPs and microsatellites) located near the gene of interest are assayed in a large number of dogs to determine whether a particular variant for any of these markers segregates completely with the disease. The failure of nearby markers to segregate completely with the disease phenotype excludes the gene near the marker as a possible candidate gene. This test is based on the following underlying assumptions:

- All affected dogs share the same underlying causative mutation for ocular melanosis that is identical by descent due to a founder event
- There has been no recombination between the marker and the causative mutation since the mutation originally appeared
- There have been no new mutations in either the marker or the gene

No single shared allele was detected at any of the 22 marker sites selected around the 11 candidate genes, showing that it is highly unlikely that a variant in any of them is causative for OM (62).

Table 1.1 – **Primers used to amplify markers around candidate genes** Reproduced from (62).

Gene, Protein, Position[a]	Marker[b] [Restriction enzyme]	Marker Position[c]	Distance (kb)[d]	P values[e]
LYST Lysosomal Trafficking Regulator chr4:7,128,220-7,294,031	Microsat 1 (TTTTC)18(TTTTC)11	$1^{\S}$	345	1.00×10^{-5}
	Microsat 2 (GAAA)5 (GAAA)13	$2^{\S}$	368	
MC1R Melanocortin 1 receptor chr5:66,692,398-66,693,344	SNP 1 (BICF2P987741)	2^{Δ}	560	1.34×10^{-5}
	SNP 2 (BICF2S23213233) [SsiI]	1^{Δ}	24	
SILV Silver chr10:3,273,996-3,279,352	Microsat 1 (GAAA)7(GAAA)17	$2^{\S}$	60	1.00×10^{-5}
	Microsat 2 (TTTC)15(TTCC)13	$1^{\S}$	226	
TYRP1 Tyrosinase related protein 1 chr11:36,344,712-36,361,793	SNP 1 (BICF2S23051528) [BC1I]	1^{Δ}	224	2.15×10^{-5}
	In/Del	2^{Δ}	96	
GPNMB Glycoprotein NMB chr14:39,877,810-39,905,589	SNP 1 (BICF2P753624) [HpyCH4V]	M1°	26	1.59×10^{-4}
	SNP 2 (BICF2P134952)	2^{Δ}	1200	
MITF Microphthalmia transcription factor chr20:24,853,657-24,884,775	SNP 1 (BICF2G630233682) [BspHI]	2^{Δ}	73	3.80×10^{-5}
	SNP 2 (BICF2S23248988)	1^{Δ}	521	
TYR Tyrosinase chr21:13,797,070-13,891,317	Microsat 1 (GAAA)17(GGAA)20(GAAA)10	$2^{\S}$	428	1.00×10^{-9}
	Microsat 2 (TTTC)10(TTTC)4(TTTC)13	$1^{\S}$	70	
TYRP2 (*DCT*) Tyrosinase related protein 2 chr22:48,219,817-48,254,000	SNP 1 (BICF2S23137809) [sequenced]	M2°	33	8.47×10^{-4}
	SNP 2 (BICF2P452919) [RsaI]	M1°	8	
ASIP Agouti signaling protein chr24:26,327,360-26,366,307	SNP 1 (BICF2P1186810) [MesI]	1^{Δ}	340	3.57×10^{-5}
	In/Del	2^{Δ}	105	
COMT Catechol-O-Methyltransferase chr26:32,426,959-32,432,523	SNP 1 (BICF2S22923369) [ApaLI]	2^{Δ}	82	8.20×10^{-5}
	Microsat 1 (TTTA)15	$1^{\S}$	676	
GSK3B Glycogen Synthase Kinase 3-Beta chr33:26,516,949-26,699,712	Microsat 1 (CTATT)14	M2*	146	1.00×10^{-5}
	Microsat 2 (TTTA)13	M2*	143	

1.6 Conclusions

Ocular melanosis is a major health concern within the Cairn terrier population. Identification of the causal mutation would be greatly beneficial to owners and breeders, as it would allow for the creation of a screening test to be created for the disease which would facilitate the eradication of the disease from the breed by means of selective breeding.

Discovering the pathway underlying OM may also provide insight into the as-yet-unmapped form of PDS commonly seen in black populations which shares many phenotypic similarities to the disease as it manifests in the Cairn terrier. The fact that this disease seems to effect only melanocytes of the eye, but does not alter behavior of melanocytes at all other body locations suggests that this knowledge could also help to explain why uveal melanocytes behave so differently from all other melanocytes despite having a nearly identical embryological origin.

In the following chapters, the results of efforts to identify the underlying mechanisms behind OM are described. These efforts include the cultivation of uveal melanocytes from both OM-affected dogs and unaffected controls, various physiological assays performed to characterize the *in vitro* behavior of those cells, and sequencing-based efforts to map the causative mutation and determine what changes OM causes to the transcriptome of affected dogs.

REFERENCES

REFERENCES

1. Lindblad-Toh K, Wade CM, Mikkelsen TS, Karlsson EK, Jaffe DB, Kamal M, et al. Genome sequence, comparative analysis and haplotype structure of the domestic dog. Nature. 2005;438(7069):803-19.

2. Waterston RH, Lindblad-Toh K, Birney E, Rogers J, Abril JF, Agarwal P, et al. Initial sequencing and comparative analysis of the mouse genome. Nature. 2002;420(6915):520-62.

3. Venter JC, Adams MD, Myers EW, Li PW, Mural RJ, Sutton GG, et al. The sequence of the human genome. Science. 2001;291(5507):1304-51.

4. Petersen-Jones SM, Mentzer AL, Dubielzig RR, Render JA, Steficek BA, Kiupel M. Ocular melanosis in the Cairn Terrier: histopathological description of the condition, and immunohistological and ultrastructural characterization of the characteristic pigment-laden cells. Vet Ophthalmol. 2008;11(4):260-8.

5. Ophthalmic Structures. Essentials of Veterinary Ophthalmology: John Wiley & Sons, Ltd; 2014. p. 12-39.

6. Breen M, Bullerdiek J, Langford CF. The DAPI Banded Karyotype of the Domestic Dog (Canis familiaris) Generated Using Chromosome-Specific Paint Probes. Chromosome Research. 1999;7(5):401-6.

7. Cichorek M, Wachulska M, Stasiewicz A, Tymińska A. Skin melanocytes: biology and development. Advances in Dermatology and Allergology/Postępy Dermatologii I Alergologii. 2013;30(1):30-41.

8. Mort RL, Jackson IJ, Patton EE. The melanocyte lineage in development and disease. Development. 2015;142(4):620-32.

9. Petersen-Jones SM, Forcier J, Mentzer AL. Ocular melanosis in the Cairn Terrier: clinical description and investigation of mode of inheritance. Vet Ophthalmol. 2007;10 Suppl 1:63-9.

10. Neff MW, Rine J. A Fetching Model Organism. Cell. 2006;124(2):229-31.

11. Guenet JL. The mouse genome. Genome Res. 2005;15(12):1729-40.

12. Parker HG, Shearin AL, Ostrander EA. Man's best friend becomes biology's best in show: genome analyses in the domestic dog. Annu Rev Genet. 2010;44.

13. Derrien T, Thézé J, Vaysse A, André C, Ostrander EA, Galibert F, et al. Revisiting the missing protein-coding gene catalog of the domestic dog. BMC Genomics. 2009;10:62-.

14. Gelatt KN, Plummer CE. Ocular Anatomy. Color Atlas of Veterinary Ophthalmology: John Wiley & Sons, Inc.; 2017. p. 1-6.

15. Miller PE. Chapter 11 - Uvea. Slatter's Fundamentals of Veterinary Ophthalmology (Fourth Edition). Saint Louis: W.B. Saunders; 2008. p. 203-29.

16. Dubielzig RR, Ketring K, McLellan GJ, Albert DM. Chapter 9 - The uvea. Veterinary Ocular Pathology. Edinburgh: W.B. Saunders; 2010. p. 245-322.

17. Physiology of the Eye. Essentials of Veterinary Ophthalmology: John Wiley & Sons, Ltd; 2014. p. 40-54.

18. Dubielzig RR, Ketring K, McLellan GJ, Albert DM. Chapter 8 - Diseases of the cornea and sclera. Veterinary Ocular Pathology. Edinburgh: W.B. Saunders; 2010. p. 201-43.

19. Gelatt KN, Plummer CE. Canine Cornea and Sclera. Color Atlas of Veterinary Ophthalmology: John Wiley & Sons, Inc.; 2017. p. 111-41.

20. Gelatt KN, Plummer CE. Canine Anterior Uvea. Color Atlas of Veterinary Ophthalmology: John Wiley & Sons, Inc.; 2017. p. 163-86.

21. Boissy RE, Hornyak TJ. Extracutaneous Melanocytes. The Pigmentary System: Blackwell Publishing Ltd; 2007. p. 91-107.

22. Henion PD, Weston JA. Timing and pattern of cell fate restrictions in the neural crest lineage. Development. 1997;124(21):4351-9.

23. Adameyko I, Lallemend F, Furlan A, Zinin N, Aranda S, Kitambi SS, et al. Sox2 and Mitf cross-regulatory interactions consolidate progenitor and melanocyte lineages in the cranial neural crest. Development. 2012;139(2):397-410.

24. Tsukamoto K, Jackson IJ, Urabe K, Montague PM, Hearing VJ. A second tyrosinase-related protein, TRP-2, is a melanogenic enzyme termed DOPAchrome tautomerase. The EMBO Journal. 1992;11(2):519-26.

25. Ernfors P. Cellular origin and developmental mechanisms during the formation of skin melanocytes. Experimental cell research. 2010;316(8):1397-407.

26. Yoshida H, Kunisada T, Kusakabe M, Nishikawa S, Nishikawa SI. Distinct stages of melanocyte differentiation revealed by anlaysis of nonuniform pigmentation patterns. Development. 1996;122(4):1207-14.

27. Nishimura EK. Melanocyte stem cells: a melanocyte reservoir in hair follicles for hair and skin pigmentation. Pigment Cell Melanoma Res. 2011;24(3):401-10.

28. Nishimura EK, Jordan SA, Oshima H, Yoshida H, Osawa M, Moriyama M, et al. Dominant role of the niche in melanocyte stem-cell fate determination. Nature. 2002;416(6883):854-60.

29. Cadieu E, Neff MW, Quignon P, Walsh K, Chase K, Parker HG, et al. Coat variation in the domestic dog is governed by variants in three genes. Science. 2009;326.

30. Hearing VJ. Determination of melanin synthetic pathways. J Invest Dermatol. 2011;131(E1):E8-e11.

31. Tobin DJ. The cell biology of human hair follicle pigmentation. Pigment Cell Melanoma Res. 2011;24(1):75-88.

32. Woodward JKL, Rennie IG, Elshaw SR, Burn JL, Sisley K. Invasive and noninvasive uveal melanomas have different adhesive properties. Eye. 2004;19(3):342-8.

33. Folberg R, Arbieva Z, Moses J, Hayee A, Sandal T, Kadkol S, et al. Tumor Cell Plasticity in Uveal Melanoma : Microenvironment Directed Dampening of the Invasive and Metastatic Genotype and Phenotype Accompanies the Generation of Vasculogenic Mimicry Patterns. The American Journal of Pathology. 2006;169(4):1376-89.

34. Bakalian S, Marshall J-C, Logan P, Faingold D, Maloney S, Di Cesare S, et al. Molecular Pathways Mediating Liver Metastasis in Patients with Uveal Melanoma. Clinical Cancer Research. 2008;14(4):951-6.

35. Petersen-Jones SM. Abnormal ocular pigment deposition associated with glaucoma in the cairn terrier. Journal of Small Animal Practice. 1991;32(1):19-22.

36. van de Sandt RR, Boeve MH, Stades FC, Kik MJ. Abnormal ocular pigment deposition and glaucoma in the dog. Vet Ophthalmol. 2003;6(4):273-8.

37. Gelatt KN, Plummer CE. Canine Glaucomas. Color Atlas of Veterinary Ophthalmology: John Wiley & Sons, Inc.; 2017. p. 143-62.

38. Adema GJ, de Boer AJ, Vogel AM, Loenen WA, Figdor CG. Molecular characterization of the melanocyte lineage-specific antigen gp100. The Journal of biological chemistry. 1994;269(31):20126-33.

39. Steuhl KP, Rohrbach JM, Knorr M, Thiel HJ. Significance, specificity, and ultrastructural localization of HMB-45 antigen in pigmented ocular tumors. Ophthalmology. 1993;100(2):208-15.

40. Hemesath TJ, Steingrimsson E, McGill G, Hansen MJ, Vaught J, Hodgkinson CA, et al. microphthalmia, a critical factor in melanocyte development, defines a discrete transcription factor family. Genes & development. 1994;8(22):2770-80.

41. Hu DN, Ritch R, McCormick SA, Pelton-Henrion K. Isolation and cultivation of human iris pigment epithelium. Investigative ophthalmology & visual science. 1992;33(8):2443-53.

42. Hu DN, McCormick SA, Ritch R, Pelton-Henrion K. Studies of human uveal melanocytes in vitro: isolation, purification and cultivation of human uveal melanocytes. Investigative ophthalmology & visual science. 1993;34(7):2210-9.

43. Covitz D, Barthold S, Diters R, Riis R. Pigmentary glaucoma in the cairn terrier. Transactions of the Fifteenth Annual Scientific Program of the American College of Veterinary Ophthalmologists. 1984:246-50.

44. Hanselman BA. Melanocytic glaucoma in a cairn terrier. The Canadian Veterinary Journal. 2002;43(4):296-8.

45. Canine Anterior Uvea: Diseases and Surgery. Essentials of Veterinary Ophthalmology: John Wiley & Sons, Ltd; 2014. p. 276-300.

46. America CTCo. Cairn Terrier Club of America 2005 Breeder-Owner Survey. 2005.

47. Gelatt KN, MacKay EO. Prevalence of the breed-related glaucomas in pure-bred dogs in North America. Veterinary Ophthalmology. 2004;7(2):97-111.

48. Ritch R, Steinberger D, Liebmann JM. Prevalence of pigment dispersion syndrome in a population undergoing glaucoma screening. American journal of ophthalmology. 1993;115(6):707-10.

49. Mikelsaar R, Molder H, Bartsch O, Punab M. Two novel deletions (array CGH findings) in pigment dispersion syndrome. Ophthalmic genetics. 2007;28(4):216-9.

50. Paglinauan C, Haines JL, Del Bono EA, Schuman J, Stawski S, Wiggs JL. Exclusion of chromosome 1q21-q31 from linkage to three pedigrees affected by the pigment-dispersion syndrome. American Journal of Human Genetics. 1995;56(5):1240.

51. Campbell DG. Pigmentary dispersion and glaucoma: A new theory. Archives of Ophthalmology. 1979;97(9):1667-72.

52. Liu L, Ong EL, Crowston J. The concave iris in pigment dispersion syndrome. Ophthalmology. 2011;118(1):66-70.

53. Sowka J. Pigment dispersion syndrome and pigmentary glaucoma. Optometry - Journal of the American Optometric Association. 2004;75(2):115-22.

54. Roberts DK, Chaglasian MA, Meetz RE. Clinical signs of the pigment dispersion syndrome in blacks. Optometry & Vision Science. 1997;74(12):993-1006.

55. Roberts DK, Meetz RE, Chaglasian MA. The inheritance of the pigment dispersion syndrome in blacks. Journal of glaucoma. 1999;8(4):250-6.

56. Niyadurupola N, Broadway DC. Pigment dispersion syndrome and pigmentary glaucoma--a major review. Clin Exp Ophthalmol. 2008;36(9):868-82.

57. Farrar SM, Shields MB. Current concepts in pigmentary glaucoma. Survey of ophthalmology. 1993;37(4):233-52.

58. Balu G. Selective Laser Trabeculoplasty.

59. Jacobi PC, Dietlein TS, Krieglstein GK. Effect of trabecular aspiration on intraocular pressure in pigment dispersion syndrome and pigmentary glaucoma. Ophthalmology. 2000;107(3):417-21.

60. Anderson MG, Smith RS, Hawes NL, Zabaleta A, Chang B, Wiggs JL, et al. Mutations in genes encoding melanosomal proteins cause pigmentary glaucoma in DBA/2J mice. Nat Genet. 2002;30(1):81-5.

61. Schlamp CL, Li Y, Dietz JA, Janssen KT, Nickells RW. Progressive ganglion cell loss and optic nerve degeneration in DBA/2J mice is variable and asymmetric. BMC Neuroscience. 2006;7(1):66.

62. Winkler PA, Bartoe JT, Quinones CR, Venta PJ, Petersen-Jones SM. Exclusion of eleven candidate genes for ocular melanosis in Cairn terriers. J Negat Results Biomed. 2013;12:6.

CHAPTER 2

ISOLATION AND CULTIVATION OF CANINE UVEAL MELANOCYTES

Dawson-Baglien EM, Winkler PA, Bruewer AR, Petersen-Jones SM, Bartoe JT. Isolation and cultivation of canine uveal melanocytes. *Veterinary Ophthalmology*. 2015;18(4):285-290

2.1 Abstract

Objectives: To establish a method for isolation and culture of canine uveal melanocytes.

Animals studied: Uveal explants from five mixed-breed dogs.

Procedures: Donor globes were dissected, and the anterior uvea removed. The uveal explants were placed in trypsin solution for enzymatic digestion. Extracted cells were cultured in modified F12 media. Immunocytochemistry was performed to confirm the identity of the extracted cells.

Results: Melanocytes were successfully isolated from uveal explants. Contaminating cell types were not observed. Repeated passaging of the melanocytes resulted in a gradual decrease in intracellular pigment. Melanocyte cell lines could be cryopreserved, thawed, and cultures successfully reestablished.

Conclusions: This extraction technique allows for generation of large populations of canine uveal melanocytes in a relatively short period of time. This technique could be a useful tool for future studies investigating both normal cellular characteristics and alterations found in melanocytes from dogs with ocular melanocytic disorders.

2.2 Introduction

The uveal tract or vascular tunic of the mammalian eye is comprised of the adjoining iris, ciliary body, and choroid (1). Melanocytes within the uveal tract synthesize and store photon-absorbing melanin pigments. Melanin plays a critical role in protection of all other nonpigmented cell types within the eye through a combination of physical and biochemical mechanisms (2). Physical protection is mediated by the 'photo-screening effect' in which melanin directly absorbs incident ultraviolet radiation (UV), whereas biochemical protection is provided by the antioxidant/free radical scavenging properties of melanin resulting in deactivation of reactive oxygen species generated from UV-exposure or other biochemical processes.

Dysregulation of normal uveal melanocyte physiology is thought to contribute to a number of breed-related ocular disorders in dogs. For example, potentially heritable iris melanoma has been reported in Labrador retrievers (3, 4). Uveodermatologic syndrome, which was first reported in the Akita, appears similar to Vogt-Koyanagi-Harada syndrome in humans resulting from autoimmune destruction of melanocytes (5). Recently, a heritable pigmentary uveitis/glaucoma condition has been reported in Golden retrievers (6). While the specific etiology of the disease remains elusive, thickening of the iridal stroma, posterior synechiae, and pigment deposition on the anterior lens capsule have been described in affected dogs (6, 7). Ocular melanosis (OM) in the Cairn terrier appears to segregate as an autosomal dominant trait and is characterized by proliferation and enlargement of melanocytes within the uveal tract (8, 9). Ultimately these atypical melanocytes can infiltrate into the trabecular meshwork of the ciliary cleft resulting in secondary glaucoma.

Characterization of these diseases has primarily been limited to clinical and histological descriptions of the abnormal phenotypes. More recently potential candidate genes for Cairn terrier ocular melanosis have been screened (10), and genome-wide association studies are planned or underway for Golden retriever pigmentary uveitis (W.M. Townsend, personal communication) and for Cairn terrier ocular melanosis in our laboratory. We believe in vitro uveal melanocyte cultures will provide a critical resource for investigation of the intracellular pathways which become dysregulated in dogs with in ocular pigmentary diseases. A greater understanding of intracellular pathway dysregulation may highlight potential candidate genes to screen for causative mutations or suggest interventional treatment targets. The aim of the current study was to develop a technique for extraction and culture of canine uveal melanocytes.

2.3 Materials and methods

2.3.1 Globe collection and harvesting of anterior uveal tissue

Eight globes were collected aseptically from five normal, adult, mixed-breed dogs following euthanasia for reasons unrelated to the current study. Upon collection, the globes were placed in chilled, sterile phosphate-buffered saline (PBS; Sigma-Aldrich, St. Louis, MO, USA) for transport back to the laboratory.

Any residual extraocular tissue was trimmed, globes submersed in 10% povodone iodine solution (Novaplus, Irving, TX, USA) for 5 min and rinsed in sterile physiological saline. Observing sterile dissection techniques, a full-thickness sclera stab incision was made using a no. 11 Bard-Parker blade (Fisher Scientific, Pittsburgh, PA, USA) 3 mm posterior to the limbus and advanced circumferentially around the globe with tenotomy scissors. The anterior segment, including the lens, was separated from the posterior segment, including the vitreous humor. Using tissue dressing forceps and gentle traction, the residual uveal structures were carefully separated as a single piece from the corneoscleral shell.

2.3.2 Isolation of uveal melanocytes

A custom isolation protocol was developed through modification of methods reported by Hu et al (11). in the 1993 manuscript describing isolation and purification of human uveal melanocytes. Anterior uveal explants were placed in 5 mL of a 0.0625% trypsin solution and stored overnight at 4°C. This solution was made by diluting 2.5% trypsin solution (SAFC Global, St. Louis, MO, USA) in Dulbecco's modified eagle medium with D-glucose and glutamine (DMEM; Gibco, Grand Island, NY, USA) to a concentration of 0.0625%. Although the protocol

used by Hu et al. used trypsin at a concentration of 0.25%, preliminary experiments in our laboratory showed the lower concentration (0.0625%) to be effective. Uveal explants were incubated for 1 h in a 37°C water bath then transferred to 5 mL of fresh 0.0625% trypsin and returned to the water bath for another hour. The used trypsin media was centrifuged at 2000 g for 5 min to collect any suspended cells released from the uvea. Cell pellets were resuspended in 2.5 mL of culture media and plated into 25-cm^2 culture flasks (Corning, USA). Culture media consisted of F12 media with L-glutamine (Gibco, USA) 10% fetal bovine serum (FBS, Gibco, USA), 100 units/mL of penicillin (Gibco, USA), 100 µg/mL streptomycin (Gibco, USA), 20 ng/mL basic fibroblast growth factor (Sigma-Aldrich, USA), and 10 ng/mL cholera toxin (SigmaAldrich, USA). Cholera toxin is a known inhibitor of fibroblast growth in cell culture conditions (12). This process was repeated for four sequential trypsin treatments, after which the remaining uveal explant was cut into small pieces and placed into a 100x20 mm cell culture dish (Corning, NY, USA) with 5 mL of culture media. All cultures were incubated at 37 °C in 5% CO_2 with media changed every 2–3 days, as determined by change in media color indicator. During the first 2 weeks, spent media was centrifuged at 2000 g for 5 min to collect nonadherent cells which were resuspended and returned to the original flask; subsequently spent media was directly aspirated using a Pasteur pipette (Fisher Scientific) attached to culture hood vacuum apparatus. Cells were observed every other day using an Olympus IX71 inverted microscope and passaged at 80% confluence.

When passaging cells, spent media was aspirated, and the cells were washed with 2.5 mL of PBS. This PBS was then aspirated, and 2.5 mL of 0.25% trypsin EDTA solution was added (Gibco, USA). The cells were incubated at 37 °C for 5 min with intermittent agitation to

separate them from the flask. Following incubation, the trypsin was neutralized by addition of 2.5 mL of culture media to the flask. Repeated aspiration with a 5-mL pipette (Fisher Scientific) was used to further dislodge any cells that remained adherent. The resultant cellular suspension was transferred to a 15-mL centrifuge tube and spun at 2000 g for 5 min. The media was aspirated, and the cell pellet resuspended in culture media. Cells were replated at densities of $1x10^3$–$1x10^4$ cells/cm^2 as counted by hemocytometer. Any remaining cells were cryopreserved for later use. Cells grown in 5-mL culture dish from the macerated uveal explants were collected in an identical manner and transferred to a 25-cm^2 culture flasks.

When preparing cells for cryopreservation, pelleted cells were resuspended at a concentration of 1–$1.5x10^6$ cells/ mL in freezing media consisting of F12 media with L-glutamine supplemented with 9% DMSO (J.T. Baker, Center Valley, PA, USA) and 15% FBS. This cell suspension was then aliquoted into 2-mL cryotubes (Corning, USA), placed in a 80 °C freezer for 24 h, and ultimately transferred to a liquid nitrogen immersion dewar for long term storage.

When thawing cryopreserved cells, cryotubes were thawed in a 37°C waterbath. Immediately after thawing, 1 mL of FBS was added to the suspension. The cell suspension was centrifuged at 2000 g for 5 min to pellet the cells, and the freezing media was aspirated. The cell pellet was then resuspended in 2.5 mL of culture media and transferred to a 25 cm^2 culture flask.

2.3.3 Immunocytochemistry

Immunocytochemistry (ICC) was performed using antibodies recognizing S100, Melan-A, cytokeratin, and vimentin to confirm the identity and purity of the extracted cell cultures. For ICC, freshly harvested cells were grown to 80% confluence; at the first passage, a subset of cells was plated and cultured for 48 h in Nunc 8 chamber slides (Sigma-Aldrich, USA) resulting in cell density of approximately 80% confluence. ICC was also performed under identical conditions on several later-passage cell populations (table 2.2). Chambered cells were fixed in a 1:1 mixture of 100% methanol and 99.8% acetone for 10 min at 20 °C. Blocking was carried out in a 5% bovine serum albumin (BSA, Sigma-Aldrich, USA) solution in PBS (Sigma-Aldrich, USA) with 0.025% Triton X-100 (Sigma-Aldrich, USA) for 30 min at room temperature. Details and dilutions for both primary and secondary antibodies are shown in table 2.1. All primary antibody incubations were carried out at 37 °C for 1 h. All secondary antibody incubations were carried out at room temperature for 1 h in a light-proof container. As a control to delineate any nonspecific binding of the secondary antibody, ICC was performed identically on a set of slides in which the primary antibody was omitted. All cells types were counterstained with 4′,6-diamidino-2-phenylindole (DAPI; Sigma-Aldrich, USA). S100 is a calcium-binding protein and used as a cell marker for neural crest-derived cells. Anti-S100 antibodies have been shown in previous studies to label ocular melanocytes, but not fibroblasts or epithelial cells (11). Anti-MelanA recognizes a melanocyte surface protein and labels melanocytes with greater specificity than S100 (13). Vimentin is expressed by mesenchymal and neuroectodermal-derived cells in normal tissues, and antibodies directed against it have been shown to label both fibroblasts and melanocytes (11, 14). Cytokeratins are a class of intermediate filaments commonly found in epithelial cells,

but absent in melanocytes and fibroblasts (11). A broadspectrum cytokeratin antibody which labels positively for many different types of cytokeratin was used to ensure that any epithelial cell contamination was detected (11). Fibroblast cells from canine testes and MAC-T bovine mammary epithelial cells were used as positive controls for vimentin and cytokeratin, respectively (11, 14, 15). Fibroblast and MAC-T epithelial cells were cultured in DMEM media with D-glucose and glutamine supplemented with 10% FBS, 100 units/mL of penicillin, and 100 µg/mL streptomycin.

Table 2.1 - Antibody specifications for immunocytochemistry

Antibody Name	Primary Antibody Manufacturer	Type	Expected Targets	Working Concentration (Primary Antibody)	Secondary Antibody	Secondary Antibody Manufacturer	Working Concentration (Secondary Antibody)
Wide spectrum Anti-Cytokeratin	Abcam, ref. ab9377	Rabbit Polyclonal	Cytoskeleton	1/100	goat anti-rabbit	Life Technologies, ref. A11070	1/500
Anti-vimentin	Millipore, ref. AB5733	Chicken Polyclonal	Cytoskeleton	1/5000	goat anti-chicken	Abcam, ref. ab6875	1/2500
Anti-S100	Santa Cruz Biotechnology, ref. sc-71994	Mouse Monoclonal	Diffuse cytoplasmic signal	1/100	rabbit anti-mouse	Life Technologies, ref. 11062	1/500
MelanA (A103)	Abcam, ref. ab79672	Mouse Monoclonal	Endomembrane system components, melanosomes	1/100	goat anti-mouse	Life Technologies, ref. 11001	1/500

2.4 Results

2.4.1 Isolation and morphology

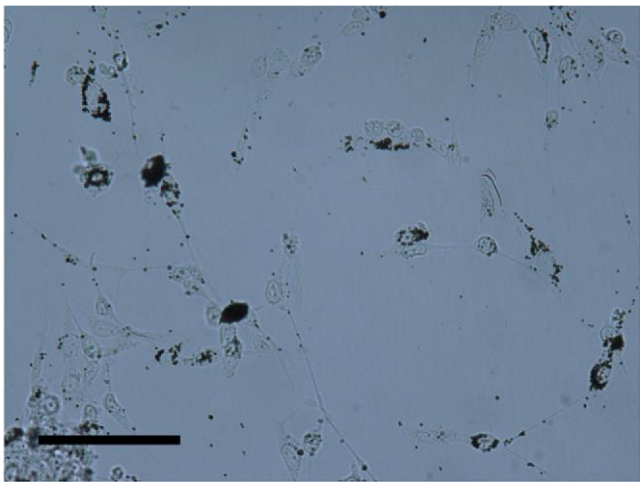

Figure 2.1 - Extracted canine uveal melanocytes develop dendritic processes after attachment to culture plates Cells were photographed 7 days after extraction. Size bar equals 100 μm.

Viable cells were isolated from both the sequential trypsin treatment suspensions and the macerated uveal explant cultures. Initially, the extracted cells were free-floating and contained dark brown pigment. The vast majority of these cells had adhered to the bottom surface of the culture flask within 7 days of isolation, although viable free-floating cells were observed as late as 3 weeks post isolation. After adhesion, cells developed a variable number of dendritic processes (figure 2.1), similar to what had previously been reported for human uveal melanocytes (11). An average of approximately $2x10^6$ cells were obtained from each uveal

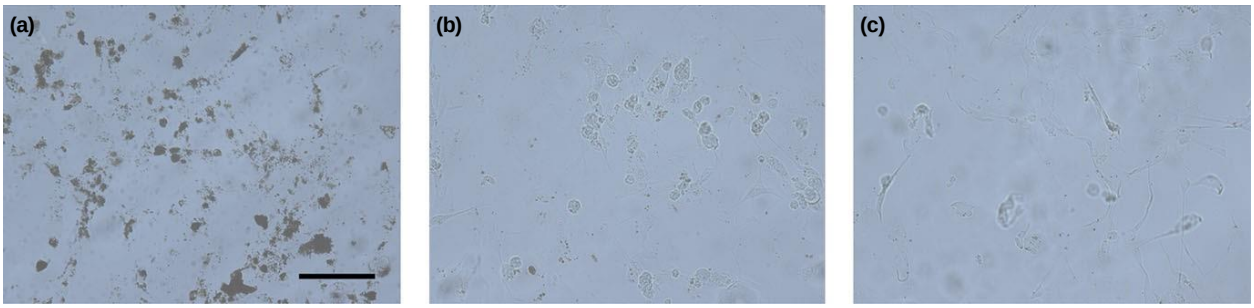

Figure 2.2 - **Extracted canine uveal melanocytes lose pigment over multiple passages**
Passage 1 (a), passage 3 (b), and passage 5 (c). Size bar equals 100 µm.

explant prior to initial passaging. In all subsequent passages (with a typical time of 1–2 weeks between passages), the cells re-adhered within 1–2 days, quickly regaining the dendritic morphology. The observed pigment was gradually lost from cultured cells over 3–5 passages (figure 2.2). This is similar to previous reports for human uveal melanocytes (11, 16). The longest-lived cell line to date has been successfully passaged 14 times. These cells do not yet show visible characteristics of senescence, which we anticipate would include an enlarged, plate-like appearance, and a loss of dendritic processes (11).

2.4.2 Cryoperservation

All four cell lines were successfully revived following cryopreservation regardless of passage number at the time of freezing. The cell line which has been cryopreserved the most often has undergone four successful freeze/thaw cycles.

2.4.3 Immunocytochemistry

Immunocytochemistry results are displayed in figure 2.3 and summarized in table 2.2. Cells extracted from canine uveal tracts labeled positively for: MelanA, S100, and vimentin

antibodies, but were not labeled by the cytokeratin antibody. These findings are consistent with previous descriptions of melanocyte cultures (11, 14). Control cell lines labeled as expected; canine testes fibroblasts labeled positive for vimentin and negative for MelanA, S100, and cytokeratin; MAC-T epithelial cells positive for cytokeratin, and negative for MelanA, vimentin, and S100.

Table 2.2 - Characterization of cell lines using immunocytochemical labeling

Cell Line	Cell Type	Number of Passages	MelanA (A103)	S100	Cytokeratin	Vimentin
MAC-T	Epithelial control	N/A	-	-	+	-
Fibroblast	Fibroblast control	3	-	-	-	+
MLN-M	Extracted uveal melanocytes	6	+	+	-	+
MLN-J	Extracted uveal melanocytes	3	+	+	-	+
MLN-R	Extracted uveal melanocytes	5	+	+	-	+
MLN-U	Extracted uveal melanocytes	5	+	+	-	+

(+) denotes a detectable signal above that seen in negative control lines. (-) denotes no detectable signal above that seen in negative control lines.

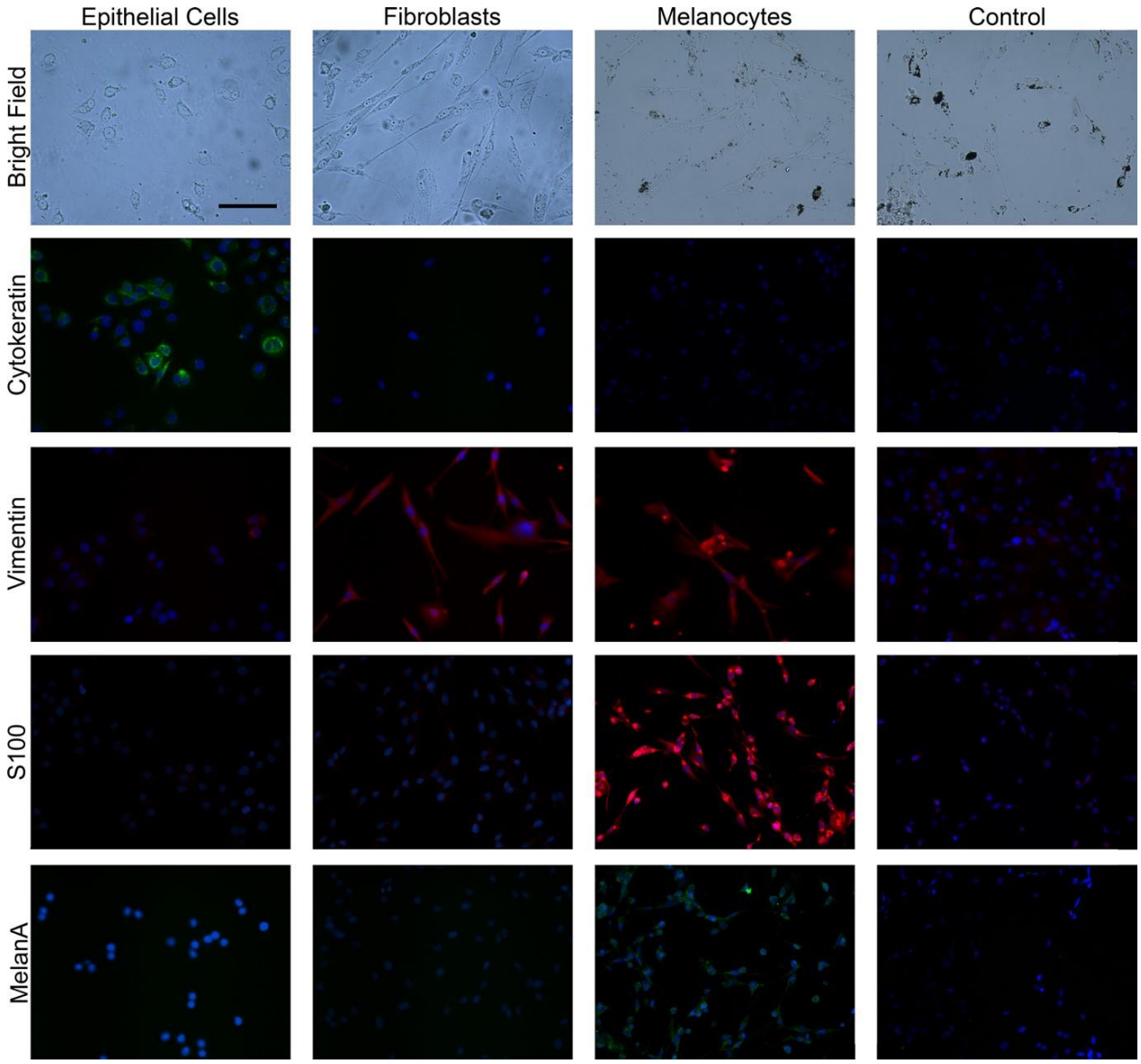

Figure 2.3 - Immunocytochemistry (ICC) of extracted first-passage canine uveal melanocytes Extracted first-passage melanocytes ('Melanocytes' column) label positively for: vimentin ('Vimentin' row; Texas Red, red color), S100 ('S100' row; Alexa Fluor 594, red color), and MelanA ('MelanA' row; Alexa Fluor 488, green color); however, are negative for cytokeratin ('Cytokeratin' row; Alexa Fluor, green color). MAC-T epithelial cells ('Epithelial Cells' column) label positively for cytokeratin and canine testes fibroblasts ('Fibroblasts' column) label positively for vimentin. The 'Control' column shows first passage canine uveal melanocytes incubated without primary antibodies to demonstrate any secondary antibody nonspecific binding. All ICC samples were counterstained with DAPI (blue color). Unlabelled cells were imaged using a bright field microscope to demonstrate typical appearance in vitro. Size bar equals 100 µm.

2.5 Conclusions

The isolation and culture techniques described here successfully generated viable uveal melanocytes from canine globes. In developing a technique to isolate human uveal melanocytes, Hu et al. observed widespread contamination of their cultures by other cell types prevalent in the uvea, most notably fibroblasts and epithelial cells. This necessitated treatment of the cultures with the selective cytotoxic agent geneticin (11). Although they did observe instances of uveal melanocytes outcompeting contaminant cells (ultimately leading to the disappearance of the contaminants), this occurred in only a minority of total cultures. Unlike the situation reported for human uveal melanocyte isolation, we did not encounter-mixed cell populations and it was not necessary to use geneticin. Our melanocyte cultures did not contain cytokeratin-positive cells, showing they were free of epithelial cell contamination. The melanocytes labeled positively for both S100 and MelanA, antibodies which do not label fibroblasts. This provided further evidence that our cultures were free of the contaminants observed by Hu et al. There were two principal differences between our culture procedures and those used by Hu et al. First, the concentration of trypsin used to treat the uveal explants differed. Hu et al. used a 0.25% trypsin solution, whereas we used only a 0.0625% trypsin solution. It is possible that at lower trypsin concentrations, the total number of cells released by the uveal explants is biased toward melanocytes, causing them to make up a much higher percentage of the total cells released than other cell types. Second, our study was performed with canine uveal tracts rather than human uveal tracts. It is possible cells of the canine uvea have different nutritional requirements than their human counterparts, and canine melanocytes will tend to outgrow other cell types in the specific culture media used in this

study. Additional study is required to definitively identify why we observed a significant reduction in contaminating cell types with our extraction methods.

In conclusion, we have established a successful method for isolation and culture of canine uveal melanocytes. We believe the techniques described here will be useful for investigation of various ocular disorders arising from aberrant melanocyte growth and replication. A future aim for our laboratory is utilization of the described techniques to generate melanocyte cell lines from OM-affected uveal tracts. We have established a donor registry of Cairn terriers affected by ocular melanosis. Following death by natural causes, owners have consented to allow us to collect OM-affected globes. Comparison of the in vitro growth characteristics of melanocyte cultures from normal and OM-affected uveal tracts may highlight critical differences. Identification of such differences may suggest potential candidate genes for the mutation causing ocular melanosis or suggest potential pharmacological targets for therapeutic intervention.

2.6 Acknowledgements

We wish to thank Drs. Lorraine Sordillo, Vilma Yuzbasiyan-Gurkan, and Steven Arnoczky for providing cell lines used as ICC controls. This study was supported by grants from the Foundation of the Cairn Terrier Club of America, the Myers-Dunlap Endowment for Canine Health, the Battle Creek Kennel Club though the Michigan State University College of Veterinary Medicine Endowed Research Funds, and Michigan State University College of Veterinary Medicine Faculty Development Funds.

2.7 Funding Sources

The funding sources had no role in the design of this study, the collection, analysis, or interpretation of data, or the writing and submission of the manuscript.

2.8 Conflict of Interest

The authors declare no competing interests for this study.

REFERENCES

REFERENCES

1. Prince JH. Comparative anatomy of the eye. Springfield, Ill.: Thomas; 1956.

2. Hu DN, Simon JD, Sarna T. Role of ocular melanin in ophthalmic physiology and pathology. Photochemistry and photobiology. 2008;84(3):639-44.

3. Cook C, Lannon A. Inherited iris melanoma in the Labrador Retriever dogs. Transactions of the American College of Veterinary Ophthalmologists. 1997;28:106.

4. Donaldson D, Sansom J, Scase T, Adams V, Mellersh C. Canine limbal melanoma: 30 cases (1992-2004). Part 1. Signalment, clinical and histological features and pedigree analysis. Vet Ophthalmol. 2006;9(2):115-9.

5. Akakura S, Takahashi T, Onishi T. Vogt-Koyanagi-Harada syndrome (uveitis diffusa acuta) in the dog. Journal of the Veterinary Medicine. 1977.

6. Sapienza JS, Simo FJ, Prades-Sapienza A. Golden Retriever uveitis: 75 cases (1994-1999). Vet Ophthalmol. 2000;3(4):241-6.

7. Esson D, Armour M, Mundy P, Schobert CS, Dubielzig RR. The histopathological and immunohistochemical characteristics of pigmentary and cystic glaucoma in the Golden Retriever. Vet Ophthalmol. 2009;12(6):361-8.

8. Petersen-Jones SM, Forcier J, Mentzer AL. Ocular melanosis in the Cairn Terrier: clinical description and investigation of mode of inheritance. Vet Ophthalmol. 2007;10 Suppl 1:63-9.

9. Petersen-Jones SM, Mentzer AL, Dubielzig RR, Render JA, Steficek BA, Kiupel M. Ocular melanosis in the Cairn Terrier: histopathological description of the condition, and immunohistological and ultrastructural characterization of the characteristic pigment-laden cells. Vet Ophthalmol. 2008;11(4):260-8.

10. Winkler PA, Bartoe JT, Quinones CR, Venta PJ, Petersen-Jones SM. Exclusion of eleven candidate genes for ocular melanosis in Cairn terriers. J Negat Results Biomed. 2013;12:6.

11. Hu DN, McCormick SA, Ritch R, Pelton-Henrion K. Studies of human uveal melanocytes in vitro: isolation, purification and cultivation of human uveal melanocytes. Investigative ophthalmology & visual science. 1993;34(7):2210-9.

12. Eisinger M, Marko O. Selective proliferation of normal human melanocytes in vitro in the presence of phorbol ester and cholera toxin. Proc Natl Acad Sci U S A. 1982;79(6):2018-22.

13. Clarkson K, Sturdgess I, Molyneux A. The usefulness of tyrosinase in the immunohistochemical assessment of melanocytic lesions: a comparison of the novel T311 antibody (anti-tyrosinase) with S-100, HMB45, and A103 (anti-melan-A). Journal of Clinical Pathology. 2001;54(3):196-200.

14. Koenig A, Wojcieszyn J, Weeks BR, Modiano JF. Expression of S100a, vimentin, NSE, and melan A/MART-1 in seven canine melanoma cells lines and twenty-nine retrospective cases of canine melanoma. Vet Pathol. 2001;38(4):427-35.

15. Huynh HT, Robitaille G, Turner JD. Establishment of bovine mammary epithelial cells (MAC-T): an in vitro model for bovine lactation. Experimental cell research. 1991;197(2):191-9.

16. Hu DN, McCormick SA, Orlow SJ, Rosemblat S, Lin AY, Wo K. Melanogenesis by human uveal melanocytes in vitro. Investigative ophthalmology & visual science. 1995;36(5):931-8.

CHAPTER 3

PHYSIOLOGICAL CHARACTERIZATION OF OCULAR MELANOSIS-AFFECTED CANINE MELANOCYTES

3.1 Abstract

Objective: Cairn terriers with ocular melanosis (OM) accumulate large, heavily pigmented melanocytes in the anterior uvea. Darkly pigmented plaques develop within the sclera, leading us to hypothesize that OM uveal melanocytes may have an abnormal migratory capacity.

Animals studied: Globes from OM-affected Cairn terriers and unaffected control eyes enucleated for reasons unrelated to this study were used for immunohistochemistry and to culture melanocytes for *in vitro* cell behavior assays.

Procedures: The scleral plaques of six dogs were immunolabeled for HMB45, MelanA, PNL2, CD18, CD204, and Iba-1 and compared with the pigment cells accumulated within the irides. Cultured uveal melanocytes from OM-affected and control dogs were compared using conventional assays measuring cell proliferation, invasion capability, and melanin production.

Results: Melanocytes isolated from OM eyes had significantly elevated levels of per-cell melanin content and production compared to controls. The majority of pigmented cells in the scleral plaques were HMB45 positive indicating a melanocytic origin. Many were also CD18 positive. No differences were observed between cultured melanocytes from OM-affected and control uvea for standard *in vitro* proliferation or invasion assays.

Conclusion: Pigmented cells which accumulate in the sclera of OM-affected Cairn terriers are predominantly melanocytes, however *in vitro* assays of uveal melanocytes did not reveal differences in migratory behavior between OM and control cells. Migratory behavior of

OM-melanocytes may be environment dependent. We suggest that RNA sequencing and differential expression analysis would be a useful next step in understanding this disease.

3.2 Introduction

Ocular melanosis (OM) in Cairn Terriers is a hereditary condition characterized by a bilateral accumulation of large, heavily pigmented, discrete round cells predominantly within the anterior uvea. These cells cause circumferential expansion and peripheral thickening of the iris root and are associated with the progressive development of pigmented scleral/episcleral plaques (figure 3.1) (1). With progression there is deposition of similar large, round, pigmented cells in other sites of the affected eye, such as the surface of the optic nerve head, the choroidal stroma, where it may obscure the tapetum, and even the meninges around the optic nerve. There is also release of pigment into the aqueous, which leads to deposition within the drainage angle and along the ventral corneal endothelial surface. Eventually the ventral opening into the ciliary cleft can be completely obscured and aqueous drainage impeded to such an extent as to cause secondary glaucoma. Our previous studies have shown that the majority of the large, pigmented cells throughout the uvea in affected dogs are melanocytes,

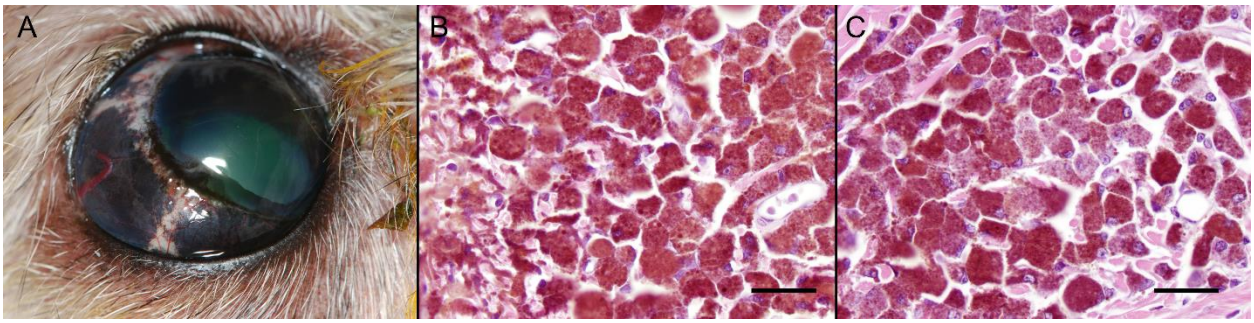

Figure 3.1 - A Cairn terrier with late-stage ocular melanosis There are extensive scleral pigmented plaques sclera adjacent to the limbus (a). The iris stroma is expanded and obscured by dense populations of large, round, densely pigmented cells; few smaller, spindloid to stellate uveal melanocytes representing normal resident populations are at the left of the image (b). Similar large round, densely pigmented cells form plaques between bundles of scleral collagen (c). Dog No. 4. Hematoxylin and eosin, post bleached, Bar = 40µm.

although a variable, but usually small number of melanophages are often also present (2). The abnormal expanded population of melanocytes in OM-affected dogs differ in morphology from normal uveal melanocytes, appearing round instead of spindle-shaped (although some spindle-shaped melanocytes can still be observed in the anterior uvea of OM-affected eyes), and packed with melanosomes of varying size. It is thought that the darkly pigmented cells that accumulate in the sclera/episclera migrate there from the uvea; however, there are no reported immunohistochemical studies to investigate whether these cells in scleral plaques are melanocytes or melanophages. The apparent invasive or migratory behavior of the cells extending into sclera and other sites in OM-affected eyes has been likened to a neoplastic behavior, but it is unclear if the large round pigment laden cells that typify ocular melanosis are overtly neoplastic. In contrast to classic anterior uveal melanocytoma in dogs which typically presents as a single expansile lesion, the large round melanocytes of ocular melanosis occur diffusely and circumferentially throughout the iris root.

We hypothesize that the pigmented cells in the scleral plaques are also melanocytes, and that the abnormal anterior uveal melanocytes of OM-affected dogs will have increased migratory capacity and melanogenesis *in vitro*. In this study, we used immunohistochemistry (IHC) to characterize the cells within the scleral/episcleral plaques in OM-affected eyes and compared them with those expanding the uvea. We also isolated and cultured melanocytes from OM-affected eyes and compared their behavior under a battery of assays testing migratory and neoplastic characteristics, with uveal melanocytes from normal control eyes.

3.3 Materials and methods

3.3.1 Animals used

Forty-eight globes from 30 dogs; 27 from 18 OM-affected dogs and 21 from 12 clinically normal dogs were used in this study. The OM-affected globes were donated by the dog's owners after being enucleated to manage painful OM-related glaucoma or when an OM-affected dog was euthanized for other health related reasons. OM was diagnosed by a veterinary ophthalmologist. Control eyes were from either elderly unaffected Cairn Terriers or crossbred dogs with dark irides which were euthanized for reasons unrelated to this study. The unaffected Cairn Terriers had been examined and found to be OM unaffected by a veterinary ophthalmologist. Forty-two globes were used for uveal culture (21 OM-affected and 21 controls) and 6 OM-affected globes were used for immunohistochemical examination. Table 3.1 provides details of the dogs used in this study.

Table 3.1 - Sources of globes used in this study

Number	Dog	Age and Sex	Breed	OM Status	# Globes Donated	Usage
1	CA76	15,M	Cairn Terrier	Affected	2	Cell Culture
2	CA166	12,F	Cairn Terrier	Affected	2	Cell Culture
3	D1	Unknown	Cairn Terrier	Affected	1	Cell Culture
4	CA599	16,M	Cairn Terrier	Affected	2	Cell Culture and IHC
5	CA569	8,F	Cairn Terrier	Affected	2	Cell Culture
6	CA538	11,F	Cairn Terrier	Affected	2	Cell Culture
7	CA319	13,F	Cairn Terrier	Affected	2	Cell Culture
8	CA524	9,F	Cairn Terrier	Affected	1	Cell Culture
9	CA518	10,F	Cairn Terrier	Affected	1	Cell Culture
10	CA239	16,F	Cairn Terrier	Affected	2	Cell Culture
11	CA67	15,M	Cairn Terrier	Affected	2	Cell Culture
12	CA537	8,F	Cairn Terrier	Affected	1	Cell Culture
13	CA609	16,M	Cairn Terrier	Affected	2	Cell Culture
14	CA393	15,F	Cairn Terrier	Unaffected	2	Cell Culture
15	CA576	16,F	Cairn Terrier	Unaffected	2	Cell Culture
16	D2	1,F	Curly Coat Retriever Mix	Unaffected	2	Cell Culture
17	D3	1,M	Curly Coat Retriever Mix	Unaffected	2	Cell Culture
18	D4	Unknown,M	Mixed Breed	Unaffected	1	Cell Culture
19	D5	Unknown,M	Mixed Breed	Unaffected	1	Cell Culture
20	D6	Unknown,F	Mixed Breed	Unaffected	1	Cell Culture
21	D7	Unknown	Unknown	Unaffected	2	Cell Culture
22	D8	Unknown	Unknown	Unaffected	2	Cell Culture
23	D9	Unknown	Mixed Breed	Unaffected	2	Cell Culture
24	D10	Unknown	Mixed Breed	Unaffected	2	Cell Culture
25	D11	Unknown	Mixed Breed	Unaffected	2	Cell Culture
26	CA530	10,M	Cairn Terrier	Affected	1	IHC
27	CA608	12,M	Cairn Terrier	Affected	1	IHC
28	CA535	12,F	Cairn Terrier	Affected	1	IHC
29	CA607	12,F	Cairn Terrier	Affected	1	IHC
30	CA642	10,F	Cairn Terrier	Affected	1	IHC

3.3.2 Immunohistochemistry

Six formalin fixed globes from OM-affected dogs (# 4, 26-30) were processed for IHC. They were sagittally bisected and one or both halves embedded in paraffin. 5µm sections were pre-bleached and routinely stained with hematoxylin and eosin (H&E), or processed for immunohistochemistry (IHC) and labeled for HMB45, MelanA, PNL2, CD18, CD204, or Iba-1 and post-bleached and counterstained with Gill's III hematoxylin. Details of IHC methods and antibodies are provided in table 3.2. Bleaching was by incubation of slides with 0.5% Potassium Permanganate for 20 minutes and 5% Oxalic Acid for 45 seconds. H&E and IHC sections were evaluated by two pathologists (DGS, EN). For each IHC marker, the percentage of the pigmented round cells in the anterior uveal stroma and within the scleral/episcleral plaques positive for antibody labelling was recorded.

Table 3.2 - Antibodies and positive control tissue

Antibody	Type/Host	Supplier	Dilution	Retrieval method	Chromogen Kit	Positive tissue
Melan A	Mouse monoclonal	Dako	1:20	Low pH PT[1]	ChromoMap V-red (Alkaline Phosphatase)	Melanoma
PNL-2	Mouse monoclonal	Santa Cruz	1:500	Low pH PT[1]	ChromoMap V-red with amplification (Alkaline Phosphatase)	Melanoma
HMB45	Mouse monoclonal	Dako	1:10	CC1[3], 32 min	ChromoMap V-red with amplification (Alkaline Phosphatase)	Melanoma
CD18	Mouse monoclonal	Peter Moore	1:20	Low pH PT[1]	ChromoMap V-red (Alkaline Phosphatase)	Histiocytic sarcoma
CD204	Mouse monoclonal	Tans Genic Inc./ Cosmo Bio	1:1000	CC1[3], 64 min	ChromoMap V-red (Alkaline Phosphatase)	Histiocytic sarcoma
IBA-1	Rabbit polyclonal	Wako Chemical USA, Inc.	1:1000	Low pH PT[2]	FLEX (AEC)	Histiocytic sarcoma

[1] Heat retrieval at low pH on the Dako PT link (Discovery Ultra, Ventana, Tucson, AZ, USA)
[2] Heat retrieval at low pH on the Dako PT link (Agilent Technologies, Santa Clara, CA, USA)
[3] Heat retrieval using CC1 (Cell Conditioning 1, Discovery Ultra, Ventana, Tucson, AZ, USA)

3.3.3 Cell culture methods

Melanocytes were isolated and cultured as previously described (3). Briefly, the anterior uvea was excised from donor eyes, placed in 5 ml of 0.0625% trypsin (SAFC Global, St. Louis, MO, USA) in Dulbecco's modified eagle medium with D-glucose and glutamine (DMEM, Gibco, Grand Island, NY, USA) and incubated at 37°C for one hour and the incubating media collected. This process was repeated 3 additional times resulting in 4 total aliquots of collected media. The media was centrifuged at 2000g for 5 minutes to collect the released cells. The cell pellets were resuspended in 2.5 ml of melanocyte media (F12 with L-glutamine [Gibco, USA], 10% fetal bovine serum [Gibco, USA], 100 units/ml of penicillin [Gibco, USA], 100 µg/ml streptomycin [Gibco, USA], 20 ng/ml basic fibroblast growth factor [Sigma-Aldrich, St. Louis, MO, USA], and 10 ng/ml cholera toxin [Sigma-Aldrich, USA]) and plated in 25 cm^2 culture flasks (Corning, Corning, NY, USA). The resulting cultures were incubated at 37°C in 5% CO_2. Media was replaced every 2-3 days, using the media pH associated color-change indicator as a guide.

Cells were passaged upon reaching approximately 80% confluence. They were washed with PBS, and incubated with 2.5ml of 0.25% Trypsin-EDTA (Gibco, USA) at 37°C for 5 minutes. Trypsin was neutralized with 2.5 mL of culture media, the cells pelleted (2000 g for 5 min at room temperature), resuspended in 5-10 mL of culture media and quantified with a hemocytometer They were then either used for assays described below, cryopreserved for later use, or re-plated for further growth.

3.3.4 Preparing ECM-treated plates

Plates were treated with extracellular matrix components (ECM) as described by Wagner *et al* 1997 for use in doubling time, scratch and cell adhesion assays (4). Five types of extracellular matrices were used: fibronectin (Sigma-Aldrich, USA), laminin (Sigma-Aldrich, USA), collagen I (Sigma-Aldrich, USA), collagen III (Millipore, Billerica, MA, USA), and collagen IV (Sigma-Aldrich, USA). All were reconstituted according to the manufacturer's instructions. For collagens I, III, and IV, 10 $\mu g/cm^2$ was added to each well of a culture plate, then air dried overnight in a laminar flow hood. Fibronectin and laminin coatings were applied at 2 $\mu g/cm^2$ and incubated at 37°C for one hour, after which any remaining solution was removed.

3.3.5 Doubling time assay

Five OM-affected (# 1-3, 5, 7) and 5 control uveal cell lines (# 20-24) were used. One 24-well plate per ECM component was used for each cell line, plus one untreated control. Seeded plates ($1x10^4$ cells in 250 µl media) were incubated at 37°C with 5% CO_2. Every 24 hours for the next 8 days, adherent cells in three wells were trypsinized and collected for counting. The total number of cells in culture each day was charted, and data points from the exponential growth phase of the curve used to calculate a doubling time using a least squares fitting method (5).

3.3.6 Cellular melanin levels

As cells were passaged, 3 ml of cell suspension was taken for cellular melanin concentration testing performed in 3 one ml technical replicates. Cells were pelleted and dissolved in 1N NaOH. The absorbance of each sample at 475 nm was measured using a

Beckman DU 650 spectrometer. The average absorbance of 3 readings from 3 technical replicates was calculated and compared to a standard curve generated by measuring the absorbance of known amounts of synthetic melanin (Sigma-Aldrich, USA) to determine the total melanin present (6). Total melanin was divided by the previously counted number of cells/ml to determine a melanin/cell ratio. Canine testes fibroblasts were used as an unpigmented cell control, and their average absorbance value was subtracted from each sample to account for the background absorbance of non-melanin cell components. Melanin production per cell was calculated using the following equation:

$$MPC = \frac{MCtP - MCo}{1.3D(P-1)}$$

where MPC is melanin produced per cell per day (in ng/cell/day), MCt is the melanin content (in ng/cell) at time *t* (in days), MCo is the melanin content per cell (ng/cell) at time 0, *P* is the population increase (in cells) during time *t*, and *D* is the average doubling time of the cell type (affected or control, in days) (7). Twelve OM-affected (# 1-3, 5-13) and 10 control uveal melanocyte cell lines (# 14-15, 18-25) were used.

3.3.7 Wound-healing rate

Seven OM-affected (# 3-4, 6-7, 10, 12-13) and 4 control uveal melanocyte cell lines (# 17, 21, 24-25) were used. Cells were plated into 24-well culture plates at a concentration of ~$1x10^5$ cells/well. Three technical replicates were performed for each cell line for each ECM component and an untreated control plate. Cells were incubated at 37°C with 5% CO_2 until confluent, with media being changed every 2-3 days as needed. A 10 µl pipette tip was then

used to create a scratch (wound) in the cell monolayer, and a razor blade was used to make a cut perpendicular to the scratch so that the same area could be reliably located for observation. An inverted microscope (Nikon Eclipse TS100) was used to capture images of the scratched area over the course of the next 72 hours (8). The program TScratch was used for automated analysis and comparison of the acquired images (9).

3.3.8 Cell adhesion assay

Cell adhesion rate was measured using a modified tetrazolium colorimetric assay (10, 11). Four OM-affected (# 1-3, 8) and 4 control uveal melanocyte cell lines (# 15, 22, 24-25) were used. $7.5x10^3$ cells in melanocyte media per well were plated into ECM coated 96-well plates or an untreated plastic control. Plates were incubated at 37°C with 5% CO_2 to allow cellular attachment, and every 10 minutes for 60 minutes post-plating, the media was aspirated from 3 wells of each cell type and replaced with serum-free media to remove any unattached cells. At the end of 60 minutes, 50 µl of a 1mg/ml solution of MTT ((3-(4,5-dimethylthiazol-2-yl)-2,5-diphenyltetrazolium bromide), Sigma-Aldrich, USA) was added to each well. The plates were then incubated for 4 hours at 37°C with 5% CO_2 to allow attached cells to reduce MTT to a blue formazan crystal. Remaining media was aspirated, each well gently washed twice with BSS to remove any unreduced MTT, and then 10% SDS-0.01 N HCl solution used to dissolve the MTT formazan. Sample absorbance at 550nm and 655nm was measured using a BioRad model 3550 plate reader. The 655nm reading was subtracted from the 550nm reading to account for background absorbance. Results were reported as a percent metabolic activity relative to the control. Additional cells from each cell line were plated at the same concentration in ECM

treated plates and allowed to attach for 2 hours to determine a maximum attachment. The previously measured metabolic activity data was compared to that of the maximum attachment samples to determine a % maximum attachment for each time point.

3.3.9 Anchorage independence

Seven OM-affected (# 1-2, 5-6, 8-9, 12) and 6 control uveal cell lines (# 15, 21-25) were used. Each well of a 6-well plate was coated with 2.5 ml of a base layer containing 0.5% agarose dissolved in melanocyte growth media as described above with 1% or 10% FBS for melanocyte lines. A negative control of canine testes fibroblasts and a positive control of MDA-MB-231 human breast adenocarcinoma cells were cultured in DMEM media with 100 units/ml of penicillin, 100 µg/ml streptomycin and 1% or 10% FBS. The base layer was allowed to cool until solid. A second layer containing $2.5x10^4$ cells in 2.5 ml of growth media with 0.35% agarose was added to the top of the base layer, and allowed to cool until solid. The plate was incubated overnight at 37ºC with 5% CO_2. Then 2.5 mL of growth media was added. Media was replaced every 3 days for 30 days. Plates were then imaged using an inverted microscope and a STEMgrid-6 plate-counting grid (STEMCELL technologies, Cambridge, MA, USA). Colonies defined as cluster of > 20 cells were counted in ten $2mm^2$ grid squares for each sample, and the averages of these counts were multiplied by the number of grid squares per plate to give a colonies-per-plate count.

3.3.10 Invasion assay

Five OM-affected (# 1-2, 7-9) and 5 control uveal cell lines (# 20, 22-25) were used. Plates for Matrigel *in vitro* cell invasion assay with 8 µm pore diameter size supports (Corning, USA) were prepared as per the manufacturer's instructions. The assay was performed in triplicate with canine testes fibroblasts as a negative control, and MDA-MB-231 cells a positive control. The chemoattractant used was 10% FBS in F12 media, and $2.5x10^4$ cells were plated in each well, as recommended in the manufacturer's protocol. Cell invasion chambers were incubated at 37ºC with 5% CO_2. After 24 hours, any remaining cells were removed from the upper chamber, the membranes were stained with Diff-Quik (Sigma-Aldrich, USA) and cells that had invaded were quantified by counting four fields near the center of each replicate.

3.4 Results

3.4.1 Immunohistochemistry

The scleral plaques within all 6 OM-affected globes examined consisted of large, round, densely pigmented cells similar in appearance to those expanding the anterior uvea. IHC (Table 3) showed the majority of these cells were immunoreactive for HMB45, but not for PNL2 or Melan A (figure 3.2). In contrast, rare round, pigmented cells in the anterior uveal stroma of 4 (# 4, 27, 29, 30) of the 6 dogs were PNL2 and MelanA immunoreactive. Between 30 and 90% of pigmented round cells both in the anterior uvea and 80 to 90% of those within the scleral plaques were immunoreactive for CD18 (figure 3.3). Rare round pigmented cells in the anterior uvea, but not in the scleral plaques, of the eye of one dog (# 29) were immunoreactive for Iba-1 and/or CD204. This eye, however, also had a more significant inflammatory response than other cases with perivascular infiltrates of lymphocytes, plasma cells, and histiocytes occurring throughout the anterior uvea. None of the large pigmented round cells in the uvea or scleral plaques of the other 5 dogs (# 4, 27-28, 3026-29, 31) were immunoreactive for Iba-1 or CD204.

3.4.2 Cellular melanin levels

Cellular melanin levels were significantly higher in early-passage melanocytes from OM-affected dogs relative to unaffected control melanocytes, both in terms of total melanin content and per-cell melanin production (figures 3.4 and 3.5). For the first three passages following isolation, OM-uveal melanocytes had an average per-cell melanin content that was more than twice the amount found in unaffected cells, including a 3.9-fold average increase in the first passage following isolation (0.37±0.19ng/cell vs. 0.094±0.064ng/cell, p=0.00185). The

Table 3.3 - Percentage of the expansile round melanocyte population with immunoreactivity for histiocytic and melanocytic markers within the anterior uvea or scleral plaques in Cairn terriers with ocular melanosis

	CD18		CD204		IBA-1		HMB45		PNL2		Melan A	
Dog No.	anterior uvea	scleral plaque	anterior uvea	scleral plaque	anterior uvea	scleral plaque	anterior uvea	scleral plaque	anterior uvea	scleral plaque	anterior uvea	scleral plaque
4	30	80	0	0	0	0	60	70	<10	0	10	0
26	30	80	0	0	0	0	60	95	0	0	0	0
27	60	90	0	0	0	0	60	60	20	0	10	0
28	90	90	0	0	0	0	60	90	0	0	0	0
29	90	90	<10	0	<10	0	30	70	<10	0	10	0
30	90	90	0	<10	0	0	60	70	0	0	10	0

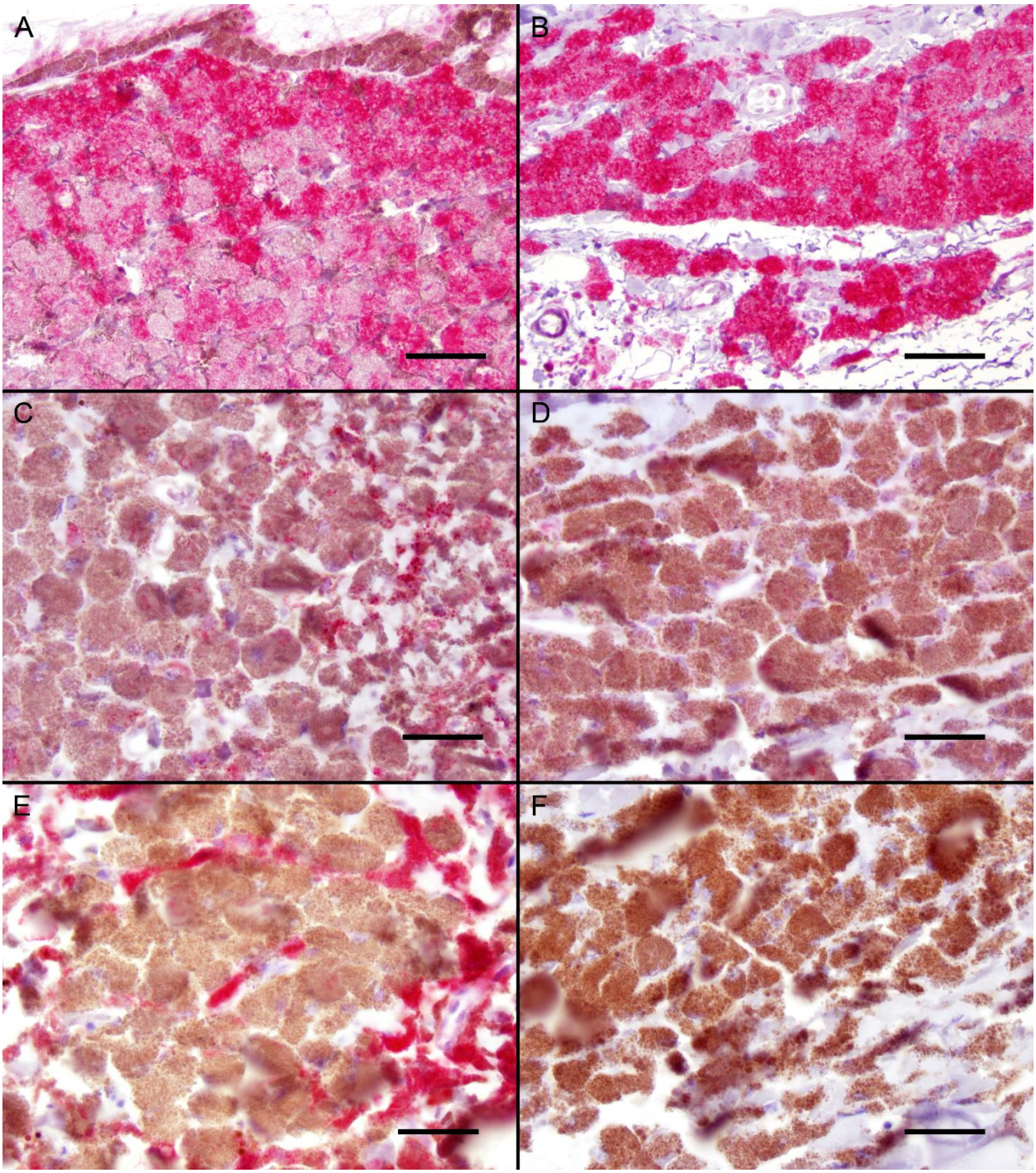

Figure 3.2 – Immunohistochemistry of ocular melanosis, anterior uvea or scleral plaque
Ocular melanosis**,** anterior uvea (a, c, e) or scleral plaque (b, d, f), dog. Large round pigmented cells show diffuse cytoplasmic red labeling for HMB45 in the anterior uvea (a) and in scleral plaques (b). Dog No. 26. IHC post bleached with hematoxylin counterstain. Only spindle to stellate shaped cells label for PNL2 (c) or Melan A (e) in the anterior uvea. Round cells are not immunoreactive for PNL2 (d) or Melan A (f) within the scleral plaques. Dog No. 4. IHC post bleached with hematoxylin counterstain. Bar = 40µm.

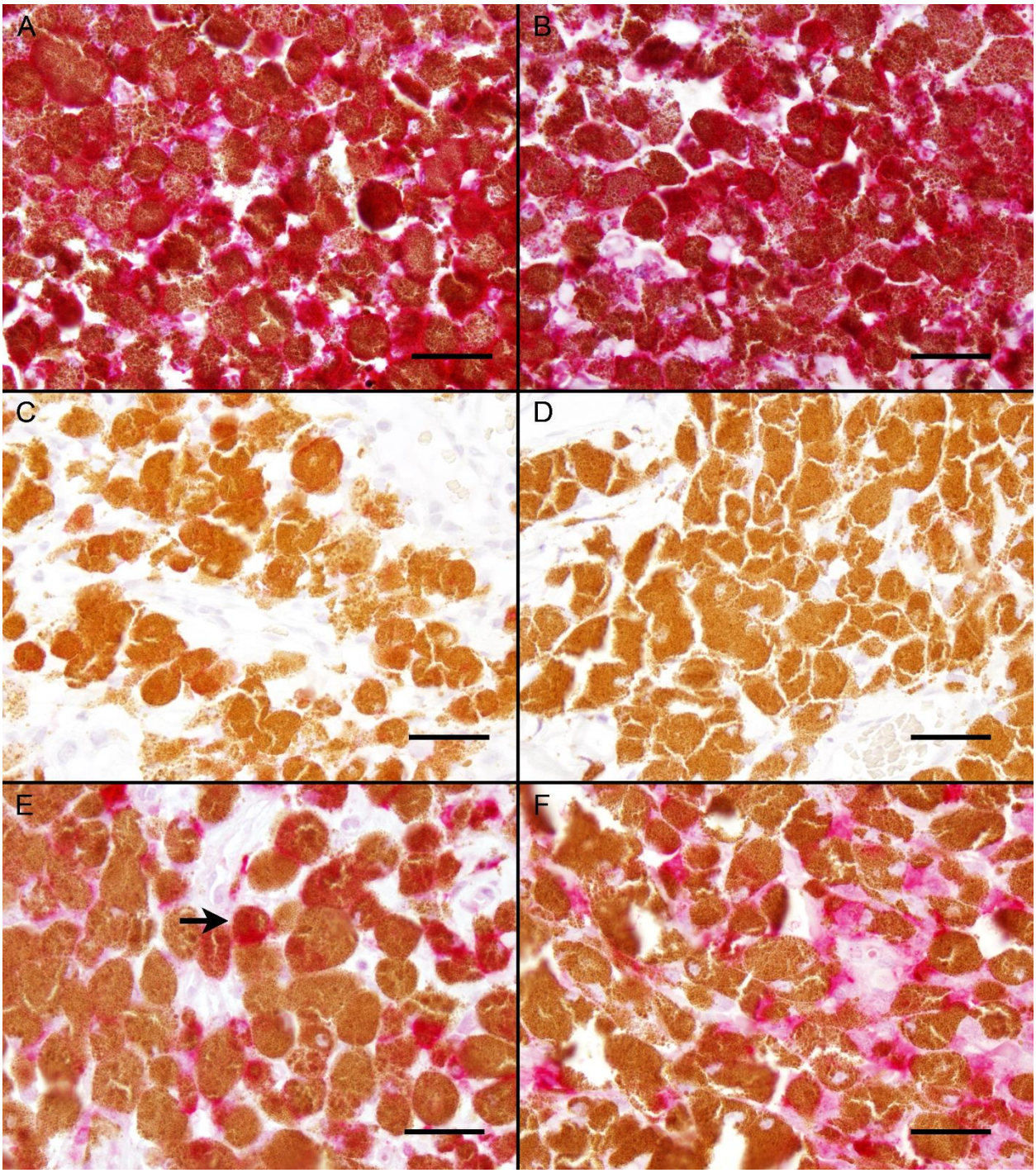

Figure 3.3 – Immunohistochemistry of ocular melanosis, anterior uvea or scleral plaque
Ocular melanosis, anterior uvea (a, c, e) or scleral plaque (b, d, f), dog. The large round pigmented cells widely show strong perimembranous to cytoplasmic labeling for CD18 in both the anterior uvea (a) and scleral plaque (b). Dog No. 4. IHC post bleached with hematoxylin counterstain. These cells are not immunoreactive for CD204 in either the anterior uvea (c) or scleral plaque (d). Only small round cells consistent with inflammatory cells label for Iba-1 in the anterior uvea (arrow) and in the scleral plaque (f). Dog No. 29. Bar = 40µm.

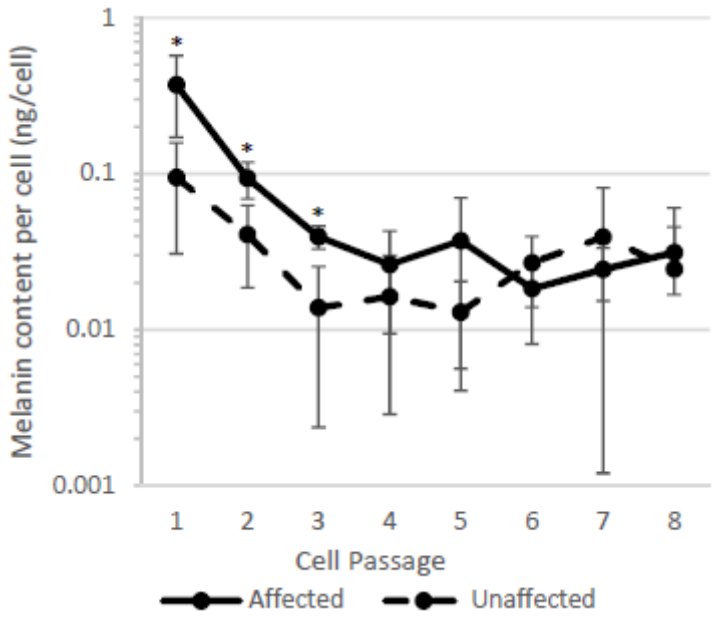

Figure 3.4 – Average melanin content of OM-uveal melanocytes Average melanin content (ng/cell) of OM-uveal melanocytes compared with unaffected melanocytes at different passages in culture. Significant differences exist between the two populations for the first three passages post-isolation (*p<0.05), after which melanin concentration in both populations equalizes. For each timepoint, n is between 5 and 9.

difference remained significant in passages 2 (2.3-fold increase, 0.094±0.025ng/cell vs. 0.041±0.022ng/cell, p=0.0052) and 3 (2.9-fold increase, 0.04±0.0066ng/cell vs. 0.014±0.011ng/cell, p=0.0017) (figure 3.4), but ceased to be significant in passage 4 and beyond. The average per-day melanin production of OM-uveal melanocytes between passage 1 and 2 was 2.8-fold higher than the unaffected control average (0.046±0.014ng/cell/day vs. 0.016±0.0084ng/cell/day, p=0.003). This increase remained significant between passages 2 and 3 (2.5-fold increase, 0.019±0.0032ng/cell/day vs. 0.0076±0.0067ng/cell/day, p=0.0021), after which there was no significant difference between the two populations (figure 3.5).

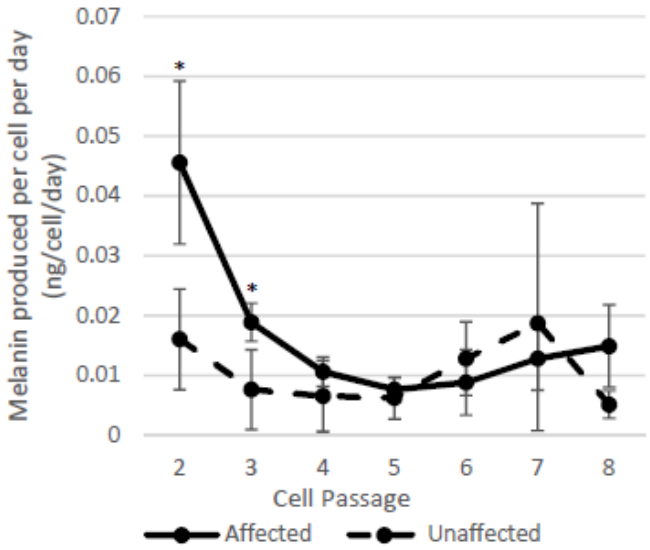

Figure 3.5 – Average melanin produced per cell per day in OM-uveal melanocytes Average melanin produced per cell per day (ng/cell/day) in OM-uveal melanocytes compared with unaffected melanocytes at different passages in culture. Significant differences exist between the two populations until after the third passage (*$p<0.05$), after which the populations equalize. Note that individual doubling time data was not available for all cell populations, so the average doubling time for affected or unaffected melanocytes was used where appropriate. For each time point, n is between 4 and 7.

3.4.3 Doubling time

No significant difference was detected between the doubling times of OM-uveal melanocytes (44±5 hrs) and those of the unaffected control melanocytes (47±3 hrs) ($p=0.3851$, figure 3.6). Similarly, no difference was detected between the average doubling time of OM-uveal melanocytes and unaffected controls in any of the 5 different ECM treatment groups (figure 3.6). Additionally, none of the ECM components tested caused a significant change in the doubling time of the uveal melanocytes when compared to the untreated control plates.

3.4.4 Anchorage independence

Both OM-uveal melanocytes and unaffected controls formed colonies at very low rates, and these rates were not significantly different from that of the negative control (canine testes fibroblasts) or from one another in either the 1% FBS or the 10% FBS soft agar treatments (table 3.4).

Table 3.4 – Average colonies per plate after 30 days incubation in soft agar

Cell Type	Colonies/plate (1% FBS)	Colonies/plate (10% FBS)
MDA-MB-231 (+ control)	285±34	503±52
Fibroblasts (- control)	15±13	38±13
Affected Avg. n=7	19±18	49±29
Unaffected Avg. n=6	20±19	43±30
p-value (A vs. U)	0.9523	0.7246

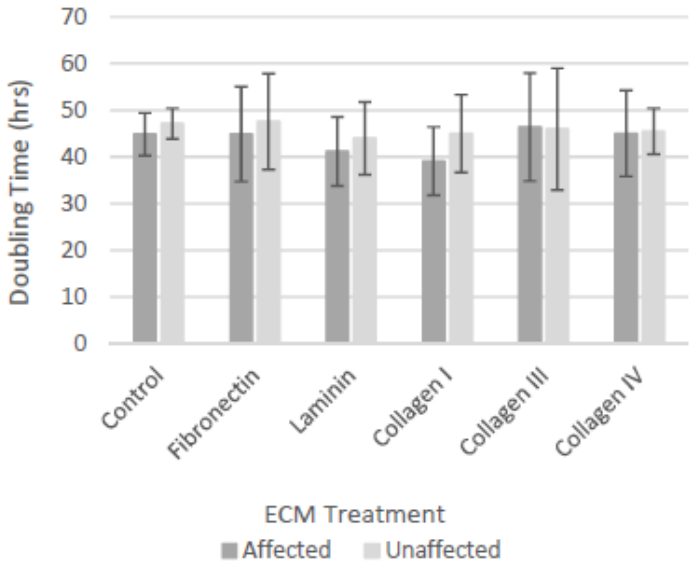

Figure 3.6 – Graph of doubling time (in hours) for melanocyte populations with different ECM treatments For all samples, n=5.

3.4.5 Invasion assay

Although both OM-uveal melanocytes and unaffected controls had migration percentages that were higher than the negative control, neither sample was very invasive compared to the positive control (table 3.5). Furthermore, there was no significant difference between the average migration percentage of OM-uveal melanocytes and melanocytes from unaffected dogs.

Table 3.5: Average percent invasion of various cell lines as determined by Matrigel assay

Cell Type	Percent Invasion
MDA-MB-231	86±4
Fibroblasts	5±2
Affected Avg. n=5	12±3
Unaffected Avg. n=5	13±4
p-value (A vs. U)	0.6870

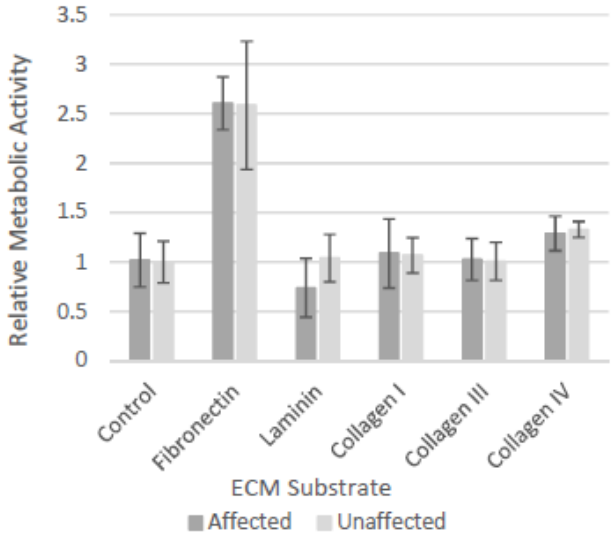

Figure 3.7 - Relative metabolic activity of melanocytes at 30-minutes time point Metabolic activity of unaffected melanocytes on the untreated plastic control was defined as 1. The difference between fibronectin the plastic control is significant at p=0.0001 as calculated by two-tailed t-test. There were no significant differences between uveal melanocytes from OM affected eye and those from control eyes. For all samples, n=4.

3.4.6 Cell adhesion

Fibronectin was the preferred binding substrate for attachment for both sets of uveal melanocytes (figure 3.7) as evidenced by cells reaching their maximum degree of attachment soonest, with cells reaching 80-100% of their maximum attachment percentage within 30 minutes of plating, compared to 40-50 minutes in trials with other ECM substrates (data not shown). No other ECM component had a rate of attachment that was significantly different from untreated plastic. There were no differences in attachment rate between OM-uveal melanocytes and unaffected controls for any of the 5 ECM substrates tested.

3.4.7 Wound-healing rate

No significant differences were detected in the rate of wound closure for OM-uveal melanocytes and unaffected controls on any of the different ECM substrates tested (figure 3.8). Although the OM-uveal melanocyte lines consistently had a higher average closure rate than the control lines, the difference was not statistically significant, and both types of cell line displayed high levels of individual variation between the different cell lines tested.

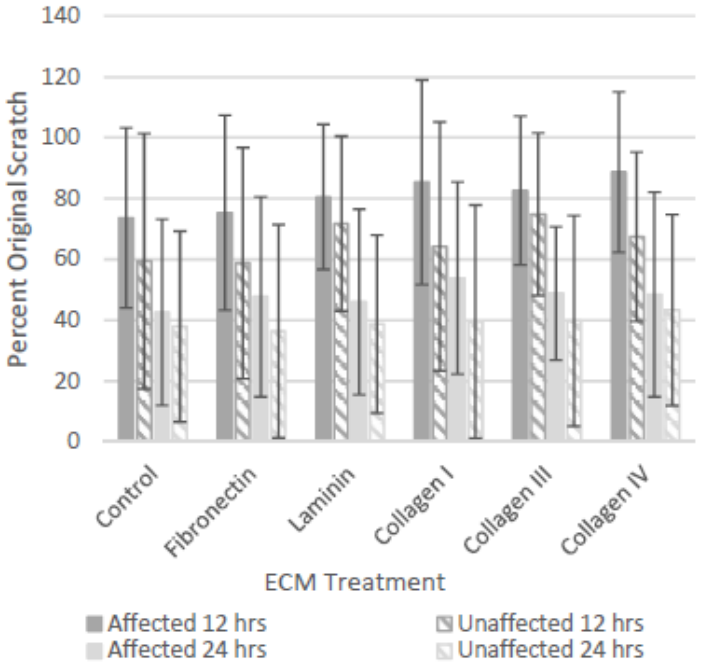

Figure 3.8 - Rate of wound closure as a percentage of the original scratch Percentage of wound remaining open after 12 or 24 hours post-scratch. No significant difference was detected for any cell type or treatment. For affected melanocytes, n=7. For unaffected melanocytes, n=4.

3.5 Discussion

Melanocytes originate from neural crest cells which migrate during development with those in the eye reaching the iris, ciliary body and choroid by following branches of the trigeminal nerve (12). Despite a common origin, melanocytes at different body sites exhibit different behavior and different responses to stimuli (13, 14). Uveal melanocytes are typically considered to be relatively quiescent, although ocular inflammation and in certain species, drugs such as prostaglandin analogues can result in an increase in iridal pigmentation. Cairn terriers with ocular melanosis develop a characteristic circumferential expansion of the iridal root primarily due to an expanded population of large melanosome-laden melanocytes (2). The reason for the altered behavior of the iridal melanocytes in OM-affected dogs is not known. The abnormal melanocytes in OM-affected eyes appear to be able to migrate to other sites in the eye, albeit at a very slow rate. This abnormal, slow expansion of the population of iridal melanocytes with a potential local migratory phenotype was the impetus to isolate and study the behavior of these cells in a number of different *in vitro* assays for growth and migration. One of the prominent additional sites of pigment accumulation in OM-affected Cairn terriers is the sclera and episclera. These lesions start as small, flat, bone-spicule shaped black pigment accumulations that over a period of years expand into larger, slightly raised plaques. We wanted to investigate whether the cells that had apparently migrated to this site, perhaps via the aqueous drainage pathways, were melanocytes or melanophages, a cell type also found in varying numbers within the irides of affected dogs. IHC for a number of antibodies demonstrated that the predominant cells in the scleral/episcleral pigmented plaques were

large, round, densely pigment melanocytes appearing morphologically very similar to those within the irides.

IHC demonstrated that a high proportion of the large, round, densely pigmented cells expanding the anterior uvea and forming the pigmented scleral plaques were positive for HMB45. This monoclonal antibody is highly specific for a glycosylated form of Pmel17 (gp100) which is present in immature melanosomes; for example, melanocytes in embryonic tissues, many melanomas and some proliferative melanocytic lesions (15). Previous EM studies identified all stages of melanosomes including many large melanosomes in these cells (2). Immunoreactivity for HMB45 conclusively shows that the abnormal pigmented cells in OM-affected dogs are of melanocytic origin. The iris stroma of affected dogs also has a background population of spindle-shaped melanocytes that morphologically resemble the melanocytes of the normal dog iris. These cells were also identified by IHC as melanocytes; typically immunoreactive for PNL2 and Melan A, but not HMB45. This suggests that the diffusely present, large, round pigmented cells are present in addition to the typical spindle-shaped melanocytes that can be found within normal iris stroma. A high proportion of the large round melanocyte cell population of ocular melanosis eyes were also positive for CD18, integrin beta-2, which plays a role in cell adhesion. No CD18 expression was detected in the spindle-shaped melanocytes within the iris stroma. Although commonly used as a leukocyte marker in dogs, CD18 can rarely be expressed in proliferative melanocytic lesions, including melanomas and we have previously reported such expression in the abnormal melanocytes of Cairn Terriers with OM (2). CD18 is one part of Leukocyte Function-Associated antigen-1 (LCA1) that is important for transendothelial migration, a feature of malignant melanomas. It is suggested that tissue

inflammatory cells provide LCA1 to melanoma cells because most melanoma cell lines do not express the LCA1 antigens (including CD18) (16). Expression of CD18 on the abnormal OM melanocytes may explain the apparent migratory behavior of the cells, although no differences in adhesion to various ECM components were detected between OM melanocytes and unaffected controls *in vitro* (figure 3.7). The lack of immunoreactivity for histiocyte markers CD204 and Iba-1 further supports that the majority of the round cells of OM are melanocytes rather than melanophages, although there were small numbers of CD18, CD204, and Iba-1 positive melanophages scattered throughout the uvea of some cases. This is consistent with our previous observations in the uvea of OM-affected dogs in which varying numbers of melanophages were also observed, admixed with the large round melanocytes (2). Clinically, OM-affected dogs have periodic episodes of anterior uveitis typically accompanied by the shedding of pigment into the aqueous, so the presence of a population of melanophages in affected tissue is expected.

Melanin content and rate of melanin production were greatly elevated in OM-uveal melanocytes relative to unaffected controls for the first several passages *in vitro*. During the period of statistically significant elevation, OM-uveal melanocytes had an average melanin content ranging from 0.37±0.19 to 0.04±0.0066 ng/cell, compared to a range of 0.094±0.064 to 0.014±0.01 ng/cell in unaffected controls. In comparison, growth-phase human uveal melanocytes from different iris colors had average per-cell melanin content ranging from 0.1020 ng/cell from melanocytes cultured from eyes with a dark iris (brown or dark green) to 0.0140 ng/cell from melanocytes cultured from eyes with a light iris (blue or light green) (6). The unaffected control average seems to correspond roughly to the normal range observed in

humans, with the melanocytes from OM-affected dogs showing levels of pigmentation ranging from well above those seen in the normal human eye down to the upper half of the normal human range. The melanin content in both unaffected control and OM-uveal melanocytes decreased rapidly in early passages before eventually stabilizing, a pattern also observed in human uveal melanocyte cultures. OM-uveal melanocytes also displayed elevated levels of melanin production, producing melanin at an average rate ranging from 0.046±0.014 to 0.019±0.0032 ng/cell/day during the significantly elevated period, compared with a range of 0.016±0.0084 to 0.0076±0.0067 ng/cell/day in unaffected control cells. The unaffected control canine melanocytes were found to be intermediate between growth-phase pigment at production levels of dark and moderately dark human uveal melanocyte melanin production rates (0.0180 and 0.0071 ng/cell/day, respectively). The OM-uveal melanocytes produced melanin at a rate higher than melanocytes from dark human irides during this period.

As the precise pathogenesis of OM and nature of the round cells comprising the lesion are presently not very well understood, a number of established *in vitro* assays were employed to evaluate basic behavioral aspects of these cells. As uveal tissue in OM-affected dogs displays increased cellularity, the doubling time of OM-uveal melanocytes was measured to determine if their replication rate was intrinsically different from that of unaffected controls. No significant difference in doubling rate was detected. The doubling rate of both OM and control uveal canine melanocytes (44±5 and 47±3 hrs respectively) were slightly faster than the range of doubling times reported for human uveal melanocytes (48-72hrs) (6). Doubling time assays were repeated in the presence of common ocular ECM components, as different ECM components are known to have differential effects on cell morphology and behavior *in vitro*,

but this had no significant impact on the doubling time of OM-uveal melanocytes or unaffected controls. OM-uveal melanocytes appear to migrate into the sclera, so a matrigel invasion assay was used to evaluate their ability to invade through a membrane, and a wound-healing assay was used to analyze their migration rate. Although no human data is available for comparison, neither test showed any significant difference between OM-uveal melanocytes and unaffected controls. Matrigel assay results for both cell types showed very little invasive potential relative to that of a known invasive cell line used as a positive control. Wound-healing assays showed no significant differences in migration rate between OM-uveal melanocytes and unaffected controls on untreated plastic or any of the different ECM substrates tested. Wound-healing assay measurements averaged from combined samples had large standard deviations, suggesting that most differences in migration rate were primarily attributable to individual variation rather than OM-affected status. Soft agar assays were performed to test the anchorage-independent growth potential of OM-uveal melanocytes. Average colony formation rates from both OM-affected and unaffected cell lines were very low, and not significantly different from the negative control, indicating that OM-uveal melanocytes are not capable of anchorage-independent growth. Previous studies have shown that transformed human uveal melanocytes have a higher attachment rate on a wider variety of extracellular matrix (ECM) components than normal uveal melanocytes, so we evaluated OM-uveal melanocytes on their attachment rates to various ECM components found in the canine eye. In humans, normal uveal melanocytes displayed a preference for fibronectin, adhering at a rate 1.5-fold greater than they adhere to untreated plastic (4). They attached significantly less well to collagens I, III, and IV, binding at roughly 80% of their attachment rate to untreated plastic. In contrast, human

uveal melanoma cells bound collagens I, III, and IV at the same rate they bound fibronectin, a 1.5-fold increase over untreated plastic. Both OM-uveal melanocytes and unaffected controls displayed a strong preference for fibronectin, adhering at a 2.5-fold greater rate over untreated plastic. No other ECM component caused a binding rate that was significantly different from untreated plastic. Although it was surprising that canine uveal melanocytes appear to bind collagens I, III, and IV at a rate higher than that reported for human uveal melanocytes, the difference was consistent across both OM-uveal melanocytes and unaffected controls.

Although IHC shows the pigmented scleral plaques to be composed primarily of melanocytes, which most likely have migrated there from the expanded population in the anterior uvea, presumably along aqueous drainage pathways, all of our assays related to cell migratory behavior showed that there were no significant differences between uveal melanocytes from OM-affected dogs and normal controls. Our melanogenesis assays, however, showed a clear difference in melanin content and production between OM-affected and unaffected dog-derived melanocyte cultures was present when examining early-passage cells, but that that difference quickly disappeared in culture, diminishing nearly 50% between passage 1 and 2 and disappearing by the fourth passage at the latest. Although we endeavored to use as early a cell passage as possible for all assays presented in this paper, the difficulties of culturing a sufficient number of melanocytes for each assay was such that most of the cells used in the assays presented here were between passage number 2 and 4 when being tested. Ocular melanosis is a very slowly progressing disease, often developing over the course of many years, so any differences in cell migration behaviors between the melanocytes of affected and unaffected eyes may be quite small in magnitude. If the difference in cell behavior being

measured experiences the same 50% reduction in effect size after a single passage in culture as melanogenesis does, this would make any difference between the two cell populations extremely difficult to detect. While OM-uveal melanocytes clearly appear to have a migratory phenotype *in vivo* based on the IHC data, we likely cannot replicate the phenotype *in vitro* due to changes in phenotype caused by differences between the intraocular environment and the environment in cell culture. In an attempt to investigate some possible environmental factors, we performed some of our assays in the presence of different uveal ECM components, but did not see any changes in cell behavior as a result of this.

Testing our hypothesis that local environmental effects may be responsible for the apparent altered behavior of OM-uveal melanocytes could require creating a uveal co-culture or similar set of conditions that mimic the uveal environment closely enough to cause the OM-uveal melanocytes to behave as they do *in vivo*. As we have no way of determining which factors are more likely to be driving the behavioral difference seen in the OM-uveal melanocytes to design a specific assay, a more plausible next step in investigating the underlying causes of the disease would be to perform RNAseq analysis on uveal tissue from both affected and unaffected Cairn Terriers and look for differential expression of individual genes or pathways that relate to either melanogenesis or cell proliferation, and direct further cell studies once a putative pathway has been identified.

In conclusion, we demonstrated that the large pigmented cells present in the pigmented scleral plaques of OM-affected dogs are primarily melanocytes, and that the characteristic uveal melanocytes of OM-affected eyes produce greatly elevated levels of pigment in culture

initially, before equalizing with the level produced by control uveal melanocytes after several passages. Despite their apparently invasive phenotype *in vivo*, we did not find evidence of invasive behaviors *in vitro*. Identification of the causal mutation for ocular melanosis and altered gene expression in affected eyes may allow us to understand the mechanism underlying this phenotype.

3.6 Acknowledgements

We would like to thank Dr. Vilma Yuzbasiyan-Gurkan for cells that were used as controls in this paper. This research was supported by grants from the Foundation of the Cairn Terrier Club of America, the Myers-Dunlap Endowment for Canine Health, and Michigan State University College of Veterinary Medicine Endowed Research funds. We would also like to thank Stephanie Eldredge and Hillary Domenech-Barreto for their contributions to some of the cell culture assays.

REFERENCES

REFERENCES

1. Petersen-Jones SM, Forcier J, Mentzer AL. Ocular melanosis in the Cairn Terrier: clinical description and investigation of mode of inheritance. Vet Ophthalmol. 2007;10 Suppl 1:63-9.

2. Petersen-Jones SM, Mentzer AL, Dubielzig RR, Render JA, Steficek BA, Kiupel M. Ocular Melanosis in the Cairn Terrier: Histopathological description of the condition and immunohistological and ultrastructural characterization of the characteristic pigment-laden cells. Veterinary Ophthalmology. 2008;11:260-8.

3. Dawson-Baglien EM, Winkler PA, Bruewer AR, Petersen-Jones SM, Bartoe JT. Isolation and cultivation of canine uveal melanocytes. Vet Ophthalmol. 2015;18(4):285-90.

4. Wagner M, Bielby S, Rennie IG, Mac Neil S. Attachment of human uveal melanocytes and melanoma cells to extracellular matrix proteins involves intracellular calcium and calmodulin. Melanoma research. 1997;7(6):439-48.

5. Weisstein EW. Least squares fitting. 2002.

6. Hu DN, McCormick SA, Orlow SJ, Rosemblat S, Lin AY, Wo K. Melanogenesis by human uveal melanocytes in vitro. Investigative ophthalmology & visual science. 1995;36(5):931-8.

7. Hu DN. Methodology for evaluation of melanin content and production of pigment cells in vitro. Photochemistry and photobiology. 2008;84(3):645-9.

8. Liang CC, Park AY, Guan JL. In vitro scratch assay: a convenient and inexpensive method for analysis of cell migration in vitro. Nat Protoc. 2007;2(2):329-33.

9. Geback T, Schulz MM, Koumoutsakos P, Detmar M. TScratch: a novel and simple software tool for automated analysis of monolayer wound healing assays. BioTechniques. 2009;46(4):265-74.

10. Mosmann T. Rapid colorimetric assay for cellular growth and survival: application to proliferation and cytotoxicity assays. J Immunol Methods. 1983;65(1-2):55-63.

11. Denizot F, Lang R. Rapid colorimetric assay for cell growth and survival. Modifications to the tetrazolium dye procedure giving improved sensitivity and reliability. J Immunol Methods. 1986;89(2):271-7.

12. Schwab C, Wackernagel W, Grinninger P, Mayer C, Schwab K, Langmann G, et al. A Unifying Concept of Uveal Pigment Cell Distribution and Dissemination Based on an Animal Model: Insights into Ocular Melanogenesis. Cells Tissues Organs. 2016;201(3):232-8.

13. Aoki H, Yamada Y, Hara A, Kunisada T. Two distinct types of mouse melanocyte: differential signaling requirement for the maintenance of non-cutaneous and dermal versus epidermal melanocytes. Development. 2009;136(15):2511-21.

14. Li L, Hu DN, Zhao H, McCormick SA, Nordlund JJ, Boissy RE. Uveal melanocytes do not respond to or express receptors for alpha-melanocyte-stimulating hormone. Investigative Ophthalmology and Visual Science. 2006;47:4507-12.

15. Kapur RP, Bigler SA, Skelly M, Gown AM. Anti-melanoma monoclonal antibody HMB45 identifies an oncofetal glycoconjugate associated with immature melanosomes. J Histochem Cytochem. 1992;40(2):207-12.

16. Ghislin S, Obino D, Middendorp S, Boggetto N, Alcaide-Loridan C, Deshayes F. LFA-1 and ICAM-1 expression induced during melanoma-endothelial cell co-culture favors the transendothelial migration of melanoma cell lines in vitro. BMC Cancer. 2012;12:455.

CHAPTER 4

OCULAR MELANOSIS LOCUS MAPPING AND CANDIDATE GENE SEQUENCING

4.1 Introduction

Ocular melanosis (OM) is an inherited eye disease of Cairn terrier dogs that is characterized by a bilateral proliferation of uveal melanocytes (1, 2). These melanocytes frequently migrate to abnormal areas of the eye, such as the sclera. Additionally, many dogs with late-stage OM develop glaucoma as a result of the eye's anterior drainage angles becoming blocked by pigmented material and cell debris, preventing the normal draining of the aqueous humor (1).

Ocular melanosis only began to reported in Cairn terrier populations relatively recently (the first cases were reported in 1984) but nonetheless is present in a significant proportion of the overall population (3, 4). This suggests that the disease is probably the result of a single mutation that arose once in a popular sire dog that spread through the breed by means of a founder effect (1). Initial candidate gene-based attempts to map the causative locus for OM examined 11 genes known to have a role in melanocyte and melanosome development or known to be associated with other pigmentation-related diseases, including a pair of genes (*Gpnmb* and *Tyrp1*) which have known mouse variants that, together, produce a mouse phenotype which strongly resembles OM as seen in Cairn terriers (5, 6). Examination of SNP and microsatellite markers near these genes showed that no single common allele was present in all OM-affected Cairn terriers for any of these 11 genes. As pedigree analysis has shown OM to be autosomal dominant, the lack of a common shared allele at these 11 loci provides evidence to exclude the loci as harboring a variant causative for OM (1, 5).

With failure of the initial candidate gene approach, we decided to take a whole-genome approach to identifying regions of the genome potentially linked to OM. Here, we report the results of a two-stage genome-wide association study performed on 94 total Cairn terriers (62 affected, 32 unaffected) using the Illumina CanineHD Beadchip system to genotype each dog at over 170,000 evenly spaced SNP markers across the canine genome. This approach identified a 7.5 megabase (Mb) region of chromosome 11 significantly associated with OM.

4.2 Materials and methods

4.2.1 Sample collection

All DNA used in this study was extracted from blood samples of Cairn terriers donated with the consent of the dog's owner. DNA was extracted using a modified version of Qiagen's PureGene commercial DNA extraction kit (Qiagen, Germantown, MD). Briefly, DNA was mixed twice with a red blood cell lysis buffer (0.32 M sucrose, 5 mM $MgCl_2$, 1% Triton-X 100, 10 mmM Tris-HCl, pH 8.0, filter sterilized) to remove red blood cell contamination. The remaining cells were pelleted and dissolved in PureGene cell lysis solution (Qiagen) to lyse white blood cells. PureGene protein precipitation solution (Qiagen) was added to remove protein. The DNA-containing supernatant was mixed with isopropanol to precipitate DNA and washed with 70% ethanol before ultimately being resuspended in DNA hydration buffer (Qiagen).

4.2.2 Whole-genome canine SNP array

For our whole-genome SNP array, we genotyped a total of 96 Cairn terriers (94 unique dogs, 2 dogs which were genotyped twice to assess reproducibility) using the Illumina CanineHD Genotyping BeadChip. We utilized two different vendors to perform this genotyping – GeneSeek (Lincoln, Nebraska) performed genotyping on an initial 48 samples using a model of the Illumina CanineHD BeadChip which used 173,662 single-nucleotide polymorphism markers (SNPs). The second 48 samples were genotyped by the University of Minnesota Genomics Core Facility (Minneapolis, Minnesota) using a newer model of the BeadChip with 220,853 markers, including all of the original 173,662 markers on the previous BeadChip. Of the 94 dogs genotyped, 62 were diagnosed as OM-affected, and 31 were unaffected control cairn terriers.

One dog possessed an atypical phenotype which superficially resembled OM but was missing several key indicators. All dogs used for genotyping are shown in Table 4.1. Since OM has a highly variable age of onset, the oldest unaffected Cairn terriers that had been examined by a veterinary ophthalmologist and shown not to have any clinical indications of OM and were therefore most likely to be true unaffecteds, were used as controls. The ages of the unaffected dogs used for controls ranged from 7 to 16 years, with a mean age of 11.9 years (Table 4.1). All 62 affected dogs that were used in this study had been diagnosed by a veterinary ophthalmologist as being OM-affected. When selecting OM-affected samples for genotyping, preference was given to more severely affected samples, as it was thought that the high variability seen in the OM phenotype might be due to zygosity differences in affected Cairn terriers.

Table 4.1 - Dogs used in GWAS study

Dog	OM Status	Age at Last Exam	Sex	Glaucoma Status
CA2	A	12	F	Yes
CA6	A	9	F	Yes
CA12	A	12	F	No
CA13	U	15	F	No
CA16	A	11	F	Yes
CA23	A	13	M	No
CA28	A	8	M	Yes
CA36	A	12	F	No
CA43	A	9	F	Yes
CA44	A	5	M	Yes
CA45	U	11	M	No
CA52	U	13	F	No
CA54	U	9	F	No
CA57	U	12	M	No
CA66	A	14	F	No
CA68	A	11	F	Yes
CA76	A	11	M	No
CA81	U	9	F	No
CA90	A	12	M	Yes
CA124	U	13	M	No
CA138	A	13	F	No
CA142	U	9	F	No
CA148	A	11	F	Yes
CA150	A	10	M	Yes
CA158	A	15	F	Yes
CA167	A	14	M	No
CA175	A	9	F	Yes
CA178	U	9	F	No
CA188	A	13	F	Yes
CA190	A	10	F	Yes
CA193	U	10	F	No
CA194	A	14	M	No
CA195	A	12	F	No
CA196	U	9	F	No
CA197	U	15	M	No
CA198	U	12	M	No
CA204	U	12	F	No
CA208	A	10	F	No
CA216	A	10	M	Yes
CA217	A	11	M	Yes
CA229	U	16	M	No
CA239	A	11	F	No
CA240	A	14	M	Yes
CA245	U	15	F	No
CA251	U	13	F	No
CA314	A	12	F	No
CA318	U	11	M	No
CA366	U	7	F	No
CA367	U	10	M	No
CA369	U	12	M	No
CA370	U	12	F	No
CA374	U	12	F	No
CA390	U	14	M	No
CA393	U	13	F	No
CA394	U	13	M	No
CA405	A	12	F	No
CA423	A	8	M	No
CA424	A	14	F	Yes

Table 4.1 (cont'd)

Dog	OM Status	Age at Last Exam	Sex	Glaucoma Status
CA483	A	Unknown	F	Unknown
CA486	A	13	F	No
CA488	A	9	F	No
CA489	A	12	F	Yes
CA490	A	12	M	Yes
CA491	A	8	M	No
CA494	A	10	M	Yes
CA509	A	12	F	Yes
CA511	A	8	F	Yes
CA518	A	10	F	Yes
CA524	A	9	F	Yes
CA540	U	11	F	No
CA541	A	10	F	Yes
CA558	U	16	M	No
CA582	A	10	F	Yes
CA593	U	14	F	No
CA595	A	16	F	No
CA599	A	12	M	No
CA602	U	16	F	No
CA605	A	10	M	No
CA606	A	12	F	Yes
CA611	U	7	M	No
CA614	A	14	F	Yes
CA615	A	14	M	Yes
CA616	A	11	F	Yes
CA617	A	12	F	Yes
CA618	A	10	F	Yes
CA619	A	18	M	Unknown
CA620	A	10	M	Yes
CA622	A	12	M	Yes
CA624	A	8	F	Yes
CA625	A	13	F	Yes
CA626	A	16	F	No
CA628	A	11	M	Yes
CA630	A	9	M	Yes
CA631	Atypical	6	M	Yes

4.2.3 Data analysis

Whole-genome SNP data was initially analyzed using the PLINK statistical software package (7). Quality cutoffs used for this data analysis removed SNPs with a minor allele frequency (MAF) of less than 5% or which were missing calls in greater than 10% of all samples genotyped. Dogs which genotyped at less than 90% of all possible SNPs were excluded from analysis as low-quality samples. Analysis was carried out using PLINK's standard case/control association test as well as PLINK's model-based association test, with correction for multiple testing carried out using the max(T) permutation procedure with 10,000 permutations. In order to control for population stratification, the program GEMMA was used to estimate a centered relatedness matrix from the genotypes for each phenotype, and the association test was performed again using the same screening criteria for SNPs with a univariate linear mixed model with the relatedness matric, phenotype, genotype, and sex all taken into account as factors, and the Wald frequentist test being used to test for significance (8-11).

4.2.4 PCR-RFLP genotyping

The UCSC genome browser (https://genome.ucsc.edu/) canfam3 reference sequence was used to retrieve sequence information near known SNPs. The webtool NEBcutter was used to determine whether the SNP being investigated led to the loss or gain of a restriction enzyme cut site (http://www.labtools.us/nebcutter-v2-0/). Primers flanking the area to be amplified were designed using the Primer3 online primer design tool (http://bioinfo.ut.ee/primer3-0.4.0/).

4.2.5 Sanger sequencing of candidate genes

The UCSC genome browser (https://genome.ucsc.edu/) canfam3 reference genome was used to retrieve the exon sequence data for genes of interest. Primers were designed flanking each exon using the Primer3 online primer design tool (http://bioinfo.ut.ee/primer3-0.4.0/). Sanger sequencing of fragments was carried out by the MSU Research Technology Support Facility (RTSF) using both the forward and reverse primers, and the resulting sequence data analyzed using the program Sequencher (Gene Codes Corporation, Ann Arbor, Michigan). A total of three affected and three unaffected dogs were sequenced for each gene.

4.3 Results

4.3.1 Genome wide SNP array

The total number of markers shared between the two SNP arrays that survived the pruning conditions described above was 118,937. The filters removed 4,657 SNPs due to low genotyping rate (> 10% of samples not genotyped) and 50,065 SNPs due to low minor allele frequency (MAF < 5%). Of the 94 dogs genotyped, 88 dogs passed the genotyping rate threshold (61 affected dogs, and 27 unaffected dogs). The total genotyping rate for the 88 remaining dogs was >99.4%. Dogs number CA13, CA36, CA142, CA370, CA374, and CA394 were filtered out for genotyping rates of less than 90%. Initial naïve analysis using PLINK had an elevated genomic inflation factor (1.69) which was corrected for using GEMMA. Following this correction, the genomic inflation factor was reduced to 1.10, which is below the level at which further adjustment for population stratification is generally required, especially as small increases in genomic inflation factor can be caused by true associations, and this effect is more pronounced in animals like dogs with large linkage disequilibrium blocks (12-14).

According to the Bonferroni correction for multiple testing, the genome-wide significance threshold for a test involving 118,937 markers is $p < 4.2 \times 10^{-7}$. Twenty-four SNPs from the combined BeadChip data had p-values below this threshold, ranging from 1.32×10^{-7} to 4.17×10^{-7}. These SNPs formed a continuous block on chromosome 11, delineating a ~7.5 megabase (Mb) region that was associated with the OM phenotype at statistically significant levels, chr11:43,919,606-51,409,494 in the canfam3 build. No SNPs from other areas of the genome reached statistical significance (Figure 4.1), although many more SNPs from

throughout the 7.5 Mb region approached genome-wide significance. No significant differences were observed when comparing the glaucoma-only population of dogs with either the non-glaucoma affected dogs or the unaffected dogs.

Examination of the transcripts annotated on both the dog and human genomes, the 7.5Mb region contains a total of 82 putative transcribed elements, some of which have multiple documented splice variants. About a third of these are Ensemble protein predictions with no supporting documentation or predicted function. There are 12 genes in the region that have been validated in dog as part of the RefSeq gene database, and an additional 32 predicted canine genes that have been validated as RefSeq genes in other species.

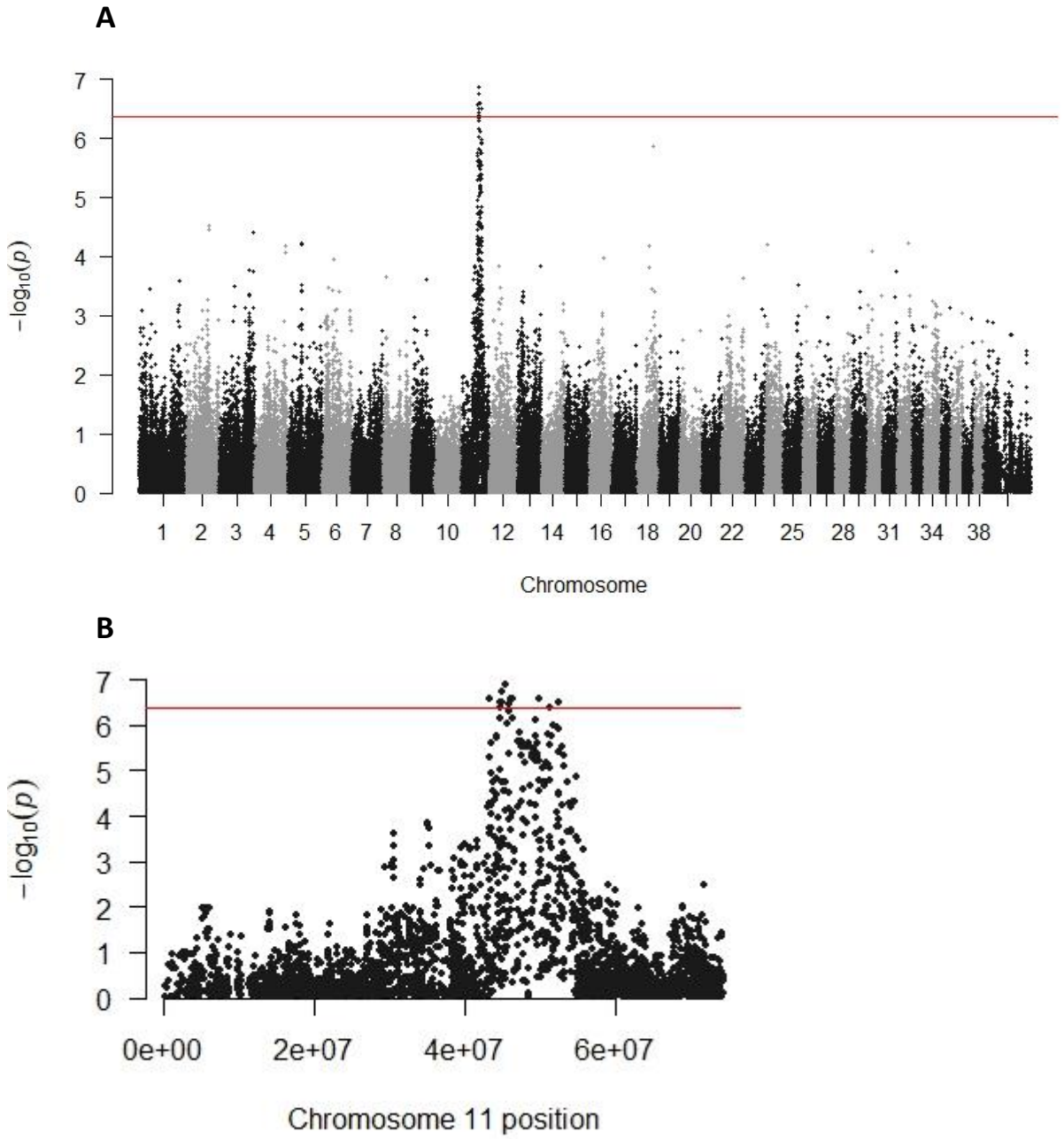

Figure 4.1 – Manhattan plots of p-values A. Manhattan plot of the –log of the p-values plotted against the genomic location for each of the 118,937 SNP markers genotyped in 88 dogs from the Illumina CanineHD BeadChip. The red line represents statistical significance (-log(4.2×10^{-7})). B. Manhattan plot of chromosome 11 only. The red line represents statistical significance.

4.3.2 Population SNP genotyping

To determine how common this haplotype was within the entire population of OM-affected dogs, it was decided to genotype one SNP located within this cluster of significant SNPs in all dogs in our database. To select this SNP, flanking primers (Table 4.2) were designed around five candidate SNPs located near the SNP with the lowest p-value as determined by PLINK, and 10 OM-affected and 10 unaffected Cairn terriers that had not been part of the SNP array (Table 4.3) were genotyped via Sanger sequencing. These SNPs were perfectly concordant in all 20 dogs, the OM affected dogs all being heterozygous for the OM-associated SNP, and the unaffected dogs all being homozygous for the SNP not associated with OM. The remaining Cairn terrier samples that we have registered in our database were genotypes at the SNP with genomic position chr11:46,303,228 (Table 4.4), where the variant associated with the affected phenotype introduces a HpyCH4IV cut site. The majority of the affected dogs we have in our database (72/83, 86.7%) have at least one copy of the allele thought to be linked to the dominant causative mutation. A lower percentage of unaffected dogs (131/184, 71.2%) were homozygous for the allele thought to correspond to recessive normal phenotype. Much of the discordance in the unaffected dog population may be due to the high variability of OM's age of onset – we have many younger Cairn terriers in our database that currently show no signs of OM and are therefore provisionally listed as unaffected, but who may end up developing the disease later in life. A chi-square test comparing the allele frequencies of these two populations produced a p-value < 0.0001, confirming the linkage we had observed with the genome-wide SNP array.

Table 4.2 – SNPs tested in trial genotyping

SNP Location	Ref. Allele	Var. Allele	F Primer	R Primer	Fragment Size
chr11:46303175	G	A	tgggacctaagtcacagtgg	atcgcatctcagcttccatt	248
chr11:46303228	C	T	tgggacctaagtcacagtgg	atcgcatctcagcttccatt	248
chr11:46413975	A	C	gaagaggtgcctttctctgc	ggcctctggagtagctgttg	221
chr11:46345226	G	A	ttgttgcagatttgatttgga	ttctgccaacctcagattctc	296
chr11:46424658	C	T	aagcagactagagatgaggctgt	gtgtgccttagcaattgtgg	224

Table 4.3 – Dogs tested in trial genotyping

OM Affected	OM Unaffected
CA570	CA526
CA548	CA519
CA539	CA514
CA540	CA243
CA551	CA239
CA552	CA220
CA556	CA511
CA571	CA250
CA402	CA485
CA527	CA421

Table 4.4 – **Population-wide SNP genotyping results** (A) represents the allele believed to be linked to the dominant OM causal gene, (a) represents the recessive wild type unaffected

Affected Status	Genotype	Number of Dogs
Unaffected	**AA**	10
	Aa	43
	aa	131
Affected	**AA**	17
	Aa	55
	aa	11

4.3.3 Candidate gene selection

Examining the 7.5 Mb region, several genes within and near the region were considered to be potential positional candidate genes. The SNPs with the highest p-values were located within the introns of *LINGO2* (leucine-rich repeat and Ig Domain Containing 2), a developmental gene thought to be restricted to neuronal tissue with several known variants that are associated with Parkinson's disease and essential tremor (15, 16). Although *LINGO2* did not seem like a good candidate gene based on the phenotypes of the diseases it is known to be associated with, we selected it for sequencing because the most highly significant SNPs were located within it. Also within the region is *ACO1* (aconitase 1), a gene which codes for a TCA-cycle enzyme that also plays a role in the regulation of cellular iron levels. Inherited mutations in *ACO1* have been linked to an increased risk of cutaneous melanoma in humans, although the mechanism by which ACO1 mutations can contribute to melanoma development is largely speculative at this time (17). Finally, *CDKN2A* was also selected for sequencing. Although upstream of the significantly associated region by about 1.5 Mb (chr11:44225749-41264280), *CDKN2A* represented by far the best candidate gene near the region identified by the genome-wide SNP array. *CDKN2A* codes for two different proteins, p16INK4a and p14arf, inhibitors of cyclin-dependent kinases CDK4 and CDK6. By blocking the activity of these proteins, the products of *CDKN2A* block the cell's transition into S phase. It is a tumor suppressor gene, mutations in which have been linked to high-penetrance familial melanoma, as well as many other cancers (18, 19). Given the migratory behavior of OM melanocytes, and the general proximity to the region identified by our genome-wide SNP array, *CDKN2A* appeared to be a very good candidate, and so its coding region was sequenced as well.

Table 4.5 – Primers for *LINGO2* sequencing

Name	F Primer	R Primer	Amplicon Size
Exons 1-3	tactcggcatccctcctaga	tcctctcttcctctggctga	453
Exon 4	aaggaaaagctcggactcgt	ccggggagatcatcctaact	197
Exon 5	ttcccaagagtttttgtttca	cattctccaaaggccaacat	175
Exon 6	gctggacctaggacatggtt	tgatcagatgccttcctcaa	250
Exon 7 pt. 1	tcttctcttcctgccttctcc	ttgagatgcttcagatgtaggc	696
Exon 7 pt. 2	atatgcccgtgtatgccttt	ggtgtcacccaggaaatcac	697
Exon 7 pt. 3	gctagtggatgaagggcaga	cttccatggaccctgcttt	691
Exons 8-13	tgagacagctggcacagtaaa	catatctccgcccatagctc	599
Exons 14-16	ggcggagatatgcagaatga	gcattccaattcttgatctcc	390

Table 4.6 – Primers for *ACO1* sequencing

Name	F Primer	R Primer	Amplicon Size
Exon 1	aggttcctgaggtccagctt	gactcttgattgctgtgagaaca	231
Exon 2	tgctttctccttttttccctaga	gacaagggaggcagtgaaga	236
Exon 3	gtggaggcaaaagctgaaaa	gaaaacccaagtatccgtcct	246
Exon 4	agcaagcctgcagacaaagt	atctcctcggcacctctctt	249
Exon 5	gtgttctttccattctcaatcct	acagaataggatcctggaacaa	238
Exon 6	agcatccttgtgtcatgctg	gtgcacttcctccctgtcac	230
Exon 7	tggagtctcaagtttttctcttgtt	actttgcacagggcattctg	248
Exon 8	tcatcacgaaatcctaatgtctgt	gaggaaatgcacgctctctc	179
Exon 9	gtccgttcctgagctcctta	ttcctcatcagagggtgaaaa	249
Exon 10	tctcagccagtgacttttgtt	gagggattcacatgcactca	351
Exon 11	ttgtcggtgtttacattgcac	aagctgacacatgctacaagg	249
Exon 12	attccccacattgctgttct	ggctcctctgcaattacctg	209
Exon 13	ccttctctgggtgacctgat	tagctgcacaaatgcaacct	220
Exon 14	ggctggatgtgatcatgaaa	acgcaggaaggcagagtg	225
Exon 15	gaatggaatgtgattagatttgct	tcaaagcaagggcaaagagt	249
Exon 16	actgacccgctgtgttcttt	gccttagtccttctccgtca	199
Exon 17	tttgctccggtcactaacct	accacccagaggctgataaa	228
Exon 18	ccttgcttttctcgtcctca	tcaccactcgagggaaagc	242
Exon 19	gtcctgtcttggctcctcag	ttccactcatttctcggtga	290
Exon 20	cctccctgattgtcctctgtt	gctggctagtggcgcttc	212
Exon 21 and 22	gtgtgctgcccacgtcac	tgtcagtcagccccactgta	338
Exon 23 and 24	cacggtaggcgaacacttg	tccaaaaccacctccaaagt	250

Table 4.7 – Primers for *CDKN2A* sequencing

Name	F Primer	R Primer	Amplicon Size
Exon 1	gcagagcggctccgagat	ggaggcctttcttacctgct	405
Exon 2	ctgtccctgtcctgaccact	ggaagctctccgagttccaa	381

Table 4.8 – Dogs for candidate gene sequencing

Name	OM Status	Sex	Age
CA318	Unaffected	M	11
CA366	Unaffected	F	13
CA367	Unaffected	M	15
CA489	Affected	F	15
CA490	Affected	M	14
CA494	Affected	M	11

4.3.4 Sanger sequencing results

The three candidate genes selected on the basis of the genome-wide SNP array were all sequenced in three affected and three unaffected dogs. No coding region variation was detected in any of the exons that segregated with the phenotype or was present in all sequenced affected dogs.

4.4 Discussion

A genome-wide association assay identified a 7.5 Mb portion of chromosome 11 that is significantly associated with the ocular melanosis phenotype. Although there was genomic inflation suggestive of population stratification present in the initial sample of 88 dogs that remained after removing dogs with low quality scores, the region remained significantly associated with OM even after correcting for this. A single SNP located in the most statistically significant region was genotyped in all dogs present in our database, and was present in one or two copies in 86.7% (72/83) of all dogs affected with OM. Although that is a very high percentage, the fact that 11 of 83 affected dogs did not have the marker indicates that even the most significant SNPs from our mapping study are not completely linked with the disease. We have been unable to find a marker which is completely linked with the affected phenotype (data not shown). This suggests four possibilities: 1. that some of the samples we have listed as OM affected have been mislabeled and are not true affected dogs, 2. that some of them have been misdiagnosed, 3. that environmental effects are producing a phenocopy in some dogs, and 4. that there is genetic heterogeneity. Mislabeling may happen due to human error, although it is unlikely that nearly 15% of our affected dog samples have been misfiled. Misdiagnosis is also a possibility, as OM can be very difficult to detect in earlier stages, although the OM phenotype becomes quite dramatic as the disease progresses. Typically, misdiagnoses will be unaffected dogs which are incorrectly called as affected. Many of the discordant affected dogs had advanced OM, making a misdiagnosis in those cases unlikely. It is also possible that environmental factors could create a phenocopy of OM – although rare, a disease with similar clinical signs to OM has been observed in other breeds. Our lab has received

samples from a spitz, a Jack Russel terrier, a Staffordshire terrier, two boxers and two Labrador retrievers that display similar clinical signs to OM. These breeds are quite diverse, and none have a documented history of a heritable OM-like condition, suggesting the cause may be environmental rather than genetic. Finally, genetic heterogeneity of the disease in Cairn terriers seems more likely in light of a dog (CA 631) that was recently examined at MSU after previously having been diagnosed as OM affected elsewhere (this dog was included on a whole-genome SNP array). Upon examination by Dr. Petersen-Jones, it became apparent that while the dog presented some of the clinical signs commonly seen in OM, such as glaucoma and pigmentation, the dog did not have a thickened iris root which has been considered a diagnostic sign. This could perhaps be a phenocopy as suggested earlier, but it could also indicate that there is genetic heterogeneity as is seen in many other hereditary conditions in dogs. This would greatly complicate genetic analysis of the disease. However, even with those potentially confounding factors, we were able to map a region of the genome which is associated with the disease.

Despite finding a genomic region significantly associated with OM, we have so far been unable to identify the causative mutation via a candidate gene approach. Several genes within the mapped locus could plausibly contribute to the phenotype seen in OM based on their annotated function, but those that had no coding region variation that was shared between all affected dogs. Many genes within the region have very little annotation information, and none of the remaining well-annotated genes have a function that suggests they would be good candidates. Our next step at this stage was to perform next-generation sequencing of the genome of several affected and unaffected Cairn terriers, as this would allow us to examine all

remaining exonic variation as well as to look for variation in intronic and regulatory sequences within the region, and also to interrogate regions of the genome other than our mapped region.

REFERENCES

REFERENCES

1. Petersen-Jones SM, Forcier J, Mentzer AL. Ocular melanosis in the Cairn Terrier: clinical description and investigation of mode of inheritance. Vet Ophthalmol. 2007;10 Suppl 1:63-9.

2. Petersen-Jones SM, Mentzer AL, Dubielzig RR, Render JA, Steficek BA, Kiupel M. Ocular melanosis in the Cairn Terrier: histopathological description of the condition, and immunohistological and ultrastructural characterization of the characteristic pigment-laden cells. Vet Ophthalmol. 2008;11(4):260-8.

3. Covitz D, Barthold S, Diters R, Riis R. Pigmentary glaucoma in the cairn terrier. Transactions of the Fifteenth Annual Scientific Program of the American College of Veterinary Ophthalmologists. 1984:246-50.

4. America CTCo. Cairn Terrier Club of America 2005 Breeder-Owner Survey. 2005.

5. Winkler PA, Bartoe JT, Quinones CR, Venta PJ, Petersen-Jones SM. Exclusion of eleven candidate genes for ocular melanosis in Cairn terriers. J Negat Results Biomed. 2013;12:6.

6. Anderson MG, Smith RS, Hawes NL, Zabaleta A, Chang B, Wiggs JL, et al. Mutations in genes encoding melanosomal proteins cause pigmentary glaucoma in DBA/2J mice. Nat Genet. 2002;30(1):81-5.

7. Purcell S, Neale B, Todd-Brown K, Thomas L, Ferreira MA, Bender D, et al. PLINK: a tool set for whole-genome association and population-based linkage analyses. Am J Hum Genet. 2007;81(3):559-75.

8. Persson ME, Wright D, Roth LSV, Batakis P, Jensen P. Genomic Regions Associated With Interspecies Communication in Dogs Contain Genes Related to Human Social Disorders. Scientific Reports. 2016;6:33439.

9. Zhou X, Stephens M. Genome-wide Efficient Mixed Model Analysis for Association Studies. Nature genetics. 2012;44(7):821-4.

10. Devlin B, Roeder K. Genomic Control for Association Studies. Biometrics. 1999;55(4):997-1004.

11. Eu-ahsunthornwattana J, Miller EN, Fakiola M, Wellcome Trust Case Control C, Jeronimo SMB, Blackwell JM, et al. Comparison of Methods to Account for Relatedness in Genome-Wide Association Studies with Family-Based Data. PLoS Genetics. 2014;10(7):e1004445.

12. Melum E, Franke A, Karlsen TH. Genome-wide association studies - A summary for the clinical gastroenterologist. World Journal of Gastroenterology : WJG. 2009;15(43):5377-96.

13. Clayton DG, Walker NM, Smyth DJ, Pask R, Cooper JD, Maier LM, et al. Population structure, differential bias and genomic control in a large-scale, case-control association study. Nat Genet. 2005;37(11):1243-6.

14. Lindblad-Toh K, Wade CM, Mikkelsen TS, Karlsson EK, Jaffe DB, Kamal M, et al. Genome sequence, comparative analysis and haplotype structure of the domestic dog. Nature. 2005;438(7069):803-19.

15. Vilariño-Güell C, Wider C, Ross OA, Jasinska-Myga B, Kachergus J, Cobb SA, et al. LINGO1 and LINGO2 variants are associated with essential tremor and Parkinson disease. Neurogenetics. 2010;11(4):401-8.

16. Wu Y-W, Prakash K, Rong T-Y, Li H-H, Xiao Q, Tan LC, et al. Lingo2 variants associated with essential tremor and Parkinson's disease. Human genetics. 2011;129(6):611-5.

17. Yang XR, Liang X, Pfeiffer RM, Wheeler W, Maeder D, Burdette L, et al. Associations of 9p21 variants with cutaneous malignant melanoma, nevi, and pigmentation phenotypes in melanoma-prone families with and without CDKN2A mutations. Fam Cancer. 2010;9(4):625-33.

18. Hayward NK. Genetics of melanoma predisposition. Oncogene. 0000;22(20):3053-62.

19. Borg Ak, Sandberg T, Nilsson K, Johannsson O, Klinker M, Måsbäck A, et al. High Frequency of Multiple Melanomas and Breast and Pancreas Carcinomas in CDKN2A Mutation-Positive Melanoma Families. JNCI: Journal of the National Cancer Institute. 2000;92(15):1260-6.

CHAPTER 5

WHOLE-GENOME SEQUENCING OF OCULAR MELANOSIS-AFFECTED CAIRN TERRIERS

5.1 Introduction

Ocular melanosis (OM) is an inherited eye disease commonly seen in the Cairn terrier dog breed. This disease is characterized by a bilateral proliferation of densely pigmented melanocytes, both within the uvea and in other areas of the eye such as the sclera and episclera (1, 2). According to pedigree analysis, the disease shows an autosomal dominant mode of inheritance, and the fact that the disease appeared relatively recently in a single breed of dog (the disease was first reported in 1984) suggests that the disease is caused by a single mutation which has been propagated throughout the breed by means of a founder effect (3).

Previous attempts to identify a causative gene for OM based on a candidate gene approach were unsuccessful (4). Our previous studies using whole-genome SNP array genotyping on a set of 94 Cairn terriers (see Chapter 4) allowed us to identify a 7.5 megabase (Mb) region on chromosome 11 that was significantly associated with the disease, however, there were no genes within our region whose function suggested them as obvious candidates. Sanger sequencing was performed on several genes within the region near the most strongly associated SNPs, as well as several genes that had previously been shown to have some connection to pigmentation or cell migratory disorders, but none of these genes showed any coding-region variation that segregated with the OM phenotype.

Without a specific target to examine, we decided to perform whole-genome sequencing (WGS) to look for the causative variant in OM, focusing most intently on genes within our previously identified region and genes known to be involved in pigmentary disorders. We initially sequenced 6 dogs using traditional PCR-based WGS, and added another 4 dogs

sequenced via PCR-free WGS, as PCR-free methods have been shown to have more even coverage of the genome and to provide better coverage of GC-rich regions that can be poorly represented using PCR-based methods (5).

5.2 Materials and methods

5.2.1 Sample collection

To ensure the highest quality DNA for sequencing and to ensure that no sample mix-ups had occurred, the owners of all dogs sequenced in this study were asked to submit a fresh blood sample from their dog, which was extracted immediately prior to sequencing using the DNA extraction protocol outlined in Chapter 4.

5.2.2 Whole-genome sequencing

Whole-genome sequencing was carried out on 10 total dogs (5 affected and 5 unaffected, see Table 5.1 for a complete list of dogs used). Sequencing was carried out using two different protocols, one using traditional PCR-based methods for library creation, and the other using PCR-free methods. Six samples (3 affected and 3 unaffected) were sent to DNA LandMarks for library preparation and sequencing (DNA LandMarks, Saint-Jean-sur-Richelieu, Quebec, Canada). Library preparation was carried out using the Illumina TruSeq kit (Illumina, San Diego, CA), and the samples were run on 4 lanes of an Illumina HiSeq 2500 sequencer (Illumina) in 100bp paired-end mode. Each affected sample was run as an individual lane, resulting in an average coverage of ~12X. The three unaffected samples were pooled and sequenced across a single lane, resulting in an average per-sample coverage of ~4X. The sequencing of the remaining 4 dogs (2 affected and 2 unaffected) was carried out at the University of Minnesota Genomics Core Facility (University of Minnesota, Minneapolis, Minnesota). Library preparation was carried out using the Illumina TruSeq PCR-Free library preparation kit (Illumina), and sequencing was performed on an Illumina HiSeq 2500 sequencer

(Illumina) using v4 chemistry in 125bp paired-end mode. One sample (CA229) was sequenced on a half-lane of a high-output flow cell, resulting in an average coverage of ~26X. The remaining three samples were pooled and run on a single lane of a high-output flow cell, resulting in an average coverage of ~17X.

Table 5.1 – Dogs used for whole-genome sequencing

Dog	OM Status	Age and Sex	Library Prep Method
CA189	Unaffected	16,M	TruSeq PCR-Free
CA204	Unaffected	12,F	TruSeq
CA229	Unaffected	16,M	TruSeq PCR-Free
CA488	Affected	9,F	TruSeq
CA491	Affected	8,M	TruSeq
CA511	Affected	8,F	TruSeq
CA593	Unaffected	14,F	TruSeq
CA602	Unaffected	16,F	TruSeq
CA628	Affected	11,M	TruSeq PCR-Free
CA630	Affected	9,M	TruSeq PCR-Free

5.2.3 Data analysis

NGS data was analyzed using two pipelines. The first pipeline was used on the 6 dogs which used PCR-based library preparation methods. The first step in sequencing involved using Sickle (https://github.com/najoshi/sickle) at default settings in paired-end mode to trim low quality score reads, reads containing multiple Ns, and very short reads. Read alignment to the genome was performed using SHRiMP (http://compbio.cs.toronto.edu/shrimp/) (6). SAMtools (http://www.htslib.org/) was used to convert the SAM alignment files these programs produced and convert them to BAM files (7). Variant calls were performed using the Freebayes toolset (8, 9) with a minimum coverage filter of 2. Annotation of called variants was done using ANNOVAR

and SnpEff (10, 11). SOAPsv (http://soap.genomics.org.cn/SOAPsv.html) was used to examine the genome for structural variation according to the program documentation (12). Finally, mapped reads from the 7.5 Mb region of interest ± 1.5 Mb were extracted and examined manually in the integrative genome viewer (IGV) to look for small indels that algorithm-based variant callers sometimes have difficulty detecting (13).

Later, all data (both the original PCR-based data and the new PCR-free data) was also analyzed according to the GATK Best Practices handbook as of June 2016 (figure 5.1). Raw FASTQ files were trimmed using Trimmomatic (http://www.usadellab.org/cms/?page=trimmomatic) to remove Illumina sequence adapters, remove reads shorter than 25 bp, to remove runs of leading or trailing bases with quality scores below 2, and to scan reads with a 4 bp window and trim where the average quality score drops below 3 (14). These reads were then mapped to the reference using the BWA-MEM Burrows-Wheeler aligner (http://bio-bwa.sourceforge.net/) (15). The PicardTools package (https://broadinstitute.github.io/picard/) was used to add read group information and mark optical duplicates. Base quality score recalibration was done using the BQSR tool in the genome analysis toolkit (GATK) (8). Calling of variants was done using GATK's Haplotypecaller in GVCF mode. At this point, the per-sample GVCFs were combined for joint genotyping using the

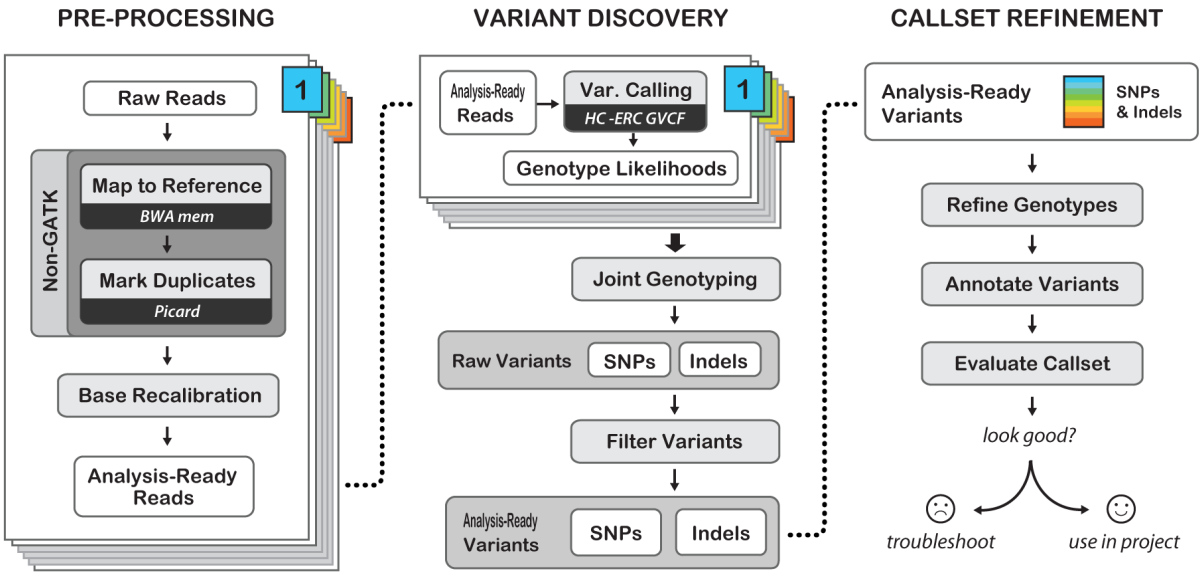

Figure 5.1 – Whole-genome sequencing pipeline according to GATK best practices handbook Reproduced from: (https://software.broadinstitute.org/gatk/best-practices/bp_3step.php?case=GermShortWGS) on June 2016

GenotypeGVCFs tools and variants were filtered according to the following criteria: SNPs were dropped if quality by depth (QD) was less than 2.0, Fisher Strand (FS) Bias Score greater than 60.0, Mapping Quality Rank Sum Test (MQRankSum) score was less than -12.5, Root Mean Square mapping quality (MQ) was less than 40.0, of alternate allele Rank Sum Test (ReadPosRankSum) was less than -8.0, and if the stand odds ratio (SOR) was greater than 3.0. Indels were dropped if QD was less than 2.0, if FS was greater than 200, ReadPosRankSum was less than -20.0, or SOR was greater than 10.0. Called variants were annotated using ANNOVAR and SnpEff (10, 11).

Once variants were called, two primary screening methods was used to examine them. Variants within 1.5 Mb of the previously mapped 7.5 Mb region of interest were examined for variants that would cause a coding region or splicing change. The list of whole-genome variants

was also compared to a list of genes from the Color Genes database, an online resource containing location information on 171 mapped genes that have been shown to be associated with pigmentation changes in mice, humans, and zebrafish. An additional database of annotated canine non-coding RNAs was provided to us by the Broad Institute was also used in these screenings.

5.2.4 Sanger sequencing of candidate genes

Sanger sequencing of regions of interest was carried out according to the protocol previously described in Chapter 4.

5.3 Results

5.3.1 PCR-based results

In total, there were 22,931 unique variants identified within the 7.5 Mb region of interest ± 1.5 Mb across all 6 dogs genotyped. The vast majority of these, 17,197, were intergenic variants. Of the total variants present, 1,943 (1,826 intergenic variants) were present in all affected dogs. Once variants were screened to remove any variants which were also present in at least one unaffected dog sample, the total number of variants was reduced to 1,155 – 1,154 intergenic variants, and a single variant present in a long non-coding RNA, lncRNA 32, a gene which had been identified as a putative tumor suppressor gene based on data from mouse cell line expression data (16, 17). This variant (chr11:45,414,338-45,414351) was called as containing a single base-pair insertion within an intron, converting a run of 13 adenine residues to a run of 14 adenine residues. Sanger sequencing of an additional 20 dogs (13 affected, 7 unaffected) showed that dogs were often heterozygous for this region, having runs of 11-15 adenine residues within the indicated intron (F Primer: TTTTTCGGTTGCCTTCATTC, R Primer: CCTCGGTCCCCTCTAATCTT, 192 bp amplicon). No particular sequence length segregated with the disease phenotype, and the region was not predicted to have any impact on splicing.

Table 5.2 – Dogs tested for variation in lncRNA32

Dog Number	OM Status	Age	Sex
CA483	A	Unknown	F
CA486	A	13	F
CA489	A	12	F
CA509	A	12	F
CA519	A	10	F
CA524	A	10	F
CA525	A	12	M
CA576	U	15	F
CA577	U	11	M
CA578	U	16	F
CA593	U	14	F
CA595	A	15	F
CA596	U	13	M
CA602	U	13	F
CA604	U	13	F
CA614	A	13	F
CA615	A	11	M
CA616	A	11	F
CA617	A	12	F
CA619	A	18	M

Fifteen coding-region variants were detected in 10 different genes (*Apc*, *Frem2*, *Pcbd1*, *Fgfr2*, *Ntrk1*, *Dock7*, *Mlph*, *Rxra*, *Atp7a*, and *Ercc2*) from the Color Genes database which were present in at least one copy in each affected dog. None of these genes were within our mapped region on chromosome 11. Of these, 12 variants were present in at least one unaffected dog as well, and 6 were present in multiple unaffected dogs. PCR primers were designed around these regions to determine whether or not they were associated with the disease phenotype. Each fragment was sequenced in 15 total dogs, 8 affected and 7 unaffected. None of the variants called via whole genome sequencing segregated with the affected phenotype.

Table 5.3 – Dogs genotyped for variants in genes in the Color Genes database

Dog Number	OM Status	Age	Sex
CA195	A	12	F
CA207	U	11	M
CA308	U	15	M
CA393	U	13	F
CA477	U	13	M
CA489	A	12	F
CA491	A	8	M
CA509	A	12	F
CA519	A	10	F
CA541	A	10	F
CA593	U	13	M
CA596	U	13	M
CA613	U	13	M
CA617	A	12	F
CA622	A	13	M

Table 5.4 – Primers for genotyping variants in genes from the Color Genes database

Primer Name	F Primer	R Primer	Amplicon Size
Apc	ATCTCAAAGGGTGGGAAAGG	TCTTGGCGAGCAGATGTAAA	170
Frem2	TTGAGGGACAGATGGGAAAG	GTTACCCTGCTGGAGCTCTG	218
Pcbd1	CGAGGGTAAGGGTGTTGAAG	GCGTCTGTGTGTCTGAGTGTG	219
Fgfr2	ATGGAGCAAGCGACGAAGT	GCGAGTTGCAGCAAAGTTAG	240
Ntrk1	ACGCTCTCACCAGAAACCAC	ATGTGCCAAGACCCACTCTC	191
Dock7	TCCAAGGCAAAAATGTAGTTCC	TGGAGCAAACTCCTATTCCA	250
Mlph	CTGAACGCGGATCTCCTTG	AGGTCTGACCCTTCCTCCTC	164
Rxra	CTTCCTGCCTCCCTTTTCTT	AACCCAGCCAGCTTCTTTCT	153
Atp7a pt.1	AAGGACGAGTAAAGGCCACA	ATCTCACACACCGGGAGAAG	167
Atp7a pt. 2	GGTATCACCTTCCTGCCTCA	AGACTGCCAAATGCAGCAC	238
Ercc2	ACGTGACCAGTTCCAGATCC	AGGAAGAGGGCAAGGAAGAG	226

Table 5.5 – Variants detected within genes from the Color Genes database via whole-genome sequencing

Variant Name	Location	Ref Seq	Variant	In Unaffecteds?	Variant Type
Apc – a	3:266419	TCAA	CCAAA	Yes (2)	Frame shift
Apc – b	3:266427	ATT	AT	Yes (1)	Frame shift
Frem2	25:2129042	TGG	TG	Yes (3)	Frame shift
Pcbd1	4:21723757	C	T	Yes (1)	Start gain
Fgfr2 – a	28:31410838	A	C	Yes (1)	Start gain
Fgfr2 – b	28:31410986	A	G	No	Start gain
Ntrk1 – a	7:41148019	TG	TCG	Yes (1)	Frame shift
Ntrk1 – b	7:41148023	CTT	CT	Yes (1)	Frame shift
Dock7	5:47482462	A	G	No	Splicing
Mlph – a	25:48160377	CCTACGGTT	GCTGCAGTGTCTC	No	Frame shift
Mlph – b	25:48160434	AGCTT	AGGAAG	Yes (2)	Frame shift
Rxra	9:50557377	CGTGTGTGTGTGTGTG TGTGTGTGTGTGTGTGTGTG	CGTGTGTGTGTGTGTG TGTGTGTGTGTGTGTGTG	Yes (2)	miRNA variant within intron
Atp7a – a	X:60203445	A	T	Yes (1)	Start Gain
Atp7a – b	X:60260558	TACA	TACACA	Yes (3)	Frame shift
Ercc2	1:110189305	GAA	GAAA	Yes (3)	Frame shift

Table 5.6 – Genotyping results for Color Genes variants

Dog#	OM Status	Apc -a	Apc -b	Frem 2	Pcbd 1	Fgfr2 -a	Fgfr2 -b	Ntrk1 -a	Ntrk1 -b	Dock 7	Mlph -a	Mlph -b	Rxr a	Atp7a -a	Atp7a -b	Ercc 2
CA195	A	V/V	V/V	V/V	V/V	R/R	V/V	R/R	R/R	V/V	V/V	V/V	*	R/R	R/R	V/V
CA207	U	V/V	V/V	V/V	V/V	R/R	V/V	R/R	R/R	V/V	V/V	V/V	*	V/V	V/V	V/V
CA308	U	V/V	V/V	V/V	V/V	R/R	V/V	V/V	V/V	R/V	V/V	V/V	*	-/-	-/-	V/V
CA393	U	V/V	V/V	V/V	R/R	R/R	V/V	R/R	R/R	V/V	V/V	V/V	*	V/V	V/V	V/V
CA477	U	V/V	V/V	V/V	V/V	R/R	V/V	R/R	R/R	V/V	V/V	V/V	*	R/V	R/V	V/V
CA489	A	V/V	V/V	V/V	R/V	R/R	V/V	R/R	R/R	V/V	V/V	V/V	*	V/V	V/V	V/V
CA491	A	V/V	V/V	V/V	V/V	R/R	V/V	R/R	R/R	R/V	V/V	V/V	*	V/V	V/V	V/V
CA509	A	V/V	V/V	V/V	R/R	R/R	V/V	R/R	R/R	R/V	V/V	V/V	*	V/V	V/V	V/V
CA519	A	V/V	V/V	V/V	V/V	R/R	V/V	R/R	R/R	V/V	V/V	V/V	*	R/R	R/R	V/V
CA541	A	V/V	V/V	V/V	R/V	R/R	V/V	R/R	R/R	V/V	V/V	V/V	*	V/V	V/V	V/V
CA593	U	V/V	V/V	V/V	V/V	R/R	V/V	R/R	R/R	V/V	V/V	V/V	*	V/V	V/V	V/V
CA596	U	V/V	V/V	V/V	V/V	R/R	V/V	R/R	R/R	R/V	V/V	V/V	*	V/V	V/V	V/V
CA613	U	V/V	V/V	V/V	-/-	R/R	V/V	R/R	R/R	-/-	V/V	V/V	*	V/V	V/V	-/-
CA617	A	V/V	V/V	V/V	V/V	R/R	V/V	R/R	R/R	V/V	V/V	V/V	*	R/V	R/V	V/V
CA622	A	V/V	V/V	V/V	V/V	R/R	V/V	R/R	R/R	V/V	V/V	V/V	*	R/V	R/V	V/V

* more than one variant allele was present for these dogs – they possessed a variable number of GT repeats, ranging from 13-18, with no particular repeat length associated with the disease phenotype

- denotes a dog that was not genotyped

"R" denotes the genotype listed as "Ref Seq" in Table 5.5

"V" denotes the genotype listed as "Variant" in Table 5.5

5.3.2 PCR-free results

A comparison of the variants called in affected dogs that had been sequenced by PCR-free methods to variants called in affected dogs sequenced by traditional PCR-based sequencing showed very little difference within the region of interest. Across the 7.5 Mb region, 20,629 total variants were called in at least one affected dog. Of those, only 59 variants were present in PCR-free sequenced dogs in regions where the traditionally sequenced dogs had lacked sufficient coverage to make a call. None of these variants were exonic. In contrast, there were 24,081 total variants called in at least one unaffected dog. Of those, 634 were unique to the dogs sequenced via PCR-free methods, although this is more likely attributable to the greater depth of coverage at which the two PCR-free unaffected samples were sequenced rather than a result of the differing sequencing techniques. The greater number of unique variants present in the PCR-free unaffected dogs should help reduce the number of variants shared by all OM-affected dogs which are absent in unaffected dogs from the 1,154 that were seen in the PCR-based data, but analysis of the PCR-free data has not yet been completed.

5.4 Discussion

Despite the presence of a strong statistical association between a 7.5 Mb pair region of chromosome 11 identified via whole-genome SNP array, no coding region variation was observed in any of the annotated genes in that region which segregated with our phenotype. Further, no variants which matched our expected inheritance pattern were detected in intronic regions likely to affect splicing or in known regulatory RNAs. The remaining variation in the region which followed our expected inheritance pattern is all intergenic. The total number of intergenic variants (1,154) are too numerous to assay individually. Additionally, no variants were found in any of 171 genes known to cause pigmentation disorders which segregated with the phenotype when tested in additional dogs.

Taken together, this suggests that the causal mutation for OM likely to be regulatory – either a cis-acting regulatory factor which is altering the expression of a gene in or near our 7.5 Mb region of interest, or a variant in a trans-acting regulatory element which is not annotated within our region. Because interrogating each of the remaining 1,154 intergenic variants is impractical, we decided to pursue a whole-transcriptome approach to determine which genes were being differentially regulated, anticipating that a single pathway would be implicated which would reduce the number of potential regulatory sites we would have to examine, while providing some clues to OM's mode of action.

The lack of any detected coding region change in our whole-genome sequencing data does not completely preclude the possibility that our variant is a coding change, however. Although quite good for a semi-model organism, the canine genome is not as well annotated as

the extensively studied mouse and human genomes, for example. *De novo* assembly of our sequence data should be performed, to help to uncover any errors that may exist in the canine reference annotation. Additionally, although SOAP was used to look for structural variants with the genome, the short-read nature of Illumina sequencing is ill-suited for finding large-scale structural changes (18, 19). Although our RNA sequencing may be able to uncover changes in gene regulation resulting from a structural rearrangement, long-read sequencing is the most robust method for detecting them (20).

REFERENCES

REFERENCES

1. Petersen-Jones SM, Forcier J, Mentzer AL. Ocular melanosis in the Cairn Terrier: clinical description and investigation of mode of inheritance. Vet Ophthalmol. 2007;10 Suppl 1:63-9.

2. Petersen-Jones SM, Mentzer AL, Dubielzig RR, Render JA, Steficek BA, Kiupel M. Ocular melanosis in the Cairn Terrier: histopathological description of the condition, and immunohistological and ultrastructural characterization of the characteristic pigment-laden cells. Vet Ophthalmol. 2008;11(4):260-8.

3. Covitz D, Barthold S, Diters R, Riis R. Pigmentary glaucoma in the cairn terrier. Transactions of the Fifteenth Annual Scientific Program of the American College of Veterinary Ophthalmologists. 1984:246-50.

4. Winkler PA, Bartoe JT, Quinones CR, Venta PJ, Petersen-Jones SM. Exclusion of eleven candidate genes for ocular melanosis in Cairn terriers. J Negat Results Biomed. 2013;12:6.

5. Williams A, Storton D, Buckles J, Llinas M, Wang W. Improvement of PCR-free NGS Library Preparation to Obtain Uniform Read Coverage of Genome with Extremely High AT Content. Journal of Biomolecular Techniques : JBT. 2012;23(Suppl):S34-S.

6. Rumble SM, Lacroute P, Dalca AV, Fiume M, Sidow A, Brudno M. SHRiMP: accurate mapping of short color-space reads. PLoS Comput Biol. 2009;5(5):e1000386.

7. Li H, Handsaker B, Wysoker A, Fennell T, Ruan J, Homer N, et al. The Sequence Alignment/Map format and SAMtools. Bioinformatics. 2009;25(16):2078-9.

8. McKenna A, Hanna M, Banks E, Sivachenko A, Cibulskis K, Kernytsky A, et al. The Genome Analysis Toolkit: a MapReduce framework for analyzing next-generation DNA sequencing data. Genome Res. 2010;20(9):1297-303.

9. Garrison E, Marth G. Haplotype-based variant detection from short-read sequencing. arXiv preprint arXiv:12073907. 2012.

10. Wang K, Li M, Hakonarson H. ANNOVAR: functional annotation of genetic variants from high-throughput sequencing data. Nucleic Acids Research. 2010;38(16):e164-e.

11. Cingolani P, Platts A, Wang LL, Coon M, Nguyen T, Wang L, et al. A program for annotating and predicting the effects of single nucleotide polymorphisms, SnpEff: SNPs in the genome of Drosophila melanogaster strain w(1118); iso-2; iso-3. Fly. 2012;6(2):80-92.

12. Li R, Li Y, Kristiansen K, Wang J. SOAP: short oligonucleotide alignment program. Bioinformatics. 2008;24(5):713-4.

13. Robinson JT, Thorvaldsdóttir H, Winckler W, Guttman M, Lander ES, Getz G, et al. Integrative Genomics Viewer. Nature biotechnology. 2011;29(1):24-6.

14. Bolger AM, Lohse M, Usadel B. Trimmomatic: a flexible trimmer for Illumina sequence data. Bioinformatics. 2014;30(15):2114-20.

15. Li H. Aligning sequence reads, clone sequences and assembly contigs with BWA-MEM. arXiv preprint arXiv:13033997. 2013.

16. Pasmant E, Laurendeau I, Heron D, Vidaud M, Vidaud D, Bieche I. Characterization of a germ-line deletion, including the entire INK4/ARF locus, in a melanoma-neural system tumor family: identification of ANRIL, an antisense noncoding RNA whose expression coclusters with ARF. Cancer Res. 2007;67(8):3963-9.

17. Kotake Y, Nakagawa T, Kitagawa K, Suzuki S, Liu N, Kitagawa M, et al. Long non-coding RNA ANRIL is required for the PRC2 recruitment to and silencing of p15INK4B tumor suppressor gene. Oncogene. 2011;30(16):1956-62.

18. Xi R, Kim TM, Park PJ. Detecting structural variations in the human genome using next generation sequencing. Brief Funct Genomics. 2010;9(5-6):405-15.

19. Guan P, Sung WK. Structural variation detection using next-generation sequencing data: A comparative technical review. Methods (San Diego, Calif). 2016;102:36-49.

20. Rhoads A, Au KF. PacBio Sequencing and Its Applications. Genomics, Proteomics & Bioinformatics. 2015;13(5):278-89.

CHAPTER 6

TRANSCRIPTOME ANALYSIS OF OCULAR MELANOSIS-AFFECTED CAIRN TERRIER IRIS TISSUE

6.1 Introduction

Ocular melanosis (OM) is an eye disease commonly seen in Cairn terrier dogs that is characterized by a bilateral proliferation of uveal melanocytes, their migration into abnormal areas of the eye such as the sclera and episclera, and the release of pigmented material into the anterior chamber of the eye (1, 2). Over time, this pigmented material builds up in the drainage pathways of the anterior chamber and impedes drainage of the aqueous humor. This leads to painful secondary glaucoma and often blindness. The pedigree analysis indicates that the disease has an autosomal dominant mode of inheritance, although it may not be completely penetrant. It has a variable rate of progression, and the age at first onset can vary widely from 2-12 years of age.

Attempts to map a causal gene using a candidate gene approach examining genes known to be involved in pigment-related disorders was unable to find any common alleles shared by all affected dogs, and whole-genome sequencing of OM-Affected dogs was unable to identify any variants that seem likely to be causal for the disease (see Chapter 5) (4). A 7.5 megabase region of chromosome 11 has been identified as significantly associated with the disease (see Chapter 4), which confirms the notion that the disease has a genetic basis, and is not a purely environmental effect which has not been identified.

Taken together, the fact that a) there is a region of chromosome 11 that is strongly associated with the OM and b) there seem to be no coding or splicing changes within the region that can account for the OM phenotype suggest that the variant being mapped is regulatory in nature. Unfortunately, the annotation of regulatory elements present within the canine

genome is quite poor, and the sheer number of intergenic variants detected via NGS that fit the expected inheritance pattern for OM makes screening them impractical. Thus, we decided to perform RNA sequencing and transcriptome analysis on a number of OM affected and unaffected Cairn terriers to determine what differences in expression level are associated with OM. In the event that the DNA variant mapped to chromosome 11 is cis-acting, we would expect to see changes in expression levels of genes within the 7.5 Mb mapped region ± 1.5 Mb, as that is the maximum distance at which cis-acting regulatory elements have been shown to be able to act (5). In the event that it is a trans-acting regulator, differences in expression levels should be observed in gene pathways under regulation. The alignments within the 7.5 Mb region identified were also assessed by eye to determine if any unannotated transcripts are present in the region.

6.2 Materials and methods

6.2.1 RNA sample collection

All RNA samples used in this study were extracted from uveal tissue donated with the consent of the owner from Cairn terrier dogs being euthanized for health reasons unrelated to OM or from eyes being enucleated for therapeutic reasons from late-stage OM dogs that had developed glaucoma. Prior to euthanasia/enucleation, veterinarians performing the operation were sent an aliquot of RNAlater (Fisher Scientific, Pittsburgh, PA), a preservation solution used to rapidly stabilize RNA in tissue samples (6). Operating veterinarians were instructed to immediately remove the anterior segment from the eye and fully submerge it in the provided RNAlater solution to allow it to penetrate into the iris, and ship the tissue back overnight in an insulated (but not refrigerated) box, as per the RNAlater usage instructions. Upon receipt of these tissue samples, the anterior chamber was removed from RNAlater. The iris was then excised from the remainder of the anterior chamber and stored at -80°C as per the RNAlater usage instructions.

6.2.2 Extraction, purification, and evaluation of RNA from iridal tissue

RNA was extracted from the collected iris tissue using a Qiagen miRNeasy mini-prep kit (Qiagen, Germantown, MD) according to the manufacturer's protocol, including the optional DNase digestion steps. RNA extracted in this way showed very high levels of melanin contamination in the final product, such that the sample was visibly dark brown in color (figure 6.1). Melanin complicates most downstream applications for which RNA is used. The fact that is absorbs large amounts of light complicates attempts to quantify the RNA using a

spectrophotometer, and melanin has been shown to bind to a wide variety of DNA polymerases and reverse transcriptases and inhibit their activity (7, 8).

The RNA samples were purified of melanin using a modified CTAB-Urea purification protocol (3, 9). Cetyl-trimethylammonium bromide (CTAB) is a cationic detergent. The cationic micelles that CTAB forms selectively complex with the anionic nucleic acids, leaving the uncharged melanin remaining in the supernatant. The presence of urea greatly increases the specificity of the reaction, and although the method by which it does so is not completely understood, it is thought to help sequester hydrophobic molecules that may otherwise disrupt the CTAB micelles (3). In brief, the purification was performed as follows: RNA purified via the RNeasy kit was diluted with water to a final volume of 200 µl. To the RNA, 65 µl of 5M NaCl was added, followed by 800 µl of CTAB-urea solution (1% CTAB [Sigma-Aldrich, St. Louis, MO], 4 M urea, 50 mM Tris-HCl, 1 mM EDTA, pH 7.0) and mixed via pipetting. Samples were left overnight at 4°C, and then centrifuged at 15,300g at 4°C for 15 minutes. The pigment-containing supernatant was removed, and the precipitated RNA was resuspended in 200 µl of 7 M guanidine hydrochloride (Sigma). The guanidine hydrochloride replaces the RNA via ionic exchange, and allowed the RNA to be precipitated by adding 400 µl of 100% ethanol (10, 11). The resulting mixture was incubated on ice for 1 hour, and pelleted via centrifugation at 15,300g at 4°C for 15 minutes. The pellet was then washed with 400 µl of 70% ethanol, and centrifuged for 10 min at 20,800g at 23°C. The remaining ethanol was removed, and the RNA pellet resuspended in 100 µl of water. This greatly reduced the level of melanin present in the samples (figure 6.1), but it also appeared to have an adverse effect on overall RNA quality. Following purification, RNA was quantified using a Qubit fluorimeter (Fisher) and the RNA integrity number (RIN) was

ascertained using a model 2100 Bioanalyzer (Agilent Technologies, Santa Clara, CA). RIN values varied between samples (8.3-5.7), but most were lower than those reported for human ocular tissue that had been preserved in RNAlater under similar conditions (12). Additionally, some samples retained a small amount of pigment following the initial CTAB-urea purification which were subjected to a second round of CTAB-urea purification. There samples uniformly produced RNA samples with unusably low RIN values (4.8-1.1).

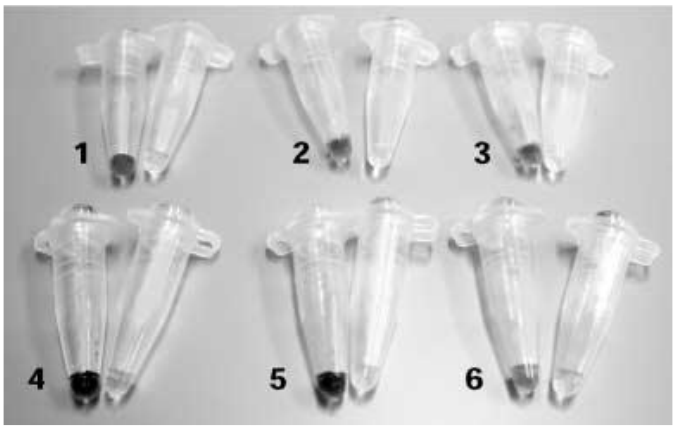

Figure 6.1 – RNA samples before and after CTAB-urea purification Six RNA samples before (left-side tubes) and after (right-side tubes) CTAB-Urea purification. Figure reproduced from (3).

6.2.3 RNA sequencing

RNA samples from 12 total dogs (7 affected and 5 unaffected, see Table 6.1 for a complete list of dogs used) were sent to Michigan State University's Research Technology Support Facility for RNA sequencing. The dogs were subdivided into two groups – a pilot group of 4 dogs to determine whether the RNA purified via CTAB-urea precipitation was of sufficient quality for sequencing, and a second group of 8 dogs to provide the power necessary for the study. The initial four dogs had higher-quality RNA as determined by RIN value. Library

preparation was performed using the Illumina TruSeq stranded mRNA library kit (Illumina). The samples were barcoded and pooled, and sequenced using an Illumina HiSeq 2500 Rapid Run flow cell v2 (Illumina, San Diego, CA) in 100bp paired-end mode. The average coverage after QC was 42.5 million reads per sample with an average yield of 8.52 Gbp of sequence data per sample. The second set of dogs used slightly lower-quality RNA, as determined by RIN value. Traditional library creation kits like the TruSeq kit used for the pilot samples isolate polyadenylated mRNA via the use of oligo-dT beads, and this can results in a strong 3' bias in degraded samples. To compensate for this, their library was created using the NuGEN Ovation RNA-Seq system (NuGEN, San Carols, CA). This library creation kit uses pseudo-random primers for first-strand cDNA synthesis, allowing for even coverage of the sample while avoiding rRNA. Samples were barcoded and pooled and sequenced on a single lane of an Illumina HiSeq 2500 High Output v4 (Illumina) in 125bp paired-end mode. The average coverage after QC was 37.5 million reads per sample with an average yield of 9.38 Gbp of sequence data per sample. According to most sources, this level of coverage should be sufficient for allowing technically precise detection of differential expression in most genes (13, 14).

Table 6.1 – Information on dogs used for RNA sequencing

Dog Number	OM Status	Age in years and Sex	RIN	Library Preparation	Coverage in read-pairs
CA614	A	14,F	7.6	Ovation	30,779,315
CA197	U	15,M	7.6	TruSeq	31,299,299
CA455	U	13,F	7.5	TruSeq	58,973,062
CA619	A	18,M	7.0	TruSeq	32,173,667
CA615	A	14,M	6.6	Ovation	35,331,298
CA621	A	10,M	7.0	TruSeq	47,856,741
CA229	U	16,M	8.3	Ovation	39,821,306
CA624	A	8,F	6.0	Ovation	31,795,705
CA456	U	16,M	6.7	Ovation	44,895,038
CA314	A	12,F	5.9	Ovation	43,249,458
CA558	U	16,M	5.9	Ovation	38,414,521
CA626	A	16,F	5.7	Ovation	35,897,872

6.2.4 Data Evaluation

RNA sequence data was used for two primary applications – examining differences in expression level, and using the data as pseudo-exome data to look for variants. All data was trimmed prior to use using Trimmomatic to remove Illumina adapter sequence, remove very short reads (less than 25bp), to trim leading or trailing bases with a quality score of below 2, and to scan reads with a 4bp sliding window and cut where the average quality score drops below 3 (15).

Expression analysis was carried out using the spliced-read mapper TopHat (http://ccb.jhu.edu/software/tophat/index.shtml) and the statistical analysis software R (https://www.r-project.org/) (16, 17). TopHat was run with the mate inner distance setting changed to reflect the insert size of each sample and with other settings set to default values. The mapped read files generated by TopHat were loaded into R and analyzed using several elements of the Bioconductor toolset (https://www.bioconductor.org/about/). The

GenomicFeatures, GenomicRanges, GenomicAlignments, Rsamtools and org.Cf.eg.db packages were used to generate per-gene read-count tables for each sample based on ensemble gene annotation (18).Tables for the affected and unaffected dogs were then compared across disease status using two different software packages - DESeq (to perform a base mean comparison between two conditions) and edgeR (to perform a genewise exact test for differences) (19-21). Genes with p-values below 0.05 (DESeq) or 0.01 (edgeR) were analyzed using PANTHER (http://pantherdb.org) to determine if any known gene families or pathways were overrepresented in the resulting data (22).

For direct data visualization, a subset of the mapped read files was created which contained the 7.5 Mb mapped region ± 1.5 Mb on either side. The IGV software package (http://software.broadinstitute.org/software/igv/) was used to visualize the data (23). All mapped reads from the 7.5 Mb region ± 1.5 Mb on either side, were extracted and loaded into IGV along with the ensemble canine gene annotation track (ver. CanFam3.1.87). Potential unannotated transcripts were called by eye in regions where more than 5 dogs had multiple reads with a mapping quality greater than zero map to the same region where no gene was annotated in the ensemble track. Sequence data from these regions was then viewed in UCSC genome browser, and converted to human (build hg38) or mouse (build mm10) to look for annotation in other organisms if necessary.

Variant calling was carried out according to the GATK Best Practices handbook as of 1/21/2017 (https://software.broadinstitute.org/gatk/documentation/article.php?id=3891). Briefly, the RNAseq reads were mapped to the reference genome (CanFam3.1) using the STAR 2-pass method, which runs an initial alignment to detect splice junctions that it then uses to

guide the final alignment (24, 25). Picard (http://broadinstitute.github.io/picard/) was used to add read groups, mark duplicates, and index the mapped reads. The genome analysis toolkit package (GATK) was used to clip out regions where exon sequence inappropriately overhangs into intronic regions, realign around indels, and perform base quality score recalibration (26). GATK's HaplotypeCaller tool was used to variants. The resulting raw variants were filtered to remove any variants with a Fisher Strand value of less than 30 or a quality by depth score of less than 20, and variant annotation was performed using ANNOVAR and SnpEff (27, 28).

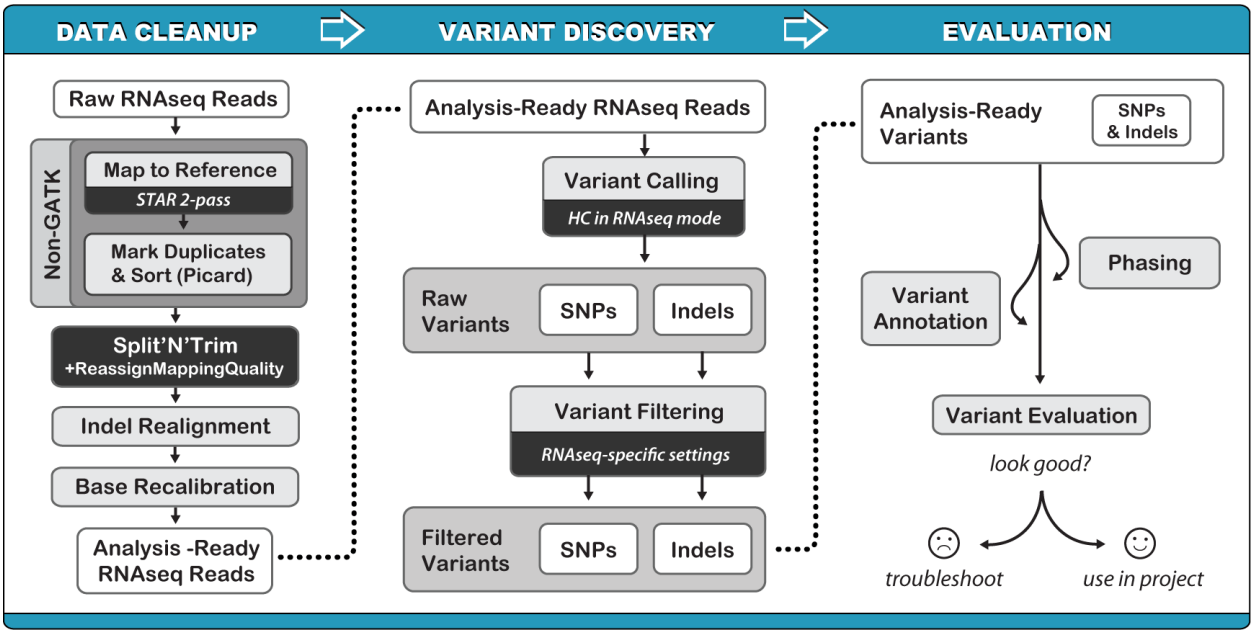

Figure 6.2 – Graphical illustration of the variant calling pipeline for RNA data Figure reproduced from (https://software.broadinstitute.org/gatk/documentation/article.php?id=3891)

6.2.5 Confirmatory qRT-PCR

To confirm differences observed in RNAseq data, quantitative real-time PCR (qRT-PCR) was carried out using. For qRT-PCR, first-stand cDNA synthesis was done using the Transcriptor first-strand cDNA synthesis kit (Roche, Indianapolis, IN) according to the manufacturer's

instructions. The qRT-PCR itself was performed using a pre-made SYBRGreen mastermix (SsoFast EvaGreen Supermix with low ROX, Biorad, Hercules CA) according to the manufacturer's protocol and run on an Applied Biosystems 7500 Fast Real-Time PCR (Fisher).

Table 6.2 – Primers used for qPCR

Gene Target	Exon Junction Spanned	Forward Primer	Reverse Primer	Product Size
COL3A1	49-50	GGTGGACAGATTCTGGTGCT	CCTTCATTTGACCCCATCAG	250
COL6A3	36-37	GGTGAACGTCAAGGAGGTGT	AACCAATCGCACTGTTTCCT	186
COL14A1	44-45	CCAGCCAATCCTCATCAGTT	ACTCTCCCCTGAAGGTCCTG	245
CXCL10	1-2	GCAGAGGAACCTCCAGTCAC	ACGATGGACTTGCAGGAATC	195
PREX1	35-36	GGCCCTGAAGGTTGTCTTCT	GCCCTGAGTTTGCGGTAATA	225
PIK3C2G Pair 1	27-28	TGCAACCAGGTCAATTCAAA	AGTGCCACCAATGAGGAAAC	200
PIK3C2G Pair 2	18-19	CGTAAAGTGGCAGTTCGACA	AGCTGCCAACAGCTTCTGAT	234
PIK3C2G Pair 3	6-7	TCAGAAAAATGGGGAAGTGC	TTGCTGGGTTTTCAATAGGC	178
GAPDH	None	ACAGTCCATGCCATCACTGCC	GCCTGCTTCACCACCTTCTTG	266

6.3 Results

6.3.1 Expression level differences

Expression levels were compared across 21,709 total annotated canine genes, giving a Bonferroni-corrected p-value of 2.3×10^{-6}. No genes reached this threshold using either analysis method. The lowest p-value for DESeq was 9.4×10^{-3}, and the lowest p-value calculated by edgeR was 2.0×10^{-4}. None of the 200 smallest p-value results from either analysis were from transcripts located within the 7.5 Mb region of interest mapped via GWAS (see Chapter 4). The transcripts with the lowest calculated p-values from each program were analyzed with PANTHER to determine if any known gene pathways or gene families were overrepresented. A cutoff p-value of 0.1 was used for DESeq samples (53 transcripts) and 0.01 for edgeR (93 transcripts). In both samples, two pathways had multiple genes map to them – integrin signaling pathways, and chemokine and cytokine-mediated inflammatory pathways. Taking both analyses into account, 4 genes classified by PANTHER as being related to chemokine or cytokine-mediated inflammation, and 4 genes related to integrin signaling were present in the lowest p-value transcripts, with 2 genes present in both groups. C-X-C Motif chemokine 10 (*CXCL10*), collagen type XIV alpha 1 chain (*COL14A1*), phosphatidylinositol 4-phosphate 3-kinase C2 domain containing subunit gamma (*PIK3C2G*), and phosphatidylinositol 3,4,5-triphosphate-dependent RAC exchanger 1 protein (*PREX1*) were classified by PANTHER as being involved chemokine and cytokine-mediated inflammatory pathways. *COL14A1* and *PIK3C2G* were also classified genes involved in integrin signaling pathways, along with collagen type III alpha I chain (*COL3A1*) and collagen type VI alpha 3 chain (*COL6A3*). All genes listed here had higher levels of expression in OM-affected dogs than in unaffected dogs. Observed average fold increases for

each gene were 4.78 (*CXCL10*), 4.04 (*COL14A1*), 3.19 (*PREX1*), 3.15 (*COL3A1*), and 3.38 (*COL6A3*). No *PIK3C2G* expression was observed in unaffected samples, so no fold change can be calculated. *PIK3C2G* expression was observed in 5 of 7 affected dogs sequenced, with a mean of 44.7 copies per dog observed among all OM affected dogs.

6.3.2 qRT-PCR confirmation

To confirm the changes in expression for each sample obtained from the RNAseq data, we used quantitative real-time PCR (qRT-PCR). Some of the samples used for RNAseq were mildly degraded (table 6.1) and replication of the results via qRT-PCR would help to confirm that the observed expression differences were not the result of library creation bias. We performed qRT-PCR on the 12 samples that we initially sent for RNA sequencing. For 5 of the 6 genes (*COL3A1*, *COL14A1*, *CXCL10*, *PREX1*, and *COL6A3*) an expression difference was observed that was significant at $P < 0.05$. For *PIK3C2G*, no fold change could be calculated. *PIK3C2G* expression was detected at very low levels in our RNAseq data (it was detected in 5 of 7 OM-affected samples, and in none of our unaffected samples). When performing qRT-PCR, we used 3 different primer pairs to attempt to amplify *PIK3C2G*, but got no amplification above the negative control background in all samples except for CA314 and CA626, both of which were OM-affected.

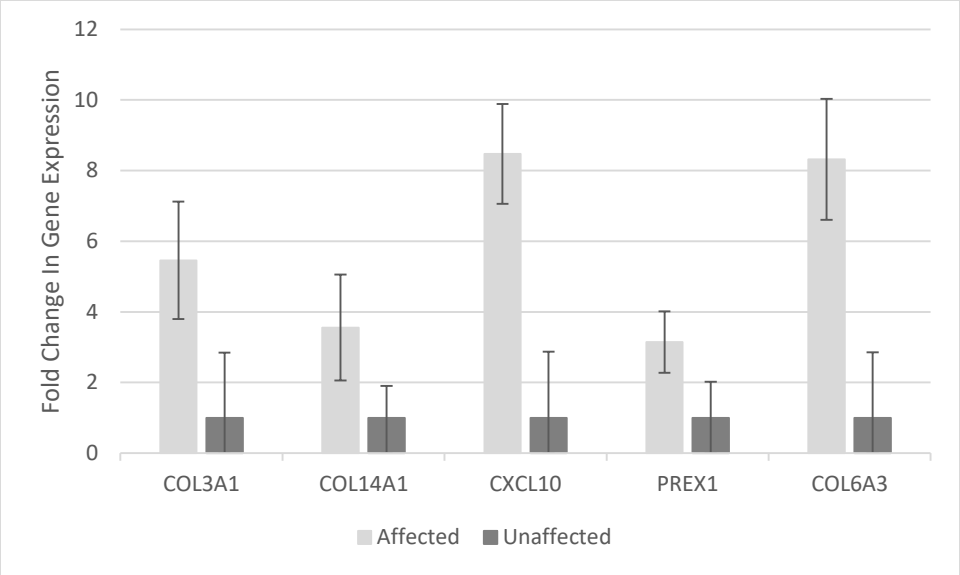

Figure 6.3 – Fold increase in gene expression as observed by qPCR Fold increase in expression level for each gene as observed by qPCR. The average unaffected expression level was defined as 1.0. *PIK3C2G* had no detectable expression in unaffected samples from which to compute a fold change.

6.3.3 Unannotated transcripts

Twenty-one regions of the genome fit our criteria for further investigation (multiple mapped reads with positive mapping quality scores from 5 or more dogs at the same location with no annotated transcript in ensemble or refgene). Upon further examination, each of these 21 regions mapped to within a known canine long interspersed nuclear element (LINE). No regions were observed that suggest an unannotated transcript.

6.3.4 RNA variant calling

Examining variants called in genes with the 7.5 Mb region identified by whole-genome SNP array, only 3 total variants were called which were present in all affected samples. There variants were also present in all unaffected samples. The genome-wide list of variants was compared to a list of genes known to be associated with pigmentation changes in human, mice,

or zebrafish (http://www.espcr.org/micemut/). A total of 17 variations were observed in all affected samples, 14 of which were present in all unaffected samples as well, and 3 of which were present in 4 of 5 unaffected samples.

6.4 Discussion

All 6 of the genes identified by PANTHER as part of a common pathway have been shown to have some effect on cell migration or invasiveness in various cancer models, suggesting that, while they may not explain the excessive pigment production observed in OM, they may provide important clues into the nature of the migratory behavior the affected melanocytes display when they migrate to the sclera.

Of the 6 genes identified, PIK3C2G seems to be the furthest upstream in this pathway – it is a member of the phosphoinositide 3-kinase (PI3K) family of proteins, which are known to play a key regulatory role in a wide variety of cellular processes, including cell survival, proliferation, migration, and oncogenic transformation (29). Changes in the activity of PI3K proteins have been linked to many different forms of cancer (29-31). Although this family of proteins is in general very well characterized, *PIK3C2G* falls into the category of class II PI3Ks, which are not as extensively characterized as class I PI3Ks. Class II PI3Ks are known to be activated by cytokine receptors, integrins, and receptor tyrosine kinases, but the exact cellular function of class II PI3Ks remains unclear.

PREX1 (often seen as P-REX1) is a guanine nucleotide exchange factor for the Rac subfamily of Rho GTPases. PREX1 activity is activated by phosphatidylinositol-3,4,5-triposphate, the product of PI3K proteins, suggesting that the increase *PREX1* expression that we see in affected OM samples may be the result of downstream result of higher *PIK3C2G* levels (32, 33). Elevated *PREX1* expression has been observed in a number of different human cancer types, including breast, prostate, and ovarian cancers, but the most interesting facet in relation to OM is that PREX1 is upregulated and drives migration and invasion in many human and mouse

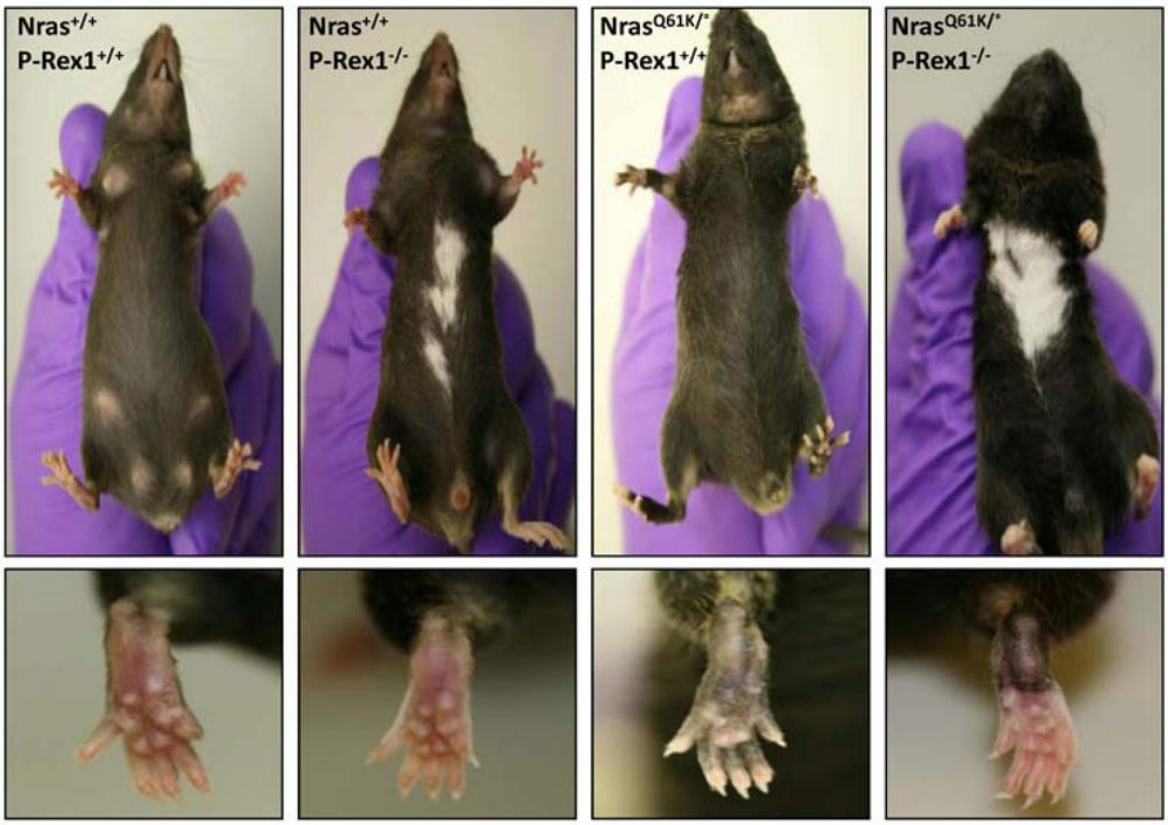

Figure 6.4 – Pigmentation patterns of various mice Note that PREX1$^{-/-}$ mice display a lack of belly and feet pigmentation regardless of background. Modified from (34).

melanomas, and that it has an important developmental role in normal melanoblast migration (34, 35). *PREX1*$^{-/-}$ mice on a C57BL6 background displayed a completely penetrant depigmentation of belly, tail and feet – the furthest points for melanoblast migration from the neural crest during embryogenesis(figure 6.4), suggesting that the loss of *PREX1* resulted in impaired

melanoblast migration (rather than a deficiency in proliferative or melanogenic capacity) (34). Further mouse studies confirmed this assessment, and also showed that *PREX1* deficiency significantly impairs melanoma metastasis in *Tyr::Nras*$^{Q61K/\circ}$*;INK4a*$^{-/-}$ mice, a genetically modified mouse model for malignant melanoma. However, metastatic cell populations driven by *PREX1* overexpression tend to be primarily anchorage independent (32). Cultured OM melanocytes did

not display anchorage independent growth characteristics *in vitro* when tested via soft agar assay (see Chapter 3).

CXCL10 is a chemokine which has been found to be overexpressed in many different types of metastatic cancer (36). This overexpression has typically been mediated by PI3K signaling pathways, suggesting that CXCL10 overexpression is a downstream effect of the observed increased PIK3C2G activity, but PREX1 has also recently been shown to have a regulatory effect on *CXCL10* (33). CXCL10 functions via activation the CXCR3 receptor. There exist two different types of CXCR3 receptor, and which kind CXCL10 binds to determine its downstream effects. CXCR3-A is the predominant isoform of the receptor, and upon binding CXCL10 it induces cell proliferation and chemotaxis. The rarer CXCR3-B isoform has the opposite effect, inhibiting cell proliferation and migration.

The expression differences in the three collagen subunits are more difficult to directly integrate into the pathway, as none of their expression is directly linked to the three proteins noted above. However, extracellular matrix rearrangement and microenvironment alteration are known to be important in all forms of cancers and cellular migratory diseases (37). The specific collagens shown to be upregulated in OM in this study have been shown to be associated with various cancer types. Mutations in *COL3A1* are known to be associated with melanoma, COL3A1 overexpression has been shown to be linked to drug resistance in ovarian cancers, and multiple carcinoma lines have been shown to secrete COL3A1 into the ECM at high levels (38-40). However, tumors implanted into *COL3A1*$^{+/-}$ mice metastasize more aggressively than those implanted into wild-type mice, suggesting that normal levels of COL3A1 provide

some protective effect (41). Likewise, COL14A1 has been shown to act as a tumor suppressor in renal carcinomas (42). COL6A3 has been shown to often be secreted in uveal melanomas (43).

Although qRT-PCR confirms that these genes are expressed at increased levels in OM affected dogs, important follow-up studies still remain to be done. Most of the OM-affected eyes used for RNA collection were enucleated from OM affected dogs in order to treat painful secondary glaucoma. As a result of this, most of the affected eyes used in this study were currently either inflamed or being treated for inflammation at the time of their submission. Although a literature search does not show that expression changes in any of these six genes have been directly linked to glaucoma, some of them, such as CXCL10, are directly involved in inflammation pathways (36, 44). If possible, immunohistochemistry of an OM affected eye that has not yet begun to experience changes related to glaucoma could show how the location and prevalence of these proteins changes between OM-affected and normal tissues, and would be useful in establishing the presence of these expression changes in early-stage OM.

Taken together with the mapping data from the genome-wide SNP array (see Chapter 4), this data supports the hypothesis that the causal mutation for OM is trans-acting and regulatory in nature. None of the six genes with elevated expression in OM affected dogs are on chromosome 11, and none of the regions that these six genes are located in are mapped as significant by the genome-wide SNP array. No genes known to regulate any of the six genes with elevated expression are within 1.5 Mb of the 7.5 Mb region, ruling out a cis-acting regulatory element or an undetected coding region change in a gene which regulates this pathway. Analysis of the mapped RNA reads by eye did not reveal any unannotated transcripts within this region.

REFERENCES

REFERENCES

1. Petersen-Jones SM, Forcier J, Mentzer AL. Ocular melanosis in the Cairn Terrier: clinical description and investigation of mode of inheritance. Vet Ophthalmol. 2007;10 Suppl 1:63-9.

2. Petersen-Jones SM, Mentzer AL, Dubielzig RR, Render JA, Steficek BA, Kiupel M. Ocular melanosis in the Cairn Terrier: histopathological description of the condition, and immunohistological and ultrastructural characterization of the characteristic pigment-laden cells. Vet Ophthalmol. 2008;11(4):260-8.

3. Lagonigro MS, De Cecco L, Carninci P, Di Stasi D, Ranzani T, Rodolfo M, et al. CTAB-urea method purifies RNA from melanin for cDNA microarray analysis. Pigment cell research. 2004;17(3):312-5.

4. Winkler PA, Bartoe JT, Quinones CR, Venta PJ, Petersen-Jones SM. Exclusion of eleven candidate genes for ocular melanosis in Cairn terriers. J Negat Results Biomed. 2013;12:6.

5. Epstein DJ. Cis-regulatory mutations in human disease. Briefings in functional genomics & proteomics. 2009;8(4):310-6.

6. Mutter GL, Zahrieh D, Liu C, Neuberg D, Finkelstein D, Baker HE, et al. Comparison of frozen and RNALater solid tissue storage methods for use in RNA expression microarrays. BMC Genomics. 2004;5(1):88.

7. Price K, Linge C. The presence of melanin in genomic DNA isolated from pigmented cell lines interferes with successful polymerase chain reaction: a solution. Melanoma research. 1999;9(1):5-9.

8. Eckhart L, Bach J, Ban J, Tschachler E. Melanin binds reversibly to thermostable DNA polymerase and inhibits its activity. Biochemical and biophysical research communications. 2000;271(3):726-30.

9. Carninci P, Hayashizaki Y. High-efficiency full-length cDNA cloning. Methods in enzymology. 1999;303:19-44.

10. Gustincich S, Manfioletti G, Del Sal G, Schneider C, Carninci P. A fast method for high-quality genomic DNA extraction from whole human blood. BioTechniques. 1991;11(3):298-300, 2.

11. Del Sal G, Manfioletti G, Schneider C. The CTAB-DNA precipitation method: a common mini-scale preparation of template DNA from phagemids, phages or plasmids suitable for sequencing. BioTechniques. 1989;7(5):514-20.

12. Kim B-J, Sprehe N, Morganti A, Wordinger RJ, Clark AF. The effect of postmortem time on the RNA quality of human ocular tissues. Molecular Vision. 2013;19:1290-5.

13. Wang Y, Ghaffari N, Johnson CD, Braga-Neto UM, Wang H, Chen R, et al. Evaluation of the coverage and depth of transcriptome by RNA-Seq in chickens. BMC Bioinformatics. 2011;12(Suppl 10):S5-S.

14. Hart SN, Therneau TM, Zhang Y, Poland GA, Kocher J-P. Calculating Sample Size Estimates for RNA Sequencing Data. Journal of Computational Biology. 2013;20(12):970-8.

15. Bolger AM, Lohse M, Usadel B. Trimmomatic: a flexible trimmer for Illumina sequence data. Bioinformatics. 2014;30(15):2114-20.

16. Trapnell C, Roberts A, Goff L, Pertea G, Kim D, Kelley DR, et al. Differential gene and transcript expression analysis of RNA-seq experiments with TopHat and Cufflinks. Nature Protocols. 2012;7(3):562-78.

17. Team RC. R: A language and environment for statistical computing. R Foundation for Statistical Computing. 2016.

18. Lawrence M, Huber W, Pagès H, Aboyoun P, Carlson M, Gentleman R, et al. Software for Computing and Annotating Genomic Ranges. PLOS Computational Biology. 2013;9(8):e1003118.

19. McCarthy DJ, Chen Y, Smyth GK. Differential expression analysis of multifactor RNA-Seq experiments with respect to biological variation. Nucleic Acids Res. 2012;40(10):4288-97.

20. Robinson MD, McCarthy DJ, Smyth GK. edgeR: a Bioconductor package for differential expression analysis of digital gene expression data. Bioinformatics. 2010;26(1):139-40.

21. Anders S, Huber W. Differential expression analysis for sequence count data. Genome Biology. 2010;11(10):R106.

22. Thomas PD, Campbell MJ, Kejariwal A, Mi H, Karlak B, Daverman R, et al. PANTHER: A Library of Protein Families and Subfamilies Indexed by Function. Genome Research. 2003;13(9):2129-41.

23. Robinson JT, Thorvaldsdóttir H, Winckler W, Guttman M, Lander ES, Getz G, et al. Integrative Genomics Viewer. Nature biotechnology. 2011;29(1):24-6.

24. Dobin A, Davis CA, Schlesinger F, Drenkow J, Zaleski C, Jha S, et al. STAR: ultrafast universal RNA-seq aligner. Bioinformatics. 2013;29(1):15-21.

25. Engstrom PG, Steijger T, Sipos B, Grant GR, Kahles A, The RC, et al. Systematic evaluation of spliced alignment programs for RNA-seq data. Nat Meth. 2013;10(12):1185-91.

26. McKenna A, Hanna M, Banks E, Sivachenko A, Cibulskis K, Kernytsky A, et al. The Genome Analysis Toolkit: a MapReduce framework for analyzing next-generation DNA sequencing data. Genome Res. 2010;20(9):1297-303.

27. Cingolani P, Platts A, Wang LL, Coon M, Nguyen T, Wang L, et al. A program for annotating and predicting the effects of single nucleotide polymorphisms, SnpEff: SNPs in the genome of Drosophila melanogaster strain w(1118); iso-2; iso-3. Fly. 2012;6(2):80-92.

28. Wang K, Li M, Hakonarson H. ANNOVAR: functional annotation of genetic variants from high-throughput sequencing data. Nucleic Acids Research. 2010;38(16):e164-e.

29. Liu P, Cheng H, Roberts TM, Zhao JJ. Targeting the phosphoinositide 3-kinase (PI3K) pathway in cancer. Nature reviews Drug discovery. 2009;8(8):627-44.

30. Krasilnikov MA. Phosphatidylinositol-3 kinase dependent pathways: the role in control of cell growth, survival, and malignant transformation. Biochemistry Biokhimiia. 2000;65(1):59-67.

31. Fruman DA, Rommel C. PI3K and Cancer: Lessons, Challenges and Opportunities. Nature reviews Drug discovery. 2014;13(2):140-56.

32. Liu H-J, Ooms LM, Srijakotre N, Man J, Vieusseux J, Waters JE, et al. PREX1 Rac-GEF Activity Promotes Breast Cancer Cell Proliferation and Tumor Growth via Activation of Extracellular-Signal-Regulated Kinase 1/2 (ERK1/2) Signaling. Journal of Biological Chemistry. 2016.

33. Liang Q, Cheng N, Zhang G, Liang Y, Qian F, Wu D, et al. Identification of P-Rex1 as an anti-inflammatory and anti-fibrogenic target for pulmonary fibrosis. Scientific Reports. 2016;6:25785.

34. Lindsay CR, Lawn S, Campbell AD, Faller WJ, Rambow F, Mort RL, et al. P-Rex1 is required for efficient melanoblast migration and melanoma metastasis. Nature Communications. 2011;2:555-.

35. Campbell AD, Lawn S, McGarry LC, Welch HC, Ozanne BW, Norman JC. P-Rex1 Cooperates with PDGFRβ to Drive Cellular Migration in 3D Microenvironments. PLOS ONE. 2013;8(1):e53982.

36. Liu M, Guo S, Stiles JK. The emerging role of CXCL10 in cancer (Review). Oncology Letters. 2011;2(4):583-9.

37. Clark AG, Vignjevic DM. Modes of cancer cell invasion and the role of the microenvironment. Current Opinion in Cell Biology. 2015;36:13-22.

38. Libby RT, Anderson MG, Pang I-H, Robinson ZH, Savinova OV, Cosma IM, et al. Inherited glaucoma in DBA/2J mice: Pertinent disease features for studying the neurodegeneration. Visual Neuroscience. 2005;22(5):637-48.

39. Januchowski R, Świerczewska M, Sterzyńska K, Wojtowicz K, Nowicki M, Zabel M. Increased Expression of Several Collagen Genes is Associated with Drug Resistance in Ovarian Cancer Cell Lines. Journal of Cancer. 2016;7(10):1295-310.

40. Naba A, Clauser KR, Lamar JM, Carr SA, Hynes RO. Extracellular matrix signatures of human mammary carcinoma identify novel metastasis promoters. eLife. 2014;3:e01308.

41. Brisson BK, Mauldin EA, Lei W, Vogel LK, Power AM, Lo A, et al. Type III Collagen Directs Stromal Organization and Limits Metastasis in a Murine Model of Breast Cancer. The American Journal of Pathology. 2015;185(5):1471-86.

42. Morris MR, Ricketts C, Gentle D, Abdulrahman M, Clarke N, Brown M, et al. Identification of candidate tumour suppressor genes frequently methylated in renal cell carcinoma. Oncogene. 2010;29(14):2104-17.

43. Daniels KJ, Boldt HC, Martin JA, Gardner LM, Meyer M, Folberg R. Expression of type VI collagen in uveal melanoma: its role in pattern formation and tumor progression. Laboratory investigation; a journal of technical methods and pathology. 1996;75(1):55-66.

44. Jakobs TC. Differential Gene Expression in Glaucoma. Cold Spring Harbor Perspectives in Medicine. 2014;4(7).

CHAPTER 7

DISCUSSION AND FUTURE DIRECTIONS

Although we have yet to identify a causal mutation, we have made great strides in understanding the genetic and physiological changes that underlie ocular melanosis (OM) as a result of the work done in this study. To summarize, we have –

- Developed methods to isolate and culture uveal melanocytes from canine eyes without contamination from other cell types
- Extensively studied the *in vitro* phenotypic differences between melanocytes cultured from OM affected eyes and those from unaffected controls
- Mapped a statistically significant region of chromosome 11 which is associated with the disease
- Performed whole-genome sequencing to interrogate possible causative mutations in OM affected dogs
- Eliminated the possibility that the primary cause of the disease is a coding-region variation in a known canine gene
- Used transcriptome sequencing to identify a putative change in pathway regulation present in OM affected dogs which suggests a possible method by which the migratory portion of the OM phenotype functions

From these results, three avenues for further investigation readily suggest themselves –

As was discussed in Chapter 3 of this work, there were no detectible *in vitro* changes in cell behavior in OM affected melanocytes related to cell migration and proliferation, only pigment production. We theorized that this loss of the migratory phenotype might be due to a lack of necessary signaling from other cell types usually present in the uvea. We suggest that

cellular co-culture experiments may be useful to attempt to re-create the *in vivo* phenotype *in vitro*. There have been numerous recorded instances of melanocyte and melanoma-derived cell lines losing certain physiological characteristics in culture which are restored in co-culture – three lines of metastatic melanoma cells which normally disseminate throughout the body via extravasation were shown to regain lost expression of LFA-1 (an integrin involved in extravasation) when cultured in the presence of human umbilical vein endothelial cells (1). Cultured human melanocytes have been shown to undergo melanogenesis when exposed to UVB radiation only when cultured with keratinocytes (2). Especially given that the causal change in OM appears to be a regulatory one (see Chapter 6), performing co-culture experiments to attempt to re-create *in vivo* conditions would be a useful next step. Although there are many different cell types present in the uveal with which co-culture could be attempted, uvea melanoma / endothelial cell interactions have been previously characterized, and suggest that uveal melanoma growth and metastasis is reliant on an interplay between uveal melanoma cells and cytokines released by endothelial cells (3). *PIK3C2G*, one of the transcripts shown to be upregulated in OM uveal tissue, is known to be activated by cytokine receptor activity, so endothelial cell co-culture represents a logical starting point for these studies (4, 5). Although some of the tests outlined in Chapter 3 would be difficult to perform under co-culture conditions, two elements critical to the OM phenotype could be tested fairly easily – the ability to migrate through a membrane and elevated melanin production. There are already well-developed protocols for examining transmigration of melanoma cells in co-culture with endothelial cells using a simple transwell assay, and for measuring differences in melanin synthesis rates for co-cultured cells (2, 3). Furthermore, if these co-culture experiments prove

successful in recreating the *in vivo* phenotype, analysis of culture media to obtain a cytokine profile and use of anti-cytokine antibodies to prevent cytokine signaling could help to provide additional clues to the exact pathways which must be active to produce the OM phenotype, and provide insight into how to best treat affected dogs.

Another possible avenue of investigation involves determining whether the six proteins corresponding to the six genes shown by RNAseq to have elevated expression levels, *PREX1*, *PIK3C2G*, *COL31A*, *COL6A3*, *COL14A1*, and *CXCL10* are actually present in elevated levels in the uvea of OM affected dogs. As many of these genes are known to be associated with inflammation, it would be best if these studies could be done on early-to-mid stage OM affected eyes rather than eyes which were enucleated as the result of glaucoma. While it is rare for us to receive such eyes via donation, an appeal could be made to the breed club that any owner with an older affected dog which is clear for glaucoma should keep our lab in mind in the even that their dog needs to be euthanized for therapeutic reasons unrelated to OM. Ideally, part of each sample can be used to extract total protein to quantitatively analyze protein levels via Western blot, and the remainder can be used for immunohistochemistry to determine whether or not these proteins co-localize with the large, pigmented cells characteristic of OM.

Given the difficulties in obtaining sample tissue for RNA sequencing, one possible alternative is to extract RNA from early-passage cultured melanocytes. Although OM affected melanocytes do lose their pigmented phenotype *in vitro*, they retain it for the first few passages immediately following isolation (see Chapter 3). Although these cells are likely undergoing expression changes in culture, they are also not in an actively inflammatory environment, as they would be in a glaucomatous eye, which may help to decrease background noise when

comparing differences between cell populations. Additionally, comparing expression changes between affected cells in culture and affected iris tissue may highlight which changes in expression are causing the loss of the pigmented phenotype in cultured cells.

We can also attempt to leverage our existing whole-genome sequencing data in new ways. To date, our study has focused primarily on genes near the 7.5 MB region mapped by the whole genome SNP array, and genes with a known connection to pigmentary disorders. There has been no extensive screening done of genes known to be involved in cytokine or integrin signaling pathways. The results of our transcriptome analysis indicate that signaling in these two pathways may be driving the changes in OM melanocyte migratory behavior that we observe *in vivo*. Both of these pathways are fairly well understood, which give us a good pool of target genes to examine for possible causative variants.

The 7.5 MB mapped region on chromosome 11 continues to present questions, however. No genes within that region showed significant expression differences as determined by either method of transcription level analysis, and whole-genome sequencing has not revealed any variants in that region that would seem to explain OM. Though the region is statistically significant in its association with OM, no annotated element within it is a strong candidate to be linked with the OM phenotype. To date, we have also been unable to find a completely linked marker within the region that segregates perfectly with the OM phenotype, finding at best ~85% concordance between a marker and the affected phenotype. Although we have observed a recent clinical case of a Cairn terrier with a phenotype that appears similar to OM but lacks some of the distinctive features, the vast majority of dogs diagnosed with OM by other physicians have been confirmed as true cases when examined by Dr. Petersen-Jones. This

makes it unlikely that misdiagnosis is occurring at a high enough rate to account for the discrepancy. At present, this seems like an impasse. We propose to use *de novo* assembly of our existing RNA sequencing data to try to detect the presence of any further unannotated transcripts within the region which may explain this difference.

Although we found no structural rearrangements when examining the sequencing data near the mapped region of interest, the short-sequence reads employed in Illumina-based workflows for efficient whole-genome sequencing create technical problems that make structural variation very difficult to detect systematically with existing software packages (6). In order to more fully investigate the possibility of a structural rearrangement within the mapped region, we suggest sequencing several OM-affected and unaffected Cairn terriers using a sequencing method which produces long average read lengths, such as Pacific Bioscience's SMRT-sequencing platform (Pacific Biosciences, Menlo Park, CA), which has an average read length of 10,000 bp (7, 8). This method would also allow us to span the gaps in the canine genome via *de novo* sequencing.

Finally, although we would obviously prefer to identify the underlying cause of OM, for owners and breeders, simply finding a perfectly linked marker would be sufficient to begin the process of selectively breeding away from the disease. Although the ~170k beadchip used in this study was dense enough to allow us to map a 7.5 MB region, increasing our marker density may allow us to narrow down the region even further, and allows us to test a large number of markers across a large number of dogs for concordance with the disease simultaneously. A new canine SNP array using ~1.2 million SNP markers is currently in development by Affymetrix (Santa Clara, CA). Although the commercial release of the chip will have less markers than that,

it should still have enough to allow us to look for mapped regions at a much higher resolution than had previously been possibly with the ~170k beadchip.

In addition to these other proposed studies, it may also be beneficial for us to try incorporating samples from another, closely related breed into some of the other analyses we have already performed. The West Highland white terrier dog breed is very closely related to the Cairn terrier, but does not develop ocular melanosis. Sequencing of several West Highland white terriers (Westies) would allow us to generate a set of background variants which could be subtracted from our Carin terrier variants to help us remove most of the variation unique to these particular dog breeds. Additionally, melanocytes from unaffected Westie iris tissue may provide better controls for cell culture studies, as they are very closely related to Cairn terriers, but there are no doubts as to their OM status, unlike the older Cairn terriers we have previously used. It should also be easier to procure these samples, as samples could be taken from dogs of any age.

REFERENCES

REFERENCES

1. Ghislin S, Obino D, Middendorp S, Boggetto N, Alcaide-Loridan C, Deshayes F. LFA-1 and ICAM-1 expression induced during melanoma-endothelial cell co-culture favors the transendothelial migration of melanoma cell lines in vitro. BMC Cancer. 2012;12(1):455.

2. Duval C, RÉGnier M, Schmidt R. Distinct Melanogenic Response of Human Melanocytes in Mono-culture, in Co-Culture with Keratinocytes and in Reconstructed Epidermis, to UV Exposure. Pigment cell research. 2001;14(5):348-55.

3. Boyd SR, Tan DSW, de Souza L, Neale MH, Myatt NE, Alexander RA, et al. Uveal melanomas express vascular endothelial growth factor and basic fibroblast growth factor and support endothelial cell growth. The British Journal of Ophthalmology. 2002;86(4):440-7.

4. Fruman DA, Rommel C. PI3K and Cancer: Lessons, Challenges and Opportunities. Nature reviews Drug discovery. 2014;13(2):140-56.

5. Krasilnikov MA. Phosphatidylinositol-3 kinase dependent pathways: the role in control of cell growth, survival, and malignant transformation. Biochemistry Biokhimiia. 2000;65(1):59-67.

6. Guan P, Sung WK. Structural variation detection using next-generation sequencing data: A comparative technical review. Methods (San Diego, Calif). 2016;102:36-49.

7. Rhoads A, Au KF. PacBio Sequencing and Its Applications. Genomics, Proteomics & Bioinformatics. 2015;13(5):278-89.

8. Sakai H, Naito K, Ogiso-Tanaka E, Takahashi Y, Iseki K, Muto C, et al. The power of single molecule real-time sequencing technology in the de novo assembly of a eukaryotic genome. Scientific Reports. 2015;5:16780.